UNIVERSITY OF SOUTHAMPTON

FACULTY OF ENGINEERING, SCIENCE AND MATHEMATICS

School of Civil Engineering and the Environment

Micro-modelling of wave fields

by

Dimitris Stagonas

Thesis for the degree of Doctor of Philosophy

February 2010

Abstract

Physical models transfer part of the natural world into controlled laboratory conditions without the oversimplifying assumptions required by numerical models. However large scale hydraulic facilities are associated with large expenditure, require a high level of preparation, while at the same time access, to them is restricted for the majority of researchers and engineers.

This thesis explores the potential of small scale physical models of waves (termed wave micro-models) as a modelling tool for coastal engineers and scientists. Length scales smaller than 1:50 are applied in micro-models and as such the requirements in facility size, technical and experimental personnel and experimental time ($t = \sqrt{\frac{1}{length\ scale}}$ for a Froude scaled model) are significantly reduced. However, the problem of scale effects must be assessed. Accordingly the first steps of the large experimental effort presented here, were focused on establishing the validity range of wave micro-models for both breaking and non-breaking waves. Using that as a starting base several micro-models were then designed and developed in order to 1. assess the effectiveness of culverts as flushing elements in marinas, 2. develop a new composite seawall for overtopping based wave energy conversion and 3. test geometry variations in an existed yacht harbour.

The obtained experimental findings demonstrated that the micro-modelling of non-breaking waves is possible for water depths larger than 0.03m and wave periods longer than 0.35sec. On the contrary small scale breaking waves are strongly influenced by surface tension but when the freshwater was replaced by an isopropyl-alcohol and distilled water solution with reduced surface tension, very encouraging results were achieved. Undistorted plunging breakers were created, air entrainment was observed to increase significantly and the energy dissipation values exceeded even those reported in the literature for large scale experiments. It is believed that such a fluid could potentialy be used in other areas of hydraulic research, e.g hydraulic jumps, dam break events, etc.

Useful insights regarding the operation of culverts were also acquired and it was shown that efficient flushing is almost potentially impossible with symetric culverts. In conjunction with this, the measurements of the hydraulic power potential of the composite seawall were very promising and when a modelling fluid with reduced surface tension was used run-up and overtopping at small scale were significantly improved.

Finally, geometry effects on wave fields were observed with a novel, purposely developed, mapping method. The velocities of floating particles were used to extract wave heights and although inaccuracies were observed, partly because linear theory was employed, the 3D evolution of a wave field was mapped for the first time. Wave mapping in combination with wave micro-models appears attractive since the comparatively small areas allow for the measurement of the whole wave field rather than using single point measurements as it is usually applied in physical model tests.

Contents

List of Figures

List of Tables

Form of declaration

I, Dimitris Stagonas, declare that the thesis entitled Micro-modelling of wave fields, and the work presented in the thesis are both my own, and have been generated by me as the result of my own original research.

I confirm that:

- This work was done wholly while in candidature for a research degree at this University.
- Where any part of this thesis has previously been submitted for a degree or any other qualification at this university or any other institution, this has been clearly stated.
- Where I have consulted the published work of others, this is always clearly attributed.
- Where I have quoted from the work of others, the source is always given. With the exception of such quotations, this thesis is entirely my own work.
- I have acknowledged all main sources of help.
- Where the thesis is based on work done by myself jointly with others, I have made clear exactly what was done by others and what I have contributed myself.
- Part of this work has been published as Stagonas and Muller, 2007.

Signed:.....

Date:.....

Acknowledgments

My most sincere acknowledgements are dedicated to..

my supervisor, Dr. Gerald Muller, for his constant and valuable support..

Prof. A.F. Velegrakis for starting the journey..

Prof. J.R Chaplin, for all his help with my laboratory experiments, and his very useful remarks and suggestions.

my friends Davide Magagna, Dave Warbrick, and Rhys Jenkins for their help and support during the endless laboratory hours.

To Alexandros Onassis foundation for the economic support during the last two years of my study. Between September 2007 and September 2009 I was honoured to be a scholar of the Alexandros Onassis foundation.

..and above all, to my parents Vasileio and Theodora, for making everything possible..

Chapter 1

Introduction

1.1 Motivation

Climate change is becoming an established fact and as such sea level rise and increased storminess challenge coastal scientists and engineers to provide valid answers and protective solutions for and against various natural hazards like floods, tsunamis and increasing coastal erosion. Hydraulic research is for the first time required to move beyond traditional civil engineering problems and become part of a more complex and dynamic network of needs, which involves the environmental and socio-economic aspects of the coastal zone and changes every day as new insights on global warming are revealed.

To meet with these challenges, the coastal engineer / scientist needs now more than ever to exploit the synergy between numerical / theoretical models, physical models and field studies as a comprehensive tool that will aid him to acquire a profound knowledge of the coastal environment and predict the reaction of the prototype to proposed protective measures. Although during the past decades numerical modelling has become a powerful tool it mainly be applied in cases where the surface motion is relatively mild. Intense wave breaking for example is complicated by the large number of boundary conditions and equations required to describe the air-water interaction. Large Eddy Simulation (LES) and Volume of Fluid (VOF) are numerical approaches that can sufficiently simulate fully turbulent flows (large

Reynolds numbers) but they require large computational time and their microscopic resolution is limited. On the other hand in Direct Numerical Simulations (DNS) even the smallest dissipative scales are resolved in the computational mesh, but the computational cost is prohibitive even for low Reynolds numbers (Re) since the number of needed operations grows with Re^3. Moreover, the area of applicability of the available equations describing the wave motion is mainly characterised by the wave steepness (i.e Boussnesq and shallow water wave equations) and the accuracy of the numerical model from the breaking point and onwards highly depends on experimental coefficients and the quality of the calibration / validation data.

Nevertheless, the questions related to coastal systems require deeper insight into the complex processes involved and their interactions with natural or artificial boundaries (e.g. coastal structures). Physical models explicitly include all or at least most of these processes since they are simplified replicas of the natural reality. Sextus Julius Frontinus, an administrator of water supply in Rome during the era of Emperor Trajan, was the first person to report the use of a scale hydraulic model. The model included sand and water interaction and was built to observe and understand the interaction of rivers with ducts lying on hill slopes, LeMehaute (1976).

Sextus did not understand that the small scale introduces errors in the final result of his experiment, but he immediately saw the opportunity to visualise a number of phenomena that helped him realise why parts of Rome were not provided with water. Since then hydraulic facilities have been vastly developed and used in order to understand, predict and to a certain extend tame nature. Nonetheless, the critical comparison between model and prototype indicates that a physical model is only as accurate as it is large, or in other words, as the model size decreases so does its capability to accurately reproduce reality. For example only at a scale at or near 1:1, will laboratory breaking waves be as intense as they observed to be at sea.

Table 1.1 summarises some of the largest and most sophisticated hydraulic facilities available in Europe. These facilities are part of a European consortium called HYDRALAB, which has as a goal to make them available to scientists and engineers

Facility owner	Facility name and short description
Delft Hydraulics /Deltares	Delta Flume (wave flume with special wave generation equip.)
	Oscillating water tunnel (full scale facility to study near bed processes)
	Rotating annular flume (erosion of cohesive, biochemical and polluted sediments)
	Dynamic multi-phase flow test rig (unsteady two-phase flow in pipelines)
	Tidal flume (density currents and waves)
	Multi-directional wave basin (basin with short crested waves and reflection compensation system)
	Schelde flume (glass wall wave/current flume)
Centre National de la Recherche Scientifique (CNRS)	Very large wave basin (sea keeping and manoeuvrability testing of ships and offshore structures)
	Stratified flume (stratified flow in which each layer is separately controlled)
DHI Water & Environment (DHI)	Multi-directional (3D) offshore wave basin (up to 12m deep with short-crested waves)
	Multi-directional (3D) shallow water wave basin (wave/current basin with short-crested waves and wind loading)
Hamburgishe Schiffbau-Versuchsanstalt (HSVA)	Arctic Technology facility LIMB (towing tank to study ice-breaking ships and offshore structures in arctic conditions)
	Arctic Technology facility AETB & Ice lab. (the largest tank in the world to study ice physics and arctic marine biology/chemistry and research oil spills in polar regions)
University of Hull	Total environmental simulator TES (basin for currents, waves and rainfall in fresh and salt water)
Norwegian University of Science & Technology (NTNU)	Ocean basin (large wave basin to test fixed and floating structures)
	Towing tanks (to study ship performance and wave behavior)
	Medium tanks (coriolis rotating basin and outdor seawater basins to study sedimentation and to do bio-optical studies)
	Research vessel (for bio-chemical and acoustic studies of the seabed, oceanographic and marine biological research)
	Field facilities (unique landlocked site that functions as a mesocosm)
Forschungszentrum Küste (UHANN/FZK)	Large wave channel (GWK is the longest large scale wave flume in the world to study physical processes such as morphological processes and structure response to wave impacts)
Universitat Polytecnica de Catalunia (UPC)	Large scale wave flume (CIEM is the large scale wave flume with an optical test section and clear water for non-intrusive optical observations)

Table 1.1: Large scale European hydraulic facilities, after Grune and Breteler (2010).

from all over the European Union (EU). The HYDRALAB III project was funded by the EU with approximately 15.000.000€, for 4 years (2006-2010). During this period 69 research groups were granted with access to the facilities in Table 1.1. At the end of the project most if not all the groups pointed out that a significant part of the experimental time they had available was spent preparing and whenever necessary altering the physical model.

The discussions above show that although state of the art and necessary, the use of such large scale experimental facilities is limited due to the high maintenance and operation expenses and the shortness of available experimental time. Of course more than 69 research groups operate within the European universities and thus experimental research, knowledge development and teaching needs to come from smaller scale models. Furthermore the design of hydraulic infrastructure by engineers can mainly be based on engineering intuition, experience and numerical analysis whenever possible. Only very large projects can afford the solution of large scale physical models and even then only one, final design option can normally be tested.

For similar reasons, the U.S Army Corps of Engineers (USACE) used very small scale (1:20,000), Table-top, physical models to assess river training problems, Davinroy (1994). These so-called micro-models were employed to investigate the effects of structures on sediment transport and river flow, and they proved to be an excellent communication and demonstration tool. Nonetheless, micro-models of rivers were heavily criticised (see Maynord (2006)) mainly because the modelling of sediment movement and accumulation, even under unidirectional flow, is a complex problem with many variables, most of which are impossible to be reproduced in such small scales. However, fluid flows can , up to a certain point, be modeled at micro-scales.

In coastal engineering large scale fluid flow processes need to be investigated and understood and the use of expensive large scale physical models is commonly required. On the other hand micro-models, due to their small size, offer an attractive, inexpensive and flexible alternative, but to this authors knowledge they have seldom been used for coastal research. Although a limited number of authors, e.g. Beckett and Marshall (1983) and Rankine (1991), refer to the employment of

very small scale (i.e. 1:2000) hydraulic models for the modelling of tidal flow effects in harbours, wave micro-models have never been considered before.

1.2 Aims

The current thesis investigates the use of wave micro-models for coastal engineering purposes. Their small size is directly associated with small experimental costs and low requirements for space, running time, and trained scientific and technical personnel. Accordingly wave micro-models can be an inexpensive alternative for the hydraulic laboratories of Universities and even medium consultancy firms. They are envisaged as a tool:

- for the preliminary research of wave-related coastal processes,
- for the development and initial testing of novel ideas,
- for the preliminary design of wave related coastal protection schemes and the testing of alternative design options,
- that can provide immediate answers and insights to simple coastal engineering problems,
- for the pre-design of large scale physical models

Once more the small scales involved imply that wave micro-models violate most if not all the necessary conditions for a model to be similar to the prototype. Nevertheless, the capacity of micro-models to reproduce nature is increased by the fact that sediment transport is not considered and as such only the effects of small scale on the fundamental wave processes are investigated. Accordingly the present work focuses on investigating the micro-modelling of wave propagation, wave diffraction and wave breaking. Experimental efforts are also concentrated on exploring the potentials of micro-models to provide insights on simple engineering problems, develop novel ideas, and test alternative design options.

1.3 Thesis outline

The work presented in the current thesis is divided into 8 chapters, the contents of which are described here.

Chapter 2 presents a review of the existing literature regarding the development and use of river micro-models, physical models of waves, and scale effects on wave propagation, refraction, diffraction, breaking and air entrainment.

Chapter 3 describes a novel method for the full field mapping of surface elevation within a wave basin. The development of this new technique was considered essential since traditional measuring equipment (i.e. wave probes) can only provide single point measurements and as such information on the wave field evolution is usually incomplete. A brief literature review follows and soon after the method is presented along with the experimental results for its validation.

Chapter 4 investigates scale effects on wave propagation and diffraction. Some theoretical considerations are presented first, followed by the experimental apparatus, the results and the discussion.

Chapter 5 explores scale effects on wave breaking in wave micro-models. Detailed references on the existed literature are made in order to better highlight the complexity of the phenomenon and experiments with breaking waves at small scales are conducted in freshwater and in a solution (isopropyl-alcohol and distilled water) with reduced surface tension. The findings presented in this chapter are believed to be of use for the hydraulic modelling of other fields as well.

Chapter 6 outlines a series of two-dimensional experiments designed to examine the potentials of wave micro-models as a tool for simple engineering applications and the development of novel concepts. In the first part of the chapter a micro-model is used to investigate the efficiency culvert as flushing elements in marinas, the second part focuses on the development of a composite seawall for wave energy conversion.

Chapter 7 presents a three-dimensional experiment and shows that micro-models can be used for testing different design options. For this reason an existed

yacht harbour is built within a small wave basin and two alternative entrance shapes are compared with regards to their effects on wave energy transmission.

Chapter 8 includes the conclusions made on the basis of research and experimental effort presented in the previous chapters, and also discusses recommendation areas for further research.

Chapter 2

Literature review

2.1 Introduction

A review of the existing literature is conducted in the current chapter. Reference is originally made to the development, operation, and short-comings of river micro-models, followed by a description of small scale hydraulic models used for the investigation of tidal flows in harbours. The use of large scale physical models for wave related studies is then reported and emphasis is given to the potential sources of error that exist whenever reality is modelled in laboratory conditions. The effects of solid boundaries (laboratory effects) and scaling (scale effects) on wave propagation, refraction and diffraction are referred to separately whilst a large part of the literature review is dedicated to wave breaking. Most of the energy transported inshore by the wave action is dissipated through breaking and as such laboratory breaking waves have been studied by many authors in the past. Despite the massive experimental effort though, the effects of scaling to the breaker shape, the entrainment of air, the formation of bubbles and the breaking process overall are not yet fully understood.

2.2 River micro-models

In 1993 the St. Louis District (SLD) of the U.S. Army Corps of Engineers (USACE) began development of river micro-models as an effort to provide timely assessment of

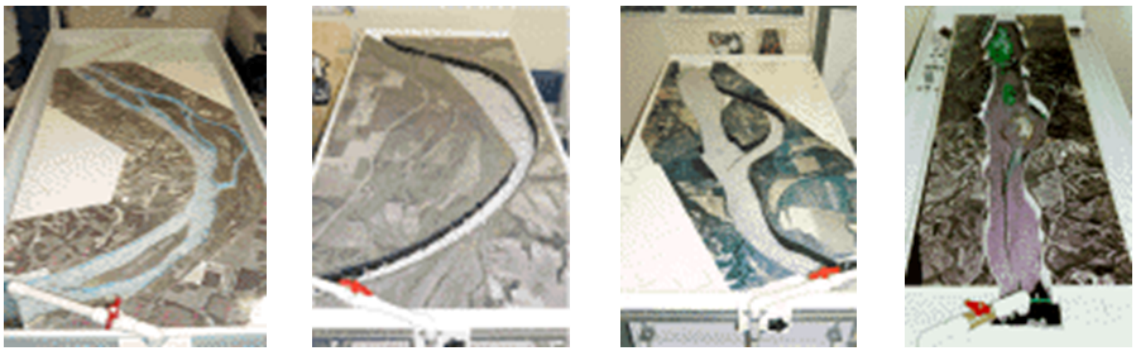

Figure 2.1: Micro-model arrangements in used by the Applied River Engineering Center in St. Louis, Missouri. From right to left, Bolter's Bar Dredging Study, Copeland Bend Environmental Dike Study, Wolf Island Environmental Study, and Lock & Dam 24 Navigation Study.

navigation plans. According to Maynord (2006) the micro-model of a river is an extremely small physical model having a movable bed, varying discharge, and numerous innovations to achieve quick answers to river engineering problems.

Davinroy (1994) describes the five main components of micro-models; which are:

- A hydraulic flume,
- a model-channel insert,
- an electronic flow controller,
- synthetic bed sediment, and
- pervious steel mesh for replicating dikes and bendway weirs

Figure 2.1 illustrates different micro-models used in the Applied River Engineering Center in St. Louis. Although a certain flexibility in size is possible, the overall dimensions of these hydraulic flumes are restricted to 1.9m long and 0.9m wide, which is the area that can by physically reached by a modeler. The model's slope is adjustable in both the longitudinal and transverse directions and a submersible pump is used to recirculate the flow and the sediment. Plastic material with a gradation between 0.25mm and 1.19mm is utilised as sediment. The material has to be light enough to be transported by the flow but it should also retain the bed configuration after each model test as to allow the collection of bathymetric data..

Investigation name (river)	Year investigation completed	Horizontal scale	Distortion (Horizontal:Vertical)	Objective/Description
Mouth of White River (Mississippi)	1998	1:12,000	10:1	Improved navigation alignment
Clarendon, AR (White)	2000	1:4,200	14:1	Improved navigation depths
Augusta, AR (White)	2000	1:3,600	20:1	Improved navigation depths
Vicksburg Front (Mississippi)	2000	1:14,400	12:1	Improved navigation alignment
Wolf Island (Mississippi)	2000	1:7,200	12:1	Evaluate features for environmental diversity
Memphis Front (Mississippi)	2000	1:4,800	8:1	Harbor entrance
Sante Fe Chute (Mississippi)	1996	1:7,200	6:1	Improve side-channel depths/ alignment
Lock and Dam 24 (Mississippi)	1998	1:9,600	16:1	Corrected currents dangerous to lock approach
SEMO Port (Mississippi) (Davinroy et al., 2000)	2000	1:3,600	6:1	Improved navigation depths at port entrance
Bolters Bar (Mississippi)	1998	1:9,600	16:1	Improved navigation depths
Savanna Bay (Mississippi)	1998	1:4,800	8:1	Improved navigation depths/side-channel protection
Marquette Chute (Mississippi)	1997	1:9,600	12.3:1	Side-channel enhancement
Copeland Bend (Missouri)	1999	1:3,600	15:1	Environmental enhancement
Big Creek (small stream)	1996	1:600	5:1	Bridge-abutment protection
Schenimann Chute (Mississippi)	2000	1:4,800	8:1	Side-channel enhancement
Morgan City/Berwick Bay (Atchafalaya)	2000	1:7,200	6:1	Improved navigation depths and alignment
New Madrid (Mississippi)	2000	1:20,000	17:1	Improved navigation depths

Table 2.1: Summary of USACE-SLD micro-model investigations, after Gaines and Maynord (2001).

2.2.1 Purpose and model scale of river micro-models

Over the past 20 years the USACE-SLD has conducted several micro-model investigations. Gaines and Maynord (2001) summarised some of these experimental efforts (Table 2.1) and deduced that micro-models were mainly used for two types of studies. The first, challenged micro-models to predict in qualitative terms the riverbed response to alternative channel control options (e.g. dykes, bendway wires etc) and the second aimed at identifying overall flow patterns and alignments. The usual goal of such model studies was to provide solution for the reduction of maintenance dredging in troublesome reaches and improve navigability.

For all these studies approximately 20km of the Mississippi river were reproduced on the 1.9m long micro-model Table. This resulted on horizontal scales of up to 1:20,000 and channel widths as small as 4cm. Since the water depth and structure size in rivers is disproportionally smaller than the modelled area, a horizontal to vertical distortion is commonly introduced. A maximum vertical distortion of 1:180 is recorded for the micro-models of Table 2.1. The gravity force is commonly considered dominant and typical hydrograph model times range from 3min to 5min. Furthermore Davinroy (2004) estimated the overall cost for construction, testing and analyses of such models, between $100,000 and $150,000.

Recently, Alam (2009) and Willson (2009) presented an extreme case of a small scale physical hydraulic model (SSPM) reproducing about 9,027km^{2}of the lower

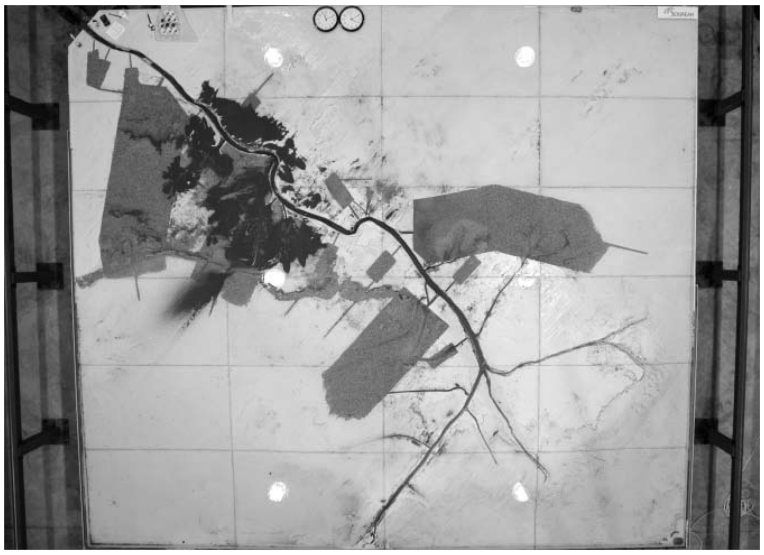

Figure 2.2: Overview of the small scale hydraulic model of the lower Mississippi river and delta, after Willson (2009).

Mississippi river and delta on a platform of 62.69m^2(Fig. 2.2). With 1:20,000 horizontal and 1:500 vertical scale, the SSPM is a distorted model aiming on the reproduction of general sediment transport trends rather than local velocity variations. According to Alam (2009) the vital requirement for comprehensive knowledge of the exact consequences of any major hydraulic structure, combined with the unsatisfactory results of sediment diversion structures designed by using numerical models, inspired the development of the SSPM.

Due to its small scale the SSPM has the capacity to simulate the Mississippi river sand transport of 1 year in prototype time within 1/2 and hour of laboratory run time. Field data were used to verify model results and both authors concluded that although qualitative in sediment transport simulation, the SSPM can reproduce fairly accurately the overall performance of alternative proposed project schemes and structures. Alam (2009) also added that the construction and operational cost of the hydraulic model (approx. $750,000) was significantly smaller than the savings in dredging costs alone.

Hence, it is seen that micro-models are used as a quick and inexpensive, qualitative alternative to large scale physical and numerical models. Their main objective is to provide a relatively reliable overview on the effects of various proposed constructions schemes and thus aid on the selection of appropriate engineering solutions.

2.2.2 Operation of river micro-models

The micro-models of rivers presented thus far largely focus on addressing sediment transport issues. Since such studies are not part of the current thesis the operation of such models is only briefly described and more detailed description can be found in Gaines and Maynord (2001).

A polystyrene sheet is used for the fabrication of the model insert, which is a semi-3D representation of the area to be studied. Aerial photographs are used for the design of the insert and the cutout plan-form of the river. Accordingly training structures, sediment and water are introduced and the model is calibrated.

According to ASCE (2000), " model calibration is the tuning of the model to reproduce a single known event ". Although such a condition does not ensure the veracity and predictive ability of models it certainly increases the confidence on the model. Freeman (1929) describes the experiments of Vernon-Harcourt and shows that the confidence level can be further increased with the validation of the calibrated model. As such, the model outcomes are compared against alternative prototype boundary conditions (validation) and if satisfactory the model is considered more reliable for prediction. The same concept is used for the evaluation of micro-models as well.

However, as soon as the micro-model is calibrated a run is conducted with a specific hydrograph and the resulting bathymetry and flow patterns are recorded with a laser scanner or a mechanical digitiser, and utilised as a base test. Changes caused by every subsequent run with the same hydrograph but different layout (i.e. alternative structures etc) are considered indicative to changes that will occur in the prototype. Maynord (2006) reports that base tests can reduce the required accuracy for the model but the necessity for resemblance of model findings and prototype conditions remains.

2.2.3 Scale effects in river micro-models

Prior to micro-models and aside from numerical models Movable-Bed hydraulic Models (MBM) were used for the study of river flow and sediment transport problems. MBMs are physical models where all or part of the model bed is composed of granular material that can be transported under the action of water flow, waves and currents. Graf (1971) categorizes this type of hydraulic models as either empirical (qualitative) or rational (quantitative) and a vast literature exists, which analyses in detail MBMs and discusses their validity, i.e. Yalin (1971); LeMehaute (1970); Kamphuis (1974); Hughes (1993) and ASCE (2000).

However, as for all physical models, in order for an MBM to accurately reproduce the prototype, geometric (length), kinematic (time and velocity), and dynamic (force) similarity needs to be maintained between the field and the laboratory or in other words all major factors influencing the modelled processes should be in proportion with the prototype. Unfortunately satisfaction of even two dynamic-similitude criteria associated with the flow (i.e. gravity and viscosity) would require for the model fluid to be different than water (prototype), Hughes (1993). If sediment transport is considered as well then the model particles will also need to have different density than those at full-scale, Yalin (1965).

However, fluids other than water and sediment material of the requisite properties can be either difficult to found or simply none existing. Hence it is deduced that the simultaneous satisfaction of all similarity criteria is possible only at a model scale of 1:1 or very nearly so. Failure of a hydraulic model to meet with similitude considerations in most cases results in unwanted scale effects. For MBM, Haque et al. (2006) discuss the consequences of these scale effects, which may even entail the improper reproduction of important processes.

From all the above it is easily derived that micro-models, due to the very small scale appear to violate similitude laws. Davinroy (1994) argued that micro-modelling seeks a direct morphologic similarity between model and prototype but Falvey (1999) and

Yalin (in Maynord (2006)) observed but not used micro-models, and heavily criticised them and doubted their veracity and predictive capacity.

Ettema and Maynord (2002) noted that micro-models include all the usual sources of scale effects in hydraulic models, such as large length scales, model distortion, amplification of channel slope and improper sediment size. In addition there is no correspondence of stage between the model and the prototype, the ratio of inertia to gravity forces is distorted, and the influence of surface tension and viscosity is greater in the laboratory than the field, Ettema (2001). Due to all that it is not possible to analytically locate the specific causes responsible for increased scale effects in micro-models. Maynord (2002) listed similarities and differences between micro-models and MBM, and defined them as totally empirical. Such classification places micro-models outside the two MBM categories of Graf (1971).

Accordingly, Maynord (2002); Ettema and Muste (2004), and Maynord (2006) compared micro-models with large scale hydraulic models and field surveys. The effect of training structures (e.g. dykes) on flow patterns and sediment transport was investigated and although not overwhelming, evidence showed a lack of predictive capability. Scaled model flow velocities were up to 3.7 times larger than field measurements and sediment accumulation areas were not the same between the micro-model the prototype. Based on that Maynord (2006) concluded that " the use of micro-model should be limited to demonstration, education, and communication for which it has been useful and should be of value to the profession ". The latter, however, contradicts USACE (2004a) who favours the use of micro-models, except in cases where the human life or the overall project were at risk.

2.2.4 Micro-models in Coastal engineering

Micro-models described so far have been used strictly for the hydraulic study of rivers. However, Beckett and Marshall (1983) reported the use of "mini-models", or very small scale hydraulic model, for the investigation of tidal flow effects on the Muara deep water port at Brunei. The physical model had a Plasticine movable bed

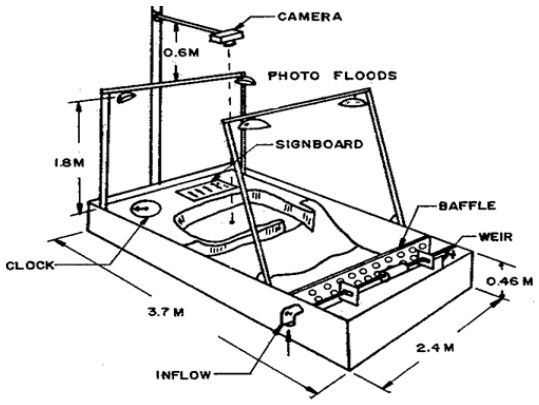

Figure 2.3: Scematic of a harbour's mini-model, after Nece (1985).

and was constructed inside a rocking tray, with a horizontal and vertical scale of 1:25,000 and 1:360 respectively. Tidal flows were simulated in order to provide preliminary indications as to whether the harbour could be economically maintained and compare the effect of different training works. According to the authors model tests were beyond doubt successful in identifying the best harbour configurations and tests the recommended scheme was then studied in a large scale MBM.

A similar small scale physical model was also used by Nece (1985) for the development of a small boat harbour (Fig. 2.3). According to the author, numerical models were unable to provide an adequate description of the complex flow field and thus a mini-model was preferred to provide answers on tidal flushing problems. The model failed to accurately predict the prototype but Nece (1985) attributed this to stratification and wind effects not taken into account. He concluded such small scale model cannot give accurate quantitative answers but they do provide the means of comparing various design options and their effect on internal circulation patterns.

Rankine (1991), describes the use and operation of mini-models for the hydraulic design of ports and emphasises the highly visual nature of this technique. When compared with the description of Gaines and Maynord (2001) for river micro-models it is seen that exactly the same approach on development, calibration and use is followed with a similar cost (approx. £60,000 at 1991). The only difference is that a titling Table is used in mini-models in order to generate the desired tidal flow.

Beckett (1992), recognised the lack of turbulent similarity, the sediment material size, the vertical distortion, and the surface tension and viscosity effects, as sources of scales effect in small scale tidal models. Therefore he suggested minimum water depths of 20mm and a horizontal to vertical distortion no larger than 6 (i.e. 1:1500 and 1:250). Under these conditions, the author concluded that scale mini-model studies can confidently predict sedimentation effects at a cost which is similar to a mathematical study.

2.2.5 Summary on small scale physical models

Overall it is seen that, either termed as micro-models or mini-models, small scale hydraulic models have been developed and used as a quick and inexpensive alternative to large scale movable bed models but the utilisation of wave has never been considered before. In any case, to this author's knowledge the term micro-model describes better small scale physical models as it includes a direct, and although approximate, quantitative reference to their scale. Thus throughout the current thesis physical models with scales smaller than 1:50, which can bee facilitated in Table-top basins (or flumes) will be referred to as micro-models.

Studies involving micro-models were mainly focused on the assessment of river training problems, but tests on harbour siltation issues have also been recorded. Micro-models have been used to provide qualitative answers about the overall effect of different construction schemes but only in flow related investigations. Due to their very small size, their veracity and capacity to reproduce the prototype were heavily criticised but micro-models are still being used for the effective management of the Mississippi river.

2.3 Short-wave physical models

Dalrymple (1985), separates wave motions into two rational categories:

- Short-waves, the periods of which in nature can range from 1sec to 20sec, and

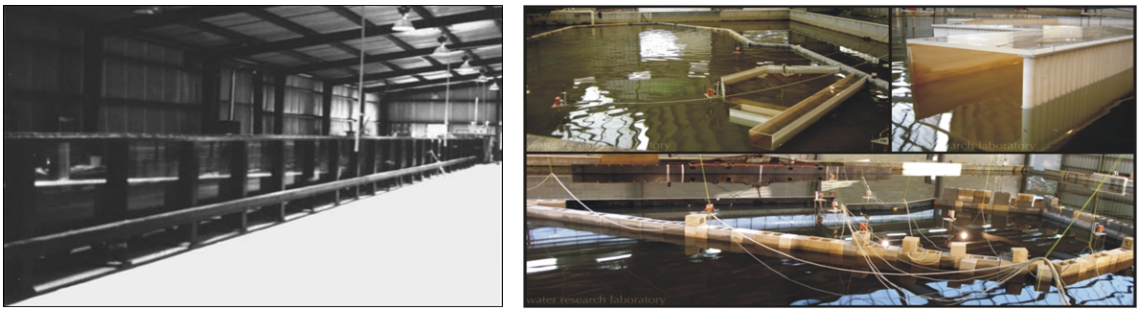

Figure 2.4: Images of a typical wave tank (left) and wave basin (right), after Hughes (1993).

- Long-waves, the periods of which in nature can range between minutes and days

Although tides could be considered as very long waves, all the micro-models presented so far to the literature refer only to the investigation of tidal flow effects on harbours. In every case, it is seen that micro-models have never before been used to study the effects of short-waves on coastal projects, except of one however, single exception. Dalrymple et al. (1977) employed a 2.44m long and 1.22m wide wave basin in order to verify analytical models of wave-induced circulation in shallow basins.

Apart from the latter exception all other physical models of short-waves are facilitated either in a, several meters long and at least 0.5m wide, (2D) wave tank or in an even longer and wider (3D) wave basin (Fig. 2.4); a vast literature exists detailing the development and operation of large physical models with scales commonly ranging from 1:10 to 1:30, like for example Hughes (1993); McCleave et al. (1999) and ASCE (2000). In either case, model results critically depend on the ability to correctly generate waves and on the influence of scale effects upon the processes under investigation.

Wave generation and wave generation systems have been described by many authors such as Dean and Dalrymple (1984) and Funke and Mansard (1987) for linear waves and more recently by Schäffer (1996) and Zhanq and Schäffer (2008) for highly non-linear waves; although interesting, the description of these complex theories rests outside the limits of the present thesis. Nevertheless, even when regular waves propagate inside a wave flume it is possible that they may not retain a constant form.

Benjamin (1967) and Benjamin and Feir (1967), observed that in deep waters and for kd > 1.363 (where $k = 2\pi/L$ is the wave number and d the water depth) regular waves show an instability to disturbances with slightly different frequencies to both sides (side-band) to which energy is transferred. Melville (1982) has experimentally shown that, for waves less steep than 0.3 (H/L < 0.3), such instabilities can cause uniform wave trains to become unstable and eventually break. This was also verified by the numerical simulations of Dold and Peregrine (1986) for wave steepness as small as 0.1. Later Longuet-Higgins and Cleaver (1994) summarised both previous studies and numerically demonstrated that such a breaking mechanism may occur for wave steepness smaller than 0.4432 but only if a propagating space of about 30-50 waves is given. Svendsen (1985) reported an equally important wave instability resulting from the development of a side wall resonant mode of oscillation and leading to unwanted wave breaking at one or the other side wall of the flume. The phenomenon, however, primalry occurred around certain wave frequencies.

Nevertheless, recent advances on wavemaker theory, i.e. Schäffer and Jakobsen (2003), and wavemaker technology (see for example HR Wallingford and / or DHI, www.hrwallingford.co.uk and www.dhigroup.com) have resulted in smoother and more reliable laboratory wave generation. In general though such instabilities are part of an overall source of inaccuracies for wave physical models, which is commonly referred to as laboratory effects. Laboratory effects arise from the presence of solid boundaries (e.g. side walls) that do not exist in the prototype and the inability to reproduce natural hydrodynamic forcing factors such as waves and current, Svendsen and Haas (1999) and Haas and Svendsen (2002). In any case, the development of passive wave absorbers, LeMehaute (1965), and active wave absorption systems, Spinnekena and Swan (2009), minimise laboratory effects from either solid (i.e. end wall) or moving boundaries (i.e. wavemaker).

2.3.1 Scale effects

Potentially more important, as an error source, than laboratory effects are scale effects. As mentioned previously, scale effects arise from the reduced capacity of a

physical model to reproduce all relevant forces of the prototype at the proper, scaled magnitude, and have concerned several investigators in the past, like LeMehaute (1976),Kamphuis (1973), Jensen and Klinting (1983), Oumeraci (1984), and Dalrymple (1989). Since the majority of models in coastal engineering involve gravity waves, gravity is taken as the dominant force and the contribution of all other forces like surface tension, friction, and elasticity are neglected despite the fact that their values might be exaggerated in the model.

The relative influence of each force in the flow / wave is expressed by the ratio of the inertia force to the force under examination. A model can only be similar to the prototype if the force ratio between them is the same and thus each force has its own similitude criterion or:

The Froude number (Fr) express the relative influence of the inertial and gravity forces in a hydraulic flow and is given by:

$$Fr = \frac{V}{\sqrt{gL}} \tag{2.1}$$

where,
V : is the velocity,
L : is the wavelength,
g : is the gravitational acceleration

For deep water propagating waves V is equal the wave celerity, $c = \frac{L}{T}$, while when waves travel in shallow waters then$V = c = \sqrt{gd}$ (T is the wave period and d is the water depth). Except of wave models, the Froude number is also useful in modelling of hydraulic jump, and ship design, where forces due to gravity and inertial forces are governing, Watson (2002).

The Reynolds number criterion becomes important when viscous forces predominate and it is given by:

$$Re = \frac{\rho LV}{\mu} \tag{2.2}$$

where,

ρ: is the fluid density,

μ: is the dynamic viscosity

The Reynolds number gives the relative importance of the inertial force on a fluid particle to the viscous force on the particle. Examples include cases of confined flows, laminar boundary layer problems and forces on cylinders with low Re, Koterayama and Hu (1996).

The Weber criterion (We) express the relative influence of surface tension and is given by:

$$We = \frac{\rho V^2 L}{\sigma} \tag{2.3}$$

where,

σ: is the surface tension

Surface tension acts on the interface between two fluids, such as air and water and it can affect both non-breaking and breaking laboratory waves, propagation, i.e. Lighthill (1975) and Duncan (2001).

Other similitude criteria, like Euler (pressure), Cauchy (elasticity) and Strouhal (convection), also exist but they are not considered relevant to the current thesis. As an example, however, the Cauchy number is important in studies of wave loads where the inertial forces can be large enough to cause changes in fluid compressibility, Bullock et al. (2001).

Figure 2.5 summarises the areas of increased influence for each similitude criterion, within a wave physical model. Although gravity effects are important for all modelled processes, it is seen that for example the significance of surface tension and viscosity increase for breaking waves and for run-up and overtopping. This entails that such a model will reproduce the prototype only if a constant ratio between their

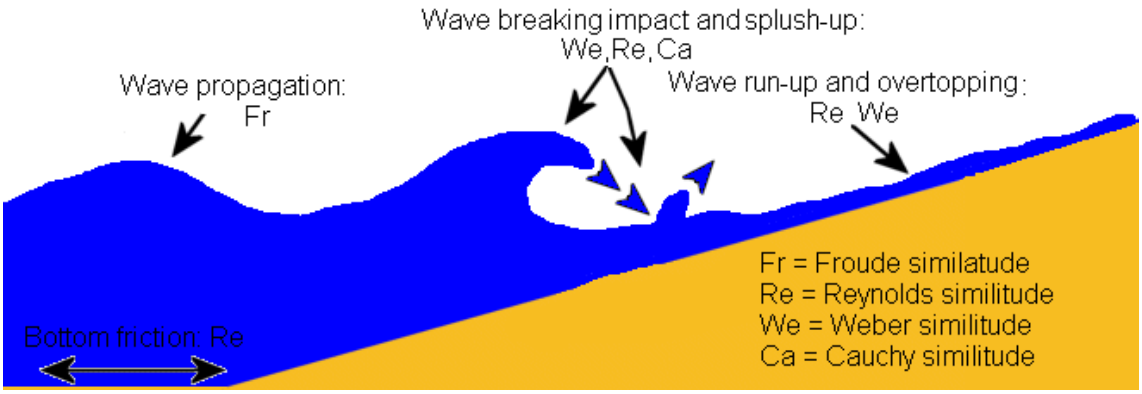

Figure 2.5: Areas of increased influence for each similitude criterion, at Froude scale physical model of waves, inspired after Fuhrboter (1986).

Force	Similitude law	Scale		
		1:1	1:10	1:100
Gravity	Froude (Fr)	1	1	1
Viscosity	Reynolds (Re)	1	1:31.6	1:1000
Surface tension	Weber (We)	1	1:100	1:10000
Elasticity	Cauchy (Ca)	1	1:10	1:31.6

Table 2.2: Required scales according to similitude laws.

lengths is maintained all over the model (geometrical similarity) and if the ratio of all forces is the same. However, as Table 2.2 shows, for a geometrically similar model scaled according to Froude criterion, different scales for friction, surface tension, and elasticity forces are required, Hughes (1993). Hence special consideration is needed since for the same physical model, scale effects may be negligible for the propagation of waves but they could become important for breaking waves. This inability to properly scale-down all fluid properties greatly increases as the model scale reduces and as such physical models of waves with a scale smaller than 1:100, or wave micro-models, will be subjected to severe scale effects.

In general short-wave physical models focus upon the simulation of wave transformation and fundamental wave-structure interactions, including 1. wave propagation, refraction and diffraction, 2. wave breaking, 3. wave reflection and transmission, 4. wave-current interaction, and 5. non-linear wave-wave interaction. However, the present work investigates the micro-modelling of propagating waves, wave diffraction and wave breaking, and as such scale effects on these processes are further analysed through the review of the existed literature.

2.3.2 Wave propagation

As it was previously shown the ratio between inertia and gravity forces (Fr) is essential for the accurate reproduction of waves in laboratory conditions. Nevertheless, when scaled according to the Froude criterion, physical models do not accurately simulate friction and surface tension effect because the Reynolds and Weber numbers are different in the model than the prototype.

As such waves travelling inside a wave tank / basin are attenuated by internal friction and side wall and bottom boundary layer friction. Either in the laboratory or in the field, the former dissipation factor is insignificant when compared with the latter, Hughes (1993) and Svendsen and Jonsson (1994). Based on the fluid viscosity, the wave characteristics, and the facility dimensions, Keulegan (1950b,a) developed expressions for estimating wave attenuation of regular waves progressing in a rectangular wave channel with a plain and constant cross-section (Chapter 4, eq. 4.1 and 4.2). Both Keulegan (1950b) and LeMehaute (1976) agree that the effect of viscous damping in non-breaking laboratory waves travelling over short distances, is negligible for water depths greater than 2cm. For these conditions and for a wave tank wider than 0.2m, wave attenuation does not exceed 5% of the original wave height per meter.

Furthermore, the propagating waves are in constant contact with air and as such a surface free energy is present on the formed interface. This interfacial energy originates from a molecular level and is the result yielded by the difference between the inward attraction of the molecules in the interior of the water and the air and those at the surface of contact. According to Adamsom (1990) the equivalent measure of this surface free energy is by means of a surface tension, which acts in a direction tangent to the surface as to reduce the expanding fluid (water) area. As such, surface tension is also the answer to the paradox created by the presence to this free interfacial energy and the principle of conservation of mechanical energy, which states that mechanical energy cannot be stored at the air-water boundary.

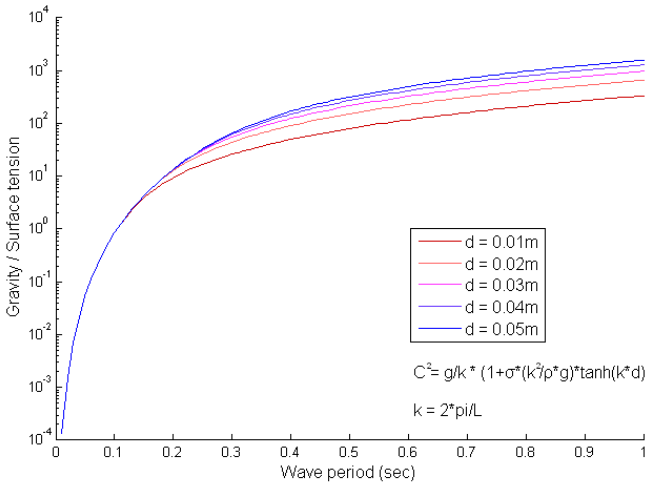

Figure 2.6: Influence of surface tension compared to the gravity force for different wave periods, equation after Tirindelli et al. (2000).

Yeh (1995) considers a small, two dimensional (2D) liquid-gas interface and assuming equilibrium condition, he modifies the dynamic boundary condition at the interface to include a term of the form $\frac{\sigma}{R}$, where $\sigma$is the surface tension and R is the local radius of curvature of the free surface; of the water in this case. Thus the effect of surface tension enters the equations of motion and its magnitude increases as the radius of the curvature in the crest region decreases. However, since the curvature is proportional to the wavelength, it yields that surface tension significantly affects short waves.

Figure 2.6 plots the ratio of the gravity force to surface tension over the wave period, for a 2D, linear wave. It is seen that for a water depth and wave period larger than 2cm and 0.35sec respectively, the surface tension becomes almost 100 times smaller than gravity, or in other words its influence becomes negligible; similar limits have also been reported by LeMehaute (1976) and Hughes (1993).

In summary, theory indicates that laboratory waves with periods longer than 0.35sec, propagating over water depths larger than 2cm are not significantly affected by surface tension and viscosity effects and the overall wave height attenuation decreases as the water depth, the wave period and the basin / tank width increases. Wave damping can be important for (e.g.) model studies of energy transmission into a harbour. As the waves approach the harbour area shoaling, refraction, reflection and diffraction occur as a direct effect of their interaction with the local topography and coastal defences. Assuming non-breaking waves those are the main wave-related processes affecting energy transmission within the protected harbour basin. Consequently if the height of the propagating and transmitted waves is attenuated due to viscous and surface tension effects the discrepancy between model and prototype can be serious.

2.3.3 Wave refraction

Wave refraction is the change in direction of a wave as a result of an alteration in its speed. When water waves approach the coastline at an angle part of them is located in shallower waters and moves slower. This causes the waves to change direction and propagate parallel to the shore. Wave refraction, shoaling and the generation of long-shore currents due to the subsequent wave energy convergence is illustrated in Figure 2.7.

The refraction of water waves over changing bathymetry can be calculated using Snell's law, which was originally formulated for optics:

$$\frac{sin\theta_1}{c_1} = \frac{sin\theta_2}{c_2} \tag{2.4}$$

where,

θ_{1and2}: is the angle between the wave crest and the local bottom depth controur at locations 1 and 2,

c : is the wave speed

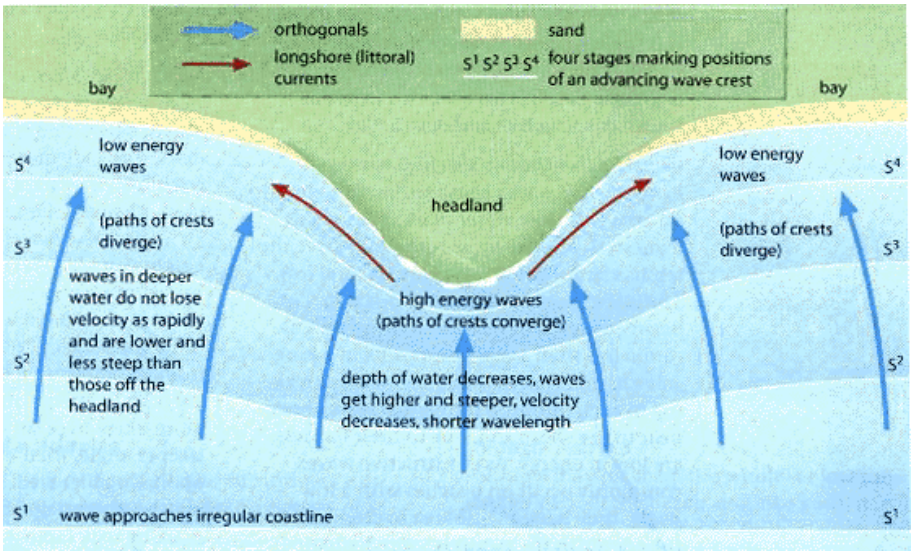

Figure 2.7: Wave refraction, shoaling and generation of long-shore currents, after www.members.tripos.com.

For linear theory and shallow water conditions equation 2.4 yields:

$$\frac{sin\theta_1}{sin\theta_2} = \frac{L_1}{L_2} = \frac{\sqrt{gd_1}}{\sqrt{gd_2}} \tag{2.5}$$

where,

L_{1and2}: is the wavelength at locations 1 and 2,

d_{1and2}: is the water depth at locations 1 and 2

For refraction to be correctly modelled it is necessary for $\left[\frac{sin\theta_1}{sin\theta_2}\right]_{prototype} = \left[\frac{sin\theta_1}{sin\theta_2}\right]_{model}$. Since g is the same for both the prototype and the model eq. 2.5 gives:

$$N_L = N_d \tag{2.6}$$

or,

$$\left[\frac{d}{L}\right]_{prototype} = \left[\frac{d}{L}\right]_{model} \tag{2.7}$$

where,

N_L: is the scale ratio for the wavelegth,

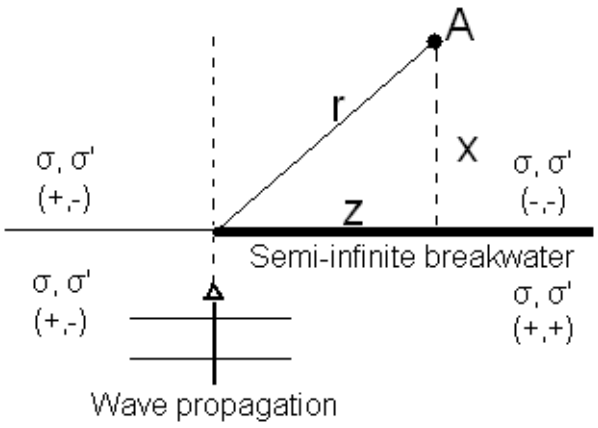

Figure 2.8: Nomenclature for wave diffraction analysis at breakwater tip, after Wiegel (1976).

N_d: is the scale ratio for the depth,

Therefore to correctly model refraction in short-wave models the wavelength scale must be equal to the vertical scale ratio, or otherwise the horizontal and vertical scales are the same. This requirement, however, is only satisfied in an undistorted model. For such a model and for negligible surface tension and viscosity effects, wave shoaling is also accurately modelled since it is also a function of d / L.

Nevertheless, Whalin and Chatham (1974) studied wave refraction in harbour models with horizontal scales ranging from 1:1 to 1:400 and distortion values between 0 and 4. The authors found no significant differences between the undistorted and distorted cases for wave periods of 1min and above but for shorter periods (i.e. 15-30sec) differences in direction and energy content were recorded.

2.3.4 Wave difraction

Wave diffraction can be described as the bending of waves around obstacles, like breakwaters, and the spreading out of waves as they pass through small openings, or in other words wave diffraction is the process by which the wave energy spreads in the lee of an obstacle. As such it is clear that a quantitative understanding of the effects of wave diffraction is relevant to the design of harbours and various coastal protection schemes.

In their pioneering work Penny and Price (1944) and Penny and Price (1952) showed that the water wave diffraction phenomenon can also be treated with the Sommerfeld solution of the diffraction of light. Thus for an infinitely thin, vertical, rigid, impermeable, semi-infinite breakwater located as illustrated in Figure 2.8:

$$F(x,z) = \frac{1+i}{2}\left\{ e^{-ikx} \int_{-\infty}^{\sigma} e^{-\pi i u^2/2} du + e^{ikx} \int_{-\infty}^{-\sigma'} e^{-\pi i u^2/2} du \right\} \tag{2.8}$$

where,

k : is the wave number or k = $\frac{2\pi}{L}$,

σ: is the value of u used in the upper limit of the definite integral,

$$\sigma^2 = \frac{4}{L}(r-x), \sigma'^2 = \frac{4}{L}(r+x) \tag{2.9}$$

where,$r = x^2 + z^2$

Figure 2.8 shows the physical interpretation of x, z, and r and the signs of $\sigma$and σ'. Wiegel (1976) shows that the diffraction coefficient (K$'$) is given by the modulus of F(x,z) ($K' = |F(x,z)|$), which is equal to 1 for the incident wave. The diffraction coefficient is defined as the ratio of the wave height in the area affected by diffraction to the wave height in the unaffected area. More details on the analytical solution of eq. 2.8 with the use of Fresnel integrals can be found in many textbooks, as for example Wiegel (1976) and Dean and Dalrymple (1984).

Diffraction diagrams and diffraction Tables for incident waves normal to the breakwater and as a function of the incident wave angle have been originally published by Penny and Price (1952) and Wiegel (1962). These diagrams depict wave fronts and contours of equal diffraction coefficients for a semi-infinite, rigid, impervious breakwater and are rendered dimensionless in terms of wavelengths. Further theories about the diffraction of waves by a single breakwater gap have been developed by Penny and Price (1952), for a relatively large gap (larger than L), and by Johnson (1952) for a smaller gap. Figure 2.9 shows the diffraction diagrams by Johnson (1952) for breakwater gaps ranging from 1L to 5L.

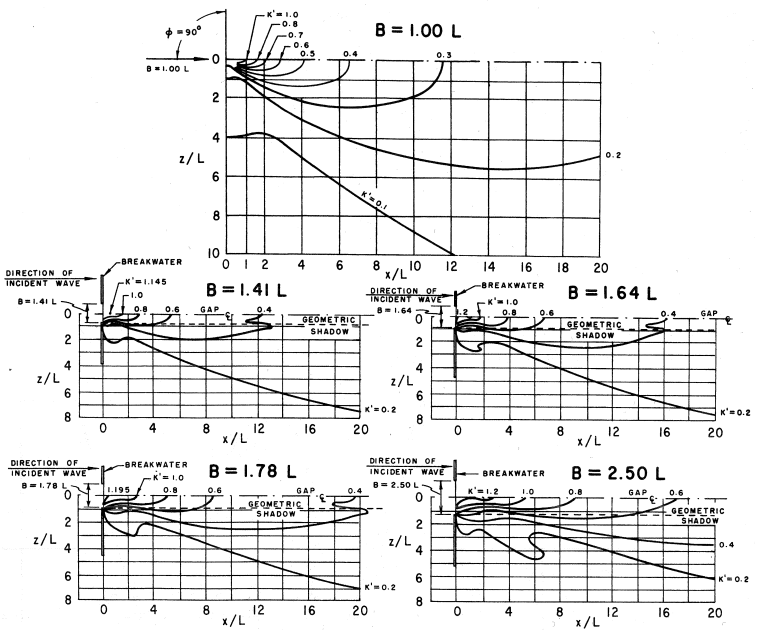

Figure 2.9: Contours of equal diffraction coefficient for wave diffraction at breakwater gap, after Johnson (1952).

Accordingly it is seen by both equation 2.8 and Figure 2.9 that wave diffraction depends on the dimensionless ratio of the horizontal distance to the wavelength. Therefore, correct reproduction of wave diffraction in a Froude scaled physical model requires the wavelength to have the same scale as the horizontal dimension, a condition once more satisfied only in a geometrically undistorted model.

2.3.5 Wave breaking

Wave breaking is the most complex process met in surface waves and is an essential consideration in most coastal engineering design studies. Upon breaking the wave shape changes rapidly, the upper part of the wave crest interacts with the underlying water surface, air is entrapped and entrained, and part of the gravity wave's energy is converted to turbulence, see for example Dean and Stokes (2002). After the initial breaking event in the field, the wave front is usually white and foamy and often covered with spray and bubbles (Fig. 2.10).

Svendsen et al. (1978) used the term 'inner region' to describe the region where the breaking induced turbulence becomes fully developed and the broken wave adopts a

Figure 2.10: Pictures of plunging breakers in shallow waters, after www.3plains.com.

steady, well organised profile which is in most cases covered with white water. Nevertheless, visual difference between breaking waves are only apparent during the breaking phase, when the wave crest overturns. Based on the different visual characteristics, Galvin (1968) classified breaker type into (Fig. 2.11):

- Spilling breakers. These breakers usually occur on a flat or gently sloping beach and are characterised by the presence of white water which spread down on the front face of the crest.
- Plunging breakers. In plunging breakers the wave crest forms a clearly pronounced jet which overturns and impacts on the front face of the wave. Air is initially entrapped between the jet and the water surface and is entrained as bubbles, white water (splash-up motions) and even spray (shooting bubbles). This breaker type is most common on moderately steep beaches.
- Surging breakers. In the case of surging breakers the large steepness of the beach cause the approaching waves to build up a crest but before a jet is formed (as in plungin breakers) the wave surges forward up to the water line.
- Collapsing breakers. Collapsing breakers are a category located between plunging and surging breakers.

Several authors like Irribarren and Nogales (1949), Galvin (1968), Yoo (1986) and Bauer and Greenwood (1988) attempted to relate breaker type to the beach slope and wave properties. Nevertheless, the most well known and vastly used breaker type

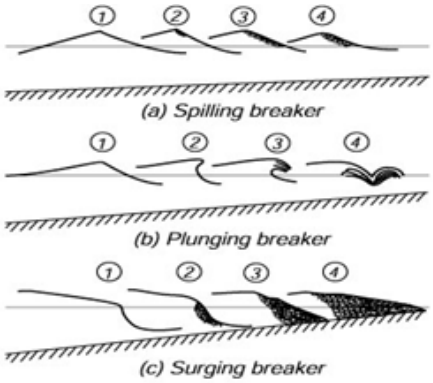

Figure 2.11: Schematic representation of the evolution of a spilling, plunging and surging breaker, after Horikawa (1988).

Breaker type	Galvin (1968)	Yoo (1986)	Battjes (1974)
Spilling	$I' < 0.6$	$\beta < 0.2$	$\xi < 0.45$
Plunging	$0.6 \leq I' \leq 2.0$	$0.2 \leq \beta \leq 2.1$	$0.45 \leq \xi \leq 3.2$
Surging	$I' > 2.0$	$\beta > 2.1$	$\xi > 3.2$

Table 2.3: Occurrence limits and / or surf similarity values for spilling, plunging and surging breakers.

criterion was proposed by Battjes (1974) and is commonly referred to as the surf similarity parameter:

$$\xi = \frac{m}{\sqrt{\frac{H_o}{L_o}}} \tag{2.10}$$

where,

m : is the slope of the beach,

H_o: is the deep water wave height,

L_o: is the deep water wavelength

Table 2.3 summarises the occurrence limits, given by different authors, for spilling, plunging, and surging breakers, whilst Figure 2.11 presents a schematic of the evolution stages of each breaker type.

Further to the surf similarity parameters a large number of authors such as Miche (1944), LeMehaute et al. (1968), Williams (1981) and Nairn (1988) worked, experimentally, on the calculation and verification of a measure of the breaker point or in other words a breaker height criterion. The breaker height criterion is defined as the

ratio of the wave height to wavelength or water depth for waves travelling in deep and shallow water respectively:

$$\gamma_s = \left(\frac{H}{d}\right)_{b,shal} \tag{2.11}$$

$$\gamma_d = \left(\frac{H}{L}\right)_{b,deep} \tag{2.12}$$

where the subscript b denotes conditions at the onset of breaking.

For all the above it is clearly seen that the observation of the physical processes involved in breaking waves and the subsequent kinematic description are mainly based on experience and data obtained from laboratory experiments. The up-scaling of such results to prototype conditions is usually carried out using the Froude similarity and therefore the effect of viscosity and surface tension are neglected. Although the influence of the former is in general not significant, the latter can dramatically affect the breaking event for waves shorter than 2m. For this reason the following review of the literature focuses on the effects of surface tension on the shape and evolution of breaking waves, air entrainment and bubble formation, and on the turbulent free surface flow.

2.3.5.1 Scale effects on wave breaking

It was earlier shown that the influence of surface tension increases as the local radius of the free surface decreases. On the other hand Stokes (1880) was the first one to indicate that deep water regular waves break when the crest becomes sharp and forms an angle of $120^o$with the water surface. The necessary criteria for the initiation of breaking have been further investigated by many researchers like Longuet-Higgins and Cokelet (1978), Bonmarin (1989) and Banner and Peregrine (1993), and all concluded that for both regular and irregular waves the crest radius rapidly decreases prior to breaking. As a result the shape and evolution of the crest during breaking is more sensitive to surface tension effects.

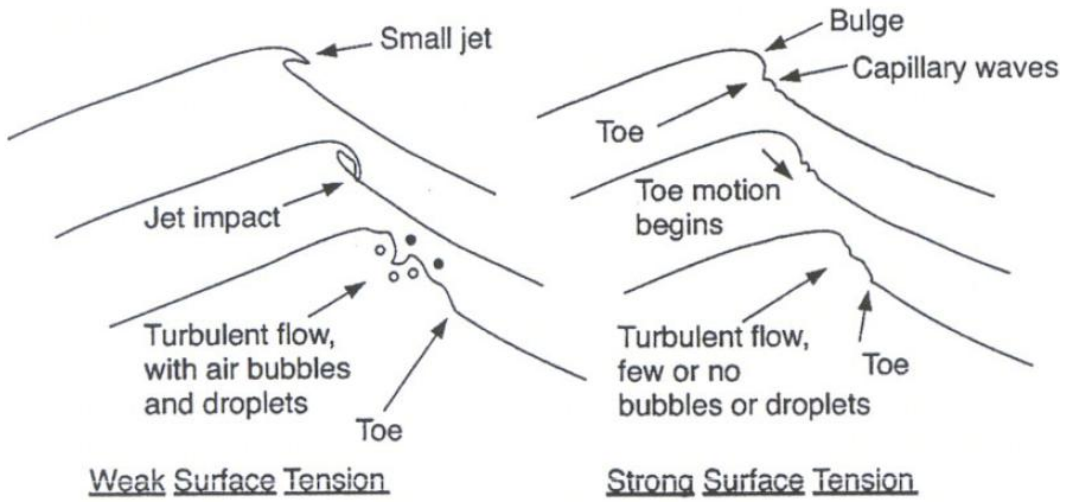

Figure 2.12: Evolution of a spilling breaker under the weak (left) and strong influence (right) of surface tension, after Duncan (2001).

Nevertheless, maintaining Froude similarity in laboratory breaking waves is impossible since water is used as the modelling fluid and as such the surface tension forces are not similar between the prototype and the physical model. Wave focusing techniques (e.g. Rapp and Melville (1990)), constructive interference techniques (e.g. Duncan et al. (1994a)) and wave shoaling (e.g. Blenkinsopp (2007)) are the main methods used to induce breaking in models of deep and shallow water waves. However the generation of any breaker type based on steepness and slope criteria is consistent with Froude scaling law and hence it ignores surface tension effects and clearly entails the possibility of scale dependent results.

Duncan (2001), in his excellent review about spilling breakers summirises the experimental work of Duncan et al. (1994a), Duncan et al. (1994b), and Duncan et al. (1999) and focuses on the effects of surface tension on weak spilling breakers. Figure 2.12 presents the evolution of a spilling breaker for a weak and strong surface tension effect. In the former case (on the left), the spilling process starts with the development of a small jet or sometimes a rough surface (not shown here, see Liu and Duncan (2003) Figure 3). The jet then curls forward from the crest and impacts with the wave face at a point very near the upper part of the crest. The impact induces turbulence, air and bubbles are entrained, and subsequent splash-up motion is triggered.

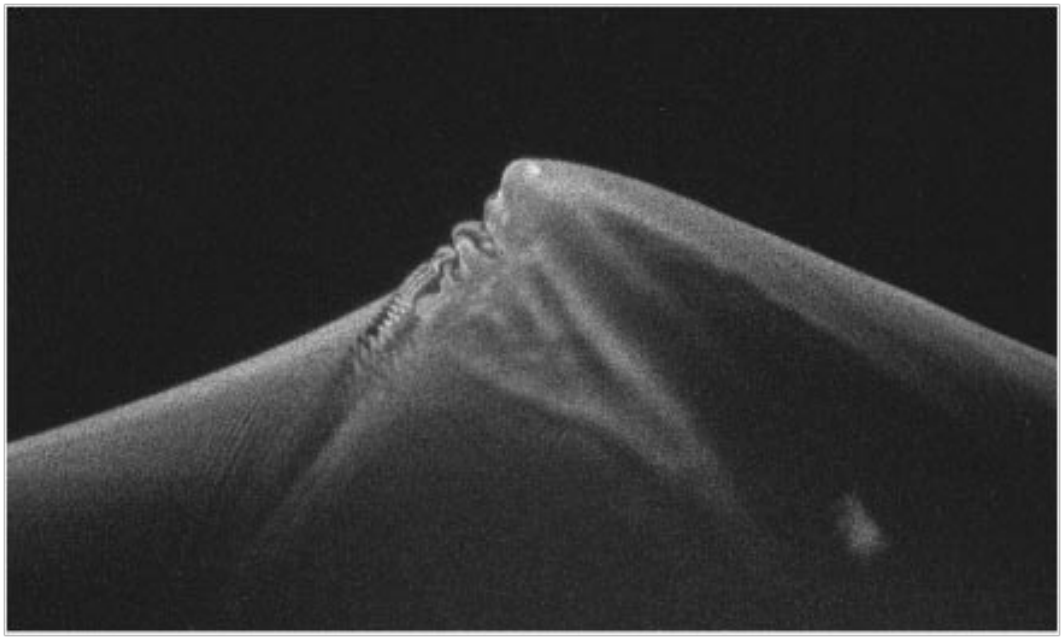

Figure 2.13: Frameshot of a small scale spilling breaker strongly influenced by surface tension. At this time instant the toe has moved and ripples are seen to develop between the toe and the crest, after Duncan et al. (1999).

On the contrary, when the process is affected by surface tension (Fig. 2.12right) the jet is replaced by a bulge form and capillary waves (waves of very small length and amplitude, see e.g. Perlin and Schultz (2000) appear upstream of the toe. As breaking evolves the bulge increases in amplitude, the toe begins to move down the wave face and ripples appear between the toe and the wave crest (Fig. 2.13). Soon after the toe movement these ripples grow rapidly and break down resulting in the appearance of vorticity downstream of the toe; as Figure 2.12 shows, the vortical region progressively extends towards the crest but no bubbles or droplets are formed. Moreover, Dimas (2007) used a new numerical approach called large wave simulation and reported that the vorticity field on the surface layer is disrupted by a vortex formed in the spilling region. The peak strength of the vortex increases with decreasing Weber number (increasing surface tension).

The formation of a spilling breaker by a jet impact for zero surface tension was also numerically verified by Longuet-Higgins and Dommermuth (1997) (Fig. 2.14 left). The authors calculated the bulge location at a horizontal distance of $0.45R_c$ahead of the highest point of the crest, where R_c is the crest radius, which scales disproportional to the wavelength. This yields that the bulge dimensions also scale

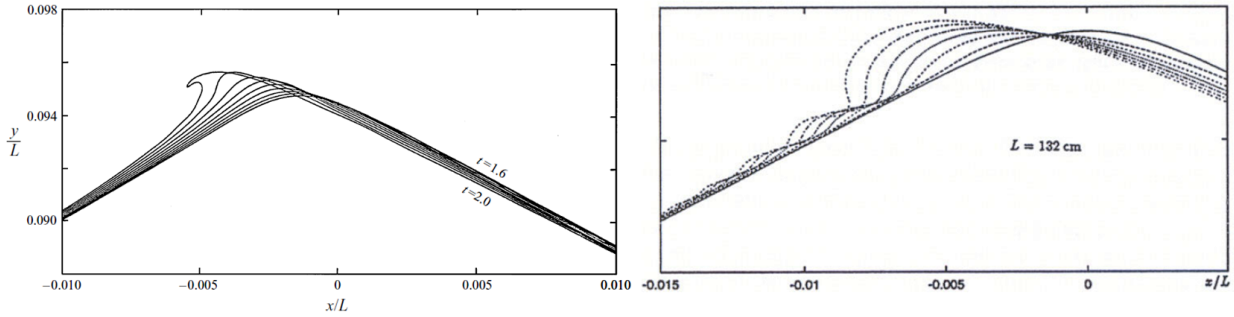

Figure 2.14: The non-linear development of the crest instability without the influence of surface tension (left) after Longuet-Higgins and Dommermuth (1997), and for surface tension equal to that of freshwater, $\sigma = 0.073N/m$, (right), after Longuet-Higgins (1997).

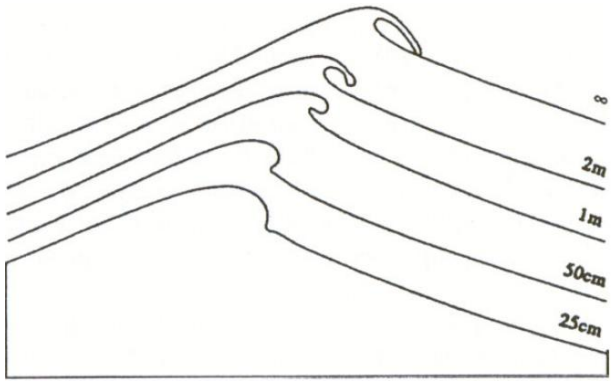

Figure 2.15: Influence of surface tension ($\sigma = 0.073N/m$)on the wave crest evolution during breaking with regards to the wavelength. Numerical calculations after Tulin (1996).

with L and thus a larger bulge structure should be expected in shorter waves.

On the contrary Figure 2.14(right), after Longuet-Higgins (1997), shows the non-linear development of the crest for a surface tension value of $\sigma = 0.073N/m$ (freshwater value). A bulge is seen to form and develop and once more capillary waves appear upstream of the toe. The profiles presented are very similar to those of Duncan et al. (1999) and are differentiated from Longuet-Higgins and Dommermuth (1997) because the effects of surface tension were included in the calculations; for further details on the formation of capillary waves during the numerical breaking process the keen reader is referred to Longuet-Higgins (1996).

Tulin (1996) and Ceniceros and Hou (1999) used boundary element calculations to investigate the effect of surface tension on plunging breakers. Figure 2.15 illustrates the results of Tulin (1996) and indicates that for waves with wavelength smaller than 2m the jet gradually becomes rounded and is finally replaced by a bulge. Ceniceros

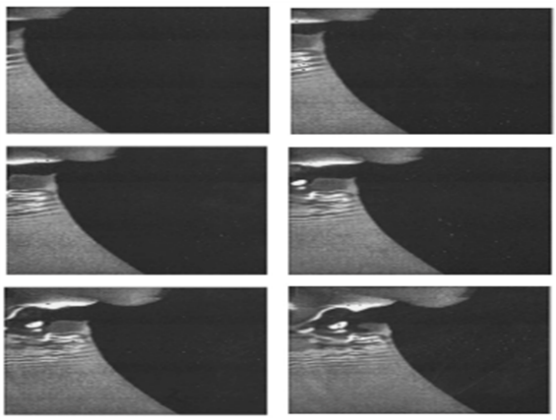

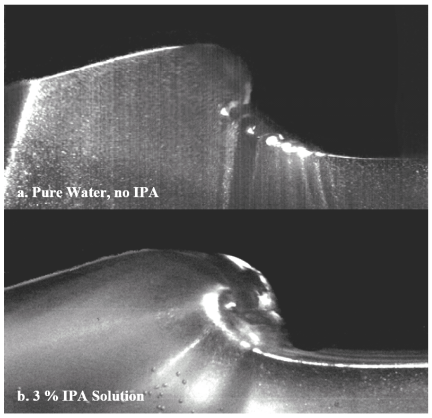

Figure 2.16: On the left, frameshots of parasitic capillary waves on the lower front face of a plunging breaker, after Perlin and He (1996).

Figure 2.17: On the right, wave crest profiles for a plunging breaker in a. pure water and b. 3% IPA solution. Capillary waves are only seen to form on the wave face for the pure water case, after McDonald (2005).

and Hou (1999) calculations showed that at a wavelength of 0.77m the jet still forms but a bulge and capillary waves also appear. This is in accordance with Perlin and He (1996) who observed the formation of capillary waves on the front face of plunging waves L = 0.8m (Fig. 2.16). Further support is also provided by McDonald (2005), who studied experimental, small scale plunging breakers (L $<$ 0.7m) in a surface tension reduced solution of 10% isopropyl-alcohol and distilled water ($\sigma = 0.0436 N/m$). The author presented evidence (Fig. McDonald (2005) that such capillary structures do not form on the crest of plunging waves with L = 0.4m and H = 0.0225m.

2.3.5.2 Scale effects on air entrainment

Wave breaking is the main mechanism responsible for atmosphere-sea interaction, wave induced sediment transport and wave-structure interaction. Upon breaking air is entrained in the form of bubbles regardless the breaker type. In plunging breakers for example air is entrapped underneath the projecting jet and above the water surface and the same can also occur between a wave and coastal structures. Depending on the intensity of the impact, the air pocket is compressed and fragments into air bubbles which are then entrained into the water column by the impact induced turbulent flow. The size of the air cavity and the overall process of

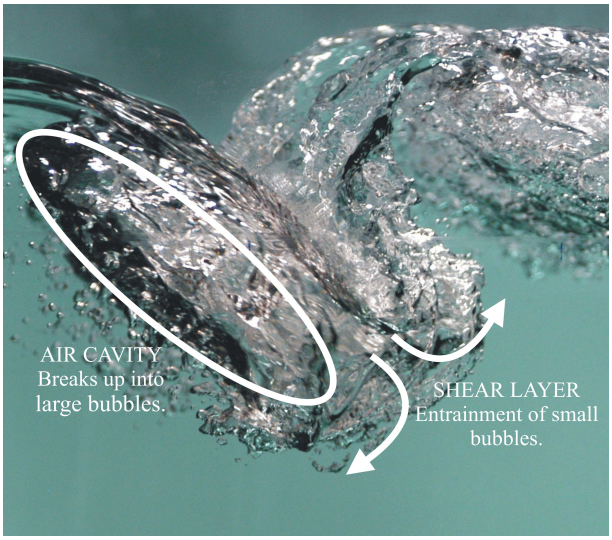

Figure 2.18: Frameshot of a laboratory plunging breaker indicating the primary mechanisms of air entrainment, after Dean and Stokes (2002).

air entrainment during breaking has been associated by many authors like Hwung et al. (1992), Chanson, Aoki and Maruyama (2002), and Blenkinsopp (2007) with the dissipation of energy by breaking waves, and with the amount of pressure acting on vertical walls, Hull and Muller (2002).

Dean and Stokes (2002), measured the bubble size distribution under oceanic and laboratory breaking waves and found important similarities. They observed that air is entrained by two main mechanisms, 1. the fragmentation of the air cavity (pocket of air formed between the projected jet and the wave face) leads to the generation of bubbles with a radius larger than 1mm, and 2. smaller bubbles are created in the shear layer developed by the impact of the jet onto the water surface and the subsequent splash-up motions (Fig. 2.18). The areas of application of each mechanism with regards to the bubble size spectrum are separated by the Hinze scale, which sets the limit above which bubbles are fragmented by turbulent and shear flow and below which the bubbles are stabilised by surface tension.

The separation point was found to be similar between the model and prototype waves, since for both cases it occurred as a change in the spectral slope of the bubble size distribution at a bubble radius of 1mm (Fig. 4 and 6 in Dean and Stokes (2002)). The comparison of the spectral slopes observed in the bubble plumes formed soon after the end of the active phase of air entrainment revealed a similar

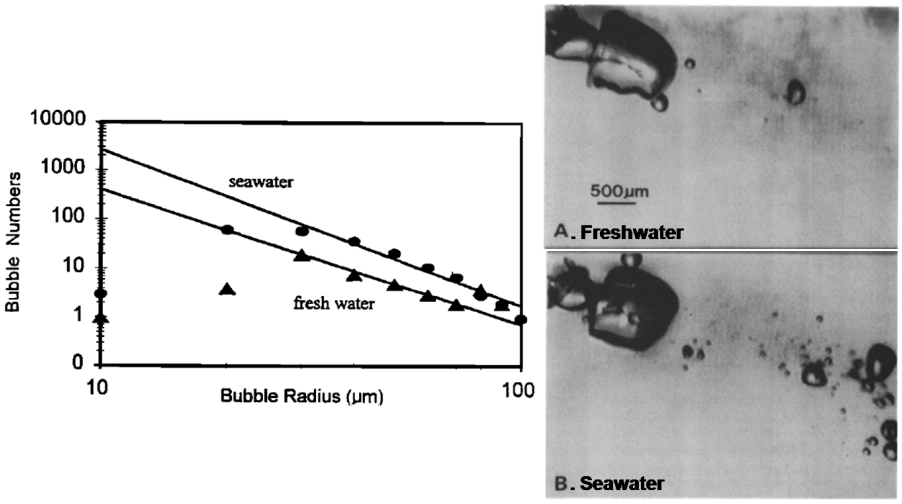

Figure 2.19: On the left, plot of the bubble distribution in seawater and freshwater, and on the right frameshots of bubble size in fresh (above) and seawater (below), after Slauenwhite and Johnson (1999).

distribution of bubble sizes within oceanic and laboratory waves. Dean and Stokes (2002) put this forward as evidence that the same formation mechanisms are operating in both environments and therefore the bubble size distribution after the initial breaking phase should not be scale-dependent. Thus it is seen that although the shape and size of the breaker can be altered with scale (see 2.3.5.1) and result in smaller amounts of entrained air, the bubble sizes encountered in laboratory and oceanic breaking waves should be at least similar regardless the model size-scale.

This however, creates a paradox when compared with authors like Wood (1991), Chanson (1997) and Chanson, Aoki and Maruyama (2002), who concluded that surface tension and viscosity can significantly affect not only the entrapment of air but also the subsequent break-up and coalescence of air bubbles and the turbulent processes in the shear region (also discussed in 2.3.5.1). Since scale effects can result from both the selection of model size (scale) and fluid type, researchers have focused not only on the differences between small and large scale but also on the differences between seawater and freshwater. Indeed Slauenwhite and Johnson (1999) compared bubble formation mechanisms in seawater and freshwater and reported that the amount of bubbles entrained in seawater was 4-5 times larger, whilst bubble sizes were in general smaller (Fig. 2.19); similar results were also reported by Haines and Johnson (1995).

On the contrary Chanson (2009) reviewed all his experimental work about air entrainment in seawater, artificial seawater and freshwater and suggested that less air is entrained in saline waters. The author also measured a smaller amount of air in natural seawater than artificial seawater and speculated that this was due to the presence of biological and / or chemical surfactants, which harden the induction trumpet at the point of impact and diminish air entrapment. Earlier, Gonzalez and Chanson (2004) compared air entrainment between physical models of stepped spillways with different scales and Reynolds numbers (Re) up to $5*10^5$, and reported the entrainment of less but larger bubbles in small scales, along with lower turbulent levels and larger turbulent length and time scales for the lowest Re. Based on all that Chanson (2009) concluded for Froude based physical models, bubble sizes, interfacial areas and turbulent levels cannot be properly scaled to prototype conditions, even for large size models with Re = $5*10^5$.

Things are further complicated by Blenkinsopp (2007) who recorded laboratory plunging breakers in seawater, artificial seawater and freshwater. He suggested that the process of air entrainment, the bubble distribution and the temporal and spatial evolution of the bubble plume do not differ significantly for all three cases despite the fact that a population of very fine bubbles (with diameter smaller than 0.3mm) was observed only for the seawater. Blenkinsopp (2007) also presented measurements of the total volume of entrained air, the cross-sectional area and the mean void fraction (Fig. 2.20), which were very similar between the three fluids.

Blenkinsopp and Chaplin (2007) discussed the effects of Froude scaling on bubble plume evolution. They argue that the bubble plume evolution scales well with the bubble rise time H_b / u_r (where, H_b the wave height at breaking and u_r the bubble rise velocity, also in Fig. 2.20) and thus the plume evolution should follow the length scale and not its square root, as suggested by the Froude law. For this reason Blenkinsopp (2007) developed a Lagrangian finite difference model capable to trace individual bubbles and include all the effect associated with bubble burst and coalescence. The numerical model was used to compare the plume evolution between the field and a physical model with scale 1:20. Indeed at model scale the bubble plume was found to almost fully disperse within a wave period, while for field

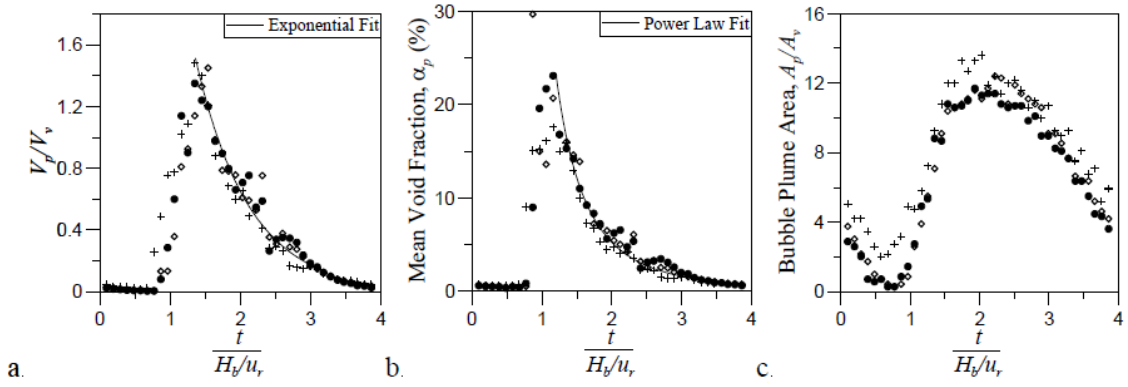

Figure 2.20: Temporal variation of a. the volume of entrained air per unit width, b. mean void fraction in the bubble plume and c. the cross-sectional area of the bubble plume, where + Freshwater, ◊ Artificial seawater, ● Natural seawater, after Blenkinsopp and Chaplin (2007).

conditions a significant amount of air remained trapped in the water column and accumulated over repeated breaking events. The importance of scale in aeration was also highlighted by Bullock et al. (2001) who compared foam production in seawater laboratory tests of wave impacts with field observations and concluded that full scale waves are characterised by higher aeration.

In summary a noticeable controversy exists between published studies about the overall number and the size distribution of bubbles entrained in fresh and seawater experiments; for more details see Table 2.2 in Blenkinsopp (2007). Blenkinsopp (2007) holds responsible for these differences, the range of validity (min. and max. bubble diameter) of the employed measuring techniques, the measuring location, the salinity and composition of the fresh / seawater and the breaker type. Some support for this is provided by Chanson and Toombes (2002) and Carosi and Chanson (2006) who conducted laboratory air-water flow measurements and reported that a wider range of bubble sizes and a larger bubble count rate were recorded by smaller sensor probes.

Nevertheless, a consensus is observed that the effects of the model scale are more important than the effects of the water type. Chanson (2009) for example suggests that smaller models of hydraulic jumps are likely to underestimate the rate of energy dissipation, while if plunging breakers are considered smaller scales may result in

smaller accumulation of air in the water column, Blenkinsopp and Chaplin (2007). Bullock et al. (2001) investigated the roll of air content on impulsive wave loadings by artificially aerating freshwater and seawater and concluded that maximum pressure is reduced and the rise time increases when the water is aerated. Thus even when seawater is used, all processes associated with breaking waves (i.e. aeration) are subject to scale effects the influence of which increases for smaller scales.

2.4 Summary of the literature review

The review of the existed literature has identified few areas where very small scale physical models have been used in the past. The effective management of large rivers, mainly through the use of training structures, is of vital importance due to its large economical and sociological impacts. However, assessing the effects of such structures on sediment transport and flow velocities is a highly complex problem that encompass many challenges including two (water-sediment) and sometimes three (air-water-sediment) phase structures, and as such a numerical approach is neither easy nor accurate. On the other hand the use of large scale experimental facilities is limited by the high maintenance and running expenses, which increase unbearably if more than one design options have to be considered.

Based on that the SLD-USACE developed river micro-models or else hydraulic models of rivers with scales as small as 1:20,000. In contraposition with numerical models, micro-models included explicitly all or at least most of the physical process occurring in the prototype, and in the same time offered a cost-effective and flexible alternative to large physical models. Nevertheless due to the very small scales involved and the large horizontal to vertical distortion required, micro-models flouted similarity laws and were thus subjected to strong scale effects. Therefore, their use was restricted to investigations where the overall project and human lives were not at risk.

In the same time, small scale physical models have seldom been used to assess the effects of tidal flows on sedimentation within harbours, and to the author's knowledge, never for wave related studies. The current thesis proposes the use of wave micro-models for coastal engineering applications. and therefore references were made to the existed literature regarding scale effects in physical models of wave processes. The critical review of the current literature yields that for water depths larger than 2cm the propagation of waves with periods larger then 0.35sec is not affected by surface tension and viscosity and if the model is undistorted, wave refraction, shoaling and diffraction are also modelled accurately. Accordingly the micro-modelling of wave fields at scales smaller than 1:50 and within Table-top basins is a feasible proposition. However, the selection of very small scale introduces significant errors to wave breaking and air entrainment processes; a new fluid with smaller surface tension than freshwater may compensate for these disadvantages.

The work presented in the remainder of the current thesis investigates several aspects of the micro-modelling of wave fields. A novel mapping method of the water surface is described (Chapter 3) and the effects of small scale on wave propagation, diffraction (Chapter 4) and wave breaking (Chapter 5) are explored. Finally wave micro-models are constructed and used to assess the effectiveness of culverts as flushing elements for marinas, develop a novel wave energy converter (Chapter 6) and to investigate alternative design options for an existed harbour (Chapter 7). Data, modelling options and ideas presented here can be used by future researchers in the field of hydraulic engineering.

Chapter 3

Wave field mapping with Particle Image Velocimetry (PIV)

3.1 Introduction

Conventional measurement techniques for waves in hydraulic laboratories employ point measurements with either resistance or capacitance type wave probes. These however do only allow for point measurements, so that the information on the two-dimensional aspects wave propagation and wave fields is usually incomplete. Worse, wave probes may not be located at the critical points or may be situated so as to measure additional local effects such as standing waves.

A number of wave techniques for the measurement of the 3D-topography of wave fields have been developed in order to overcome this situation. In the following, only some typical approaches are described, a more complete overview is given in Stagonas (2005). Barrillon developed the 'starry sky' technique described e.g. in Valembois (1951). Downwards pointing lamps are installed in a grid above a wave basin (Fig. 3.1). A camera is located above the centre of the basin. The camera's shutter is opened for a time exceeding one wave period, so that the reflection of the point lamps leaves a set of lines / ovals pointing in the direction of wave propagation, whereby the length of the line / oval is related to the steepness of the wave H / L. This technique was employed until the seventies, but fell into disuse since it required

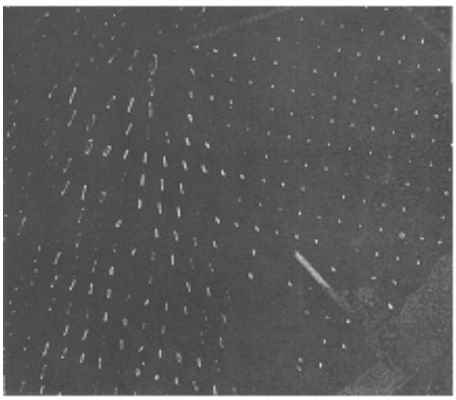

Figure 3.1: Application of the starry sky method for the visualisation of the wave field around a model of the port of Quiberon, France, after Valembois (1951).

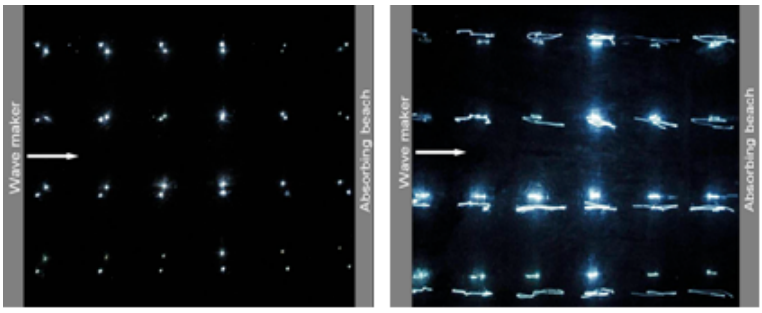

Figure 3.2: Starry sky results for a. still water conditions (left) and b. for regular propagating waves (right). Watson (2007).

a wave basin in a darkened room, cannot give any further information without additional measurements and – possibly most importantly – could not be used with random seas since the exposure time had to be equal to the wave period. Recent investigations in the University of Southampton yield similar results (Fig. 3.2).

A number of researchers employed line techniques either with a single line / set of lines at the tank bottom, e.g. Craeye et al. (1999). Lines at the tank bottom are optically shifted by the diffraction of the light; the amount of shift depends on the angle of view and the submerged depth – i.e. the wave height. Line patterns were also projected onto the water surface, employing either a projection Moire technique for analysis of a single crest, see Grant et al. (1990), or using image analysis software and photogrammetry and grey scale pattern identification to determine the surface elevation along the grid lines, Elshof et al. (2001). These techniques however are subjected to non-linear laws, perspective distortions, and require carefully controlled light conditions and suffer from the difficulty of projecting images onto the water

surface.

Curtis et al. (2002) took a different approach and employed the analysis of reflected light from the distorted water surface; here the grey scale of the image's pixels are related to the surface slope. Although this technique is practicable, again carefully controlled lighting and calibration measurements are required. A similar optical, spatial measuring technique was developed by Tzivanaki (2007), but according to Masterton and Swan (2008) it is extremely complicated to both setup and interpret, and it could not be expected to yield accurate results for small wave amplitudes, a $<$ 0.05 m.

The review of the currently available techniques, and reported experiments on wave mapping, indicates that there is a significant interest in this field without available techniques being adequate for employment in a standard hydraulic laboratory situation, Stagonas (2005).

3.2 Particle Image Velocimetry (PIV)

PIV is by now a standard optical measurement technique for the instantaneous mapping of flow fields. The flow is seeded with tracer particles which are then illuminated and their positions recorded photographically, or by video, at two successive instants. The photographic or video "flow record" of the whole 2D field is then divided into a grid of cells and, in each cell, the distance moved by the tracer particles from the time of the first image being recorded to the second is determined; this is known as the cross-correlation method, e.g. Gray and Bruce (1995). Knowing the distance travelled and the time taken, the velocity of the flow in that cell is therefore measured. This is done for every interrogation area, giving a 2D map of the "instantaneous" velocity field at the time of the recording. Implicit in the method are two basic assumptions:

- the flow field as a whole does not change over the time between first and second exposures,

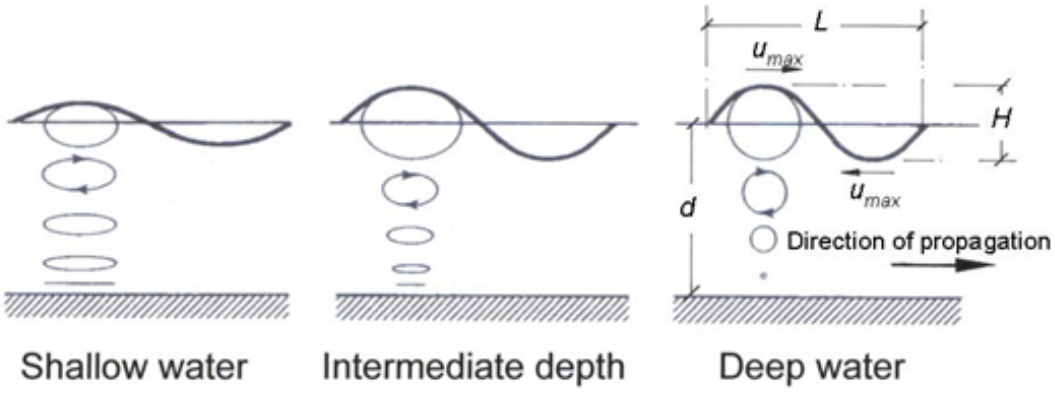

Figure 3.3: Particel motion in water waves.

- the velocity in each cell is uniform

In any real flow of interest, neither assumption will hold fully and the extent to which they hold is always an important consideration. In hydraulic engineering this technique has been applied for surface velocity measurements of water and ice flow in very uniform flow fields in river models with simple geometries, Ettema et al. (1997), Fujita et al. (1998), and in more complex flows, Müller et al. (2002). These applications showed that PIV is a powerful tool for the mapping of surface flow velocities.

3.3 Particle motion in water waves

In linear wave theory for deep water, the particle motion in water waves is circular with the largest radius at the water surface. For shallow water, the particle motion becomes elliptical, Figure 3.3.

The maximum horizontal particle velocities (u_{max}) occur at the surface and are a function of the wave height H, the wave length L, the wave period T and the still water depth d:

$$k = \frac{2\pi}{L} \tag{3.1}$$

$$L = \frac{gT^2}{2\pi} tanh(kd) \tag{3.2}$$

$$u_{max} = \frac{\pi H}{T} \frac{cosh\left[k(d+\frac{H}{2})\right]}{sin(kd)} sin(\omega t - kx) \tag{3.3}$$

The maximum horizontal velocity vector points in the direction of wave propagation at the wave crest, and against this direction in the wave trough.

3.4 Wave mapping with surface flow velocities

The relationship between maximum horizontal particle velocity and wave height and length suggests that u_{max} could be employed to map wave fields, using PIV surface measurements of horizontal particle velocities in waves –an approach which to the author's knowledge has not been described before. In order to assess this possibility, a series of experiments were conducted at Southampton University with the aim to develop surface flow mapping as a simple and robust tool to map wave fields.

3.4.1 Experimental set-up

A small scale Perspex wave basin with a length of 1.80m, a width of 0.8m and a depth of 0.15m was built (Fig. 3.4). On one side, a wave paddle – driven by an electric motor and therefore only able to produce sinusoidal waves – was installed. At the other end, a 1:3 slope of gravel (d50 $\approx$ 5 mm) was built as wave absorber. Wave heights were measured with two resistance type wave probes; cross checks with photographs through the transparent side walls gave good correlation with the wave probe measurements.

The water depth was kept constant at 90mm for all tests. Expanded polystyrene beads of 0.3 mm diameter were used as floating particles. At a height of 1.5 m above the wave basin, a Sony CyberShot DSC-P200 digital camera with video option (25 fps, 640 $\times$ 480 pixel) was installed. Surface flow velocities were determined with the Optical Flow Systems VidPIV 2.15 software with 16 $\times$16 and – for the long waves, 32 $\times$ 32 pixel interrogation cells.

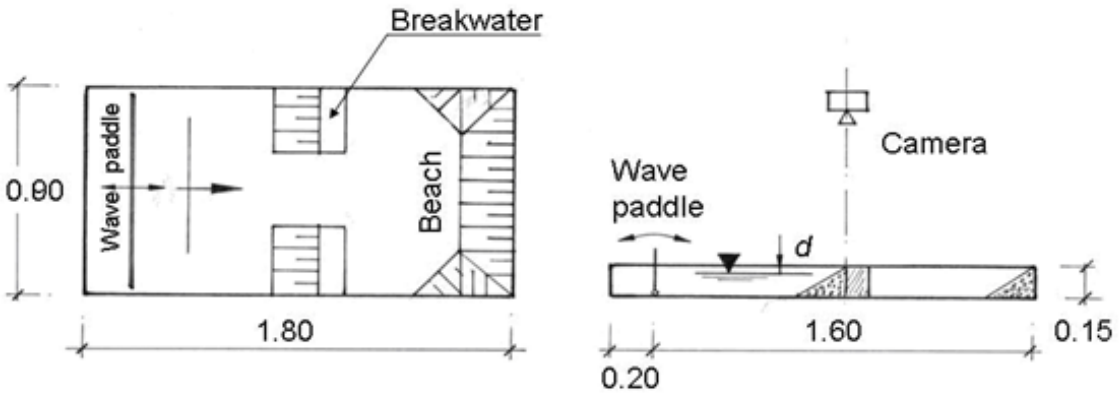

Figure 3.4: Experimental set up with (optional) breakwater model.

H / L	H(m)	T(s)	L_{cal}(m)	u_{max}(m/s)	d / L
0.0101	0.006	0.72	0.597	0.02	0.151
0.0197	0.01	0.57	0.507	0.06	0.178
0.0681	0.017	0.4	0.25	0.16	0.361

Table 3.1: Results from wave probe measurements (H, T) and calculated values for L, u_{max}.

A first series of initial tests was conducted with regular waves and a wave absorbing beach. In a second series, a harbour entrance was modelled in order to assess the wave field around an obstacle. Implicit in the experiment is the assumption that the particles on the surface move with the velocity of the water particles they are attached to. This appears reasonable since the polystyrene particles are small compared with the wave length, and since they are significantly lighter than water.

3.4.2 Experimental results

Initially a series of tests was conducted without the breakwater in order to validate the proposed technique. Wave heights were measured with wave probes, photographs were taken through the transparent side walls and the seeded water surface was videoed. Three different wave steepnesses of 0.0101, 0.0197 and 0.0681 were employed for the verification tests as shown in Table 3.1. From linear wave theory (above equations) the maximum horizontal particle velocities and the wave lengths were determined. Figure 3.5 shows a typical vector map.

In Table 3.2, the results from PIV measurements of u_{max} and L are given as well as the calculated values for T and H. Wave heights and periods are compared with wave

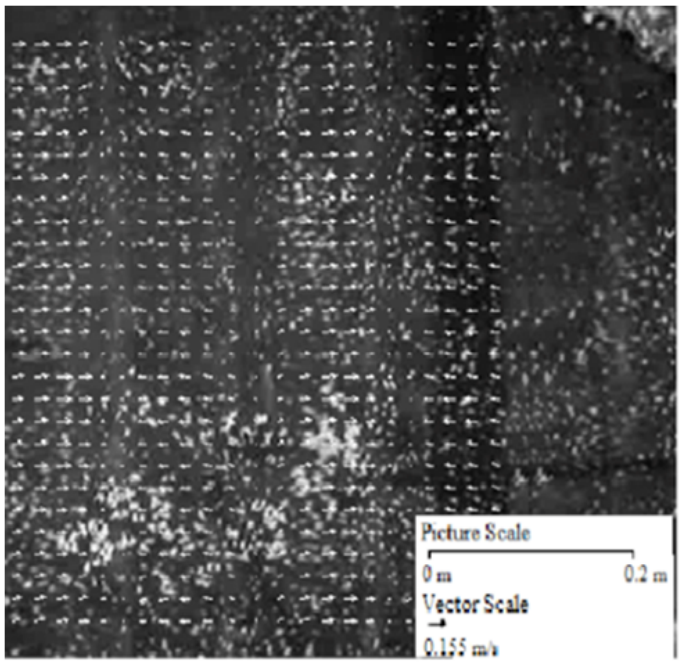

Figure 3.5: Validation tests without breakwater, Lo= 0.24m.

H / L	L(m)	u_{max} (m/s)	T_{cal}(sec)	H_{cal} (m)	d / L	Error % H	Error % T	Measuring method
0.0094	0.587	0.033	0.71	0.0055	0.153	8.3	1.39	PIV
0.0217	0.507	0.066	0.57	0.011	0.178	10	0.02	PIV
0.0625	0.24	0.14	0.396	0.015	0.391	11.3	1.01	PIV
0.0101	0.597	0.02	0.72	0.006	0.151			WP
0.0197	0.507	0.06	0.57	0.01	0.178			WP
0.0681	0.25	0.16	0.4	0.017	0.361			WP

Table 3.2: Combined results from PIV and wave probe (WP) measurements and error percentages for differences on H and T.

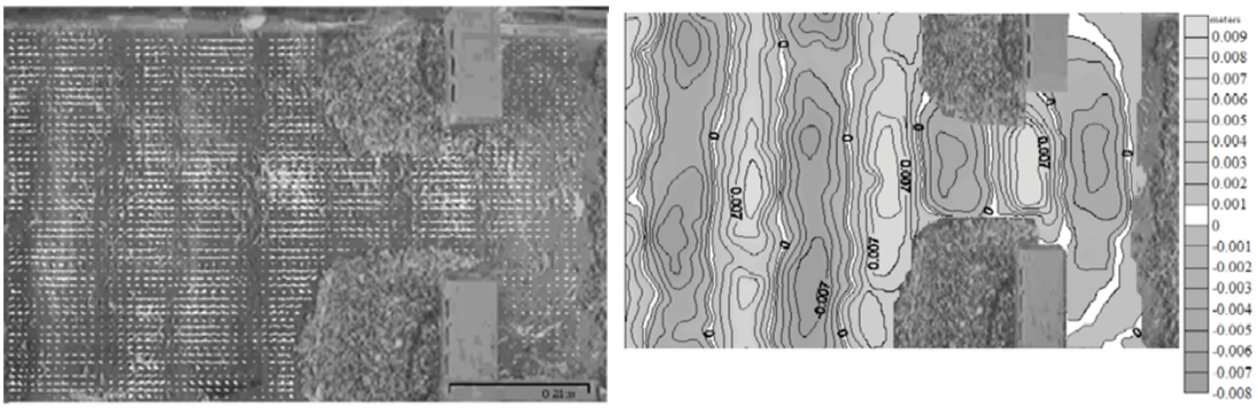

Figure 3.6: Surface flow velocities with the breakwater; a. surface velocity vectors (left) and b. surface contour map (right).

probes results and errors were found to range from 8.3 to 11.3% for H, and 0.02 to 1.30% for T.

Figure 3.6a and b shows the surface velocities and the surface contours for a wave of 0.24 m length and 0.0145 m height traveling into a harbour entrance. The diffraction of the wave is clearly visible; the low resolution of the camera did however not allow for a more accurate mapping of the distorted surface.

An interesting aspect of surface flow velocity mapping is the identification of additional wave induced features, which would probably escape the attention of the modeller working with wave probes only. Figure 3.7 shows a detail of the harbour entrance; here the diffraction around the corner of the 'breakwater' can be seen, whilst vectors directed perpendicular to the wave direction (from left to right) are possibly an artefact generated in processing the PIV data.

3.4.3 Accuracy of wave heights

The main causes of error of the described technique are:

- the underlying assumption of PIV is that velocities in one interrogation area are constant. In combination with the comparatively low pixel resolution of the camera (600 pixels for 1000 mm, with 16 × 16 pixel interrogation areas) this introduced a maximum error of 5.6 % for the 0.24 m wave length, but only

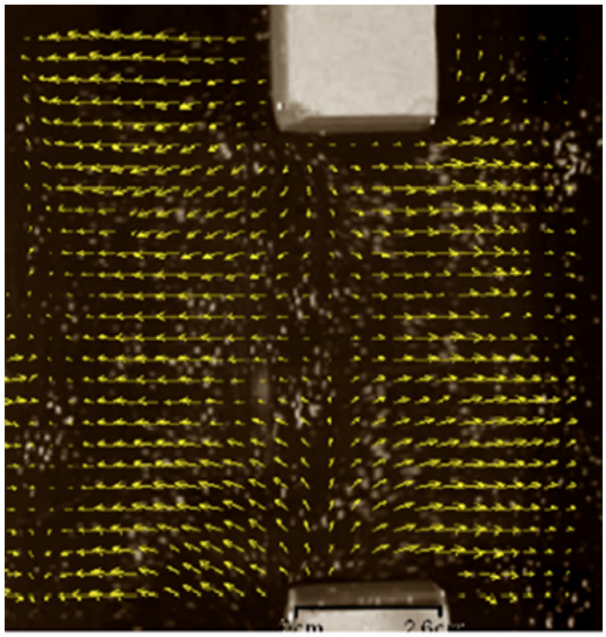

Figure 3.7: Detail of the wave diffraction at the corners of the breakwater.

– theoretically – 3% for the maximum horizontal velocity. The error in the calculation of the wave period is reduced by the fact that T is a function of the square root of L,

- the low resolution of the camera meant that one pixel covered a comparatively large area of 1.76 mm^2. This imposes an upper limit on the accuracy of the PIV analysis,

- the simplifying assumptions for the linear wave theory probably limit the accuracy of the back-calculation of wave heights for water depth to wave length ratios d / L> 1 / 20

- the method, as employed here, assumes that all wave components are proceeding in the same direction. Accordingly the presence of reflections in the tank might lead to errors in computed wave heights.

3.4.4 Discussion

Most of the techniques for wave surface mapping described in the literature suffer from the requirement for very even lighting conditions, since making the water surface visible on a photographic image is very difficult. In addition,

photogrammetry based methods rely on a carefully calibrated rig with two cameras and can only map small surface areas; again, an uneven light distribution can be expected to have significant effects on the image analysis software. Also, complex and costly equipment and complicated calibration procedures are required. All previously described techniques are therefore very difficult to apply in coastal engineering modelling, where different geometries and contrasts and uncontrolled lighting conditions are omnipresent.

Surface velocity measurements on the other hand can be conducted with standard video equipment. As long as the particles provide sufficient contrast, lighting conditions can vary over the measurement field although point reflections should be avoided. Data processing is straightforward; the velocity vector field itself already gives a qualitative overview over the wave pattern.

Currently, the analysis technique is not as yet sufficiently developed; linear theory appears to give acceptable results for deep and intermediate water depths but will probably lead to increasing errors for decreasing d/L ratios. Moreover, errors in calculated wave heights may occur when wave reflections are present in the tank. The method, as utilised here, assumes a homogenous direction of all wave components and thus it potentially ignores vectors moving towards a different direction. The latter error source can probably be minimised or even eliminated by removing the maximum horizontal velocity assumption and including the local phase information on the wave height calculation; nonetheless further research is required. Mixtures of standing and propagating waves are difficult to separate since in standing waves the maximum horizontal particle velocities occur at the node points rather than at the crests (as in propagating waves); the effect of currents needs to be investigated. However an effort was made to extend the technique for the analysis of random seas, and is presented here.

3.5 Irregular sea measurements

3.5.1 Overview

Real sea states are usually modelled using irregular seas, i.e. a prescribed spectrum of regular seas with components of varying periods, phase and amplitude, e.g. Goda (2000). The PIV mapping technique described previously cannot be directly applied to analyse irregular seas since neither wave length nor amplitude are constant in the spatial domain. It did however appear feasible to interpret a irregular sea locally as a regular wave, so that a wave height can be determined from a local wave length and maximum horizontal particle velocity. In order to test this assumption, initially a theoretical analysis was conducted and subsequently verified with irregular sea experiments.

3.5.2 Theoretical analysis

In theory two approaches exist to treat irregular seas; 1. spectral methods and 2. wave-by-wave analysis. Nonetheless, due to restrictions in space, only the wave-by-wave analysis will be referred to here, and in any case the keen reader is referred to Goda (2000) for more details. Wave train (wave-by-wave) analysis requires a wave record. In such records the manifestation of wave period / length is not one-dimensional, but can be taken as the time interval between any two adjacent zero crossing points. Maybe the most common definitions of wave period are; the time interval between successive crossings of the mean water level by the water surface in a downward direction called zero down-crossing period or zero up-crossing period for the other way round. The zero-crossing wave height is the difference in water surface elevation of the highest crest and lowest trough between successive zero crossings, Figure 3.8.

To conduct the theoretical analysis the sum of three different sinusoidal waves (Table 3.3) was used to generate a irregular sea. Following, the data were shifted from the time into the space domain. This was necessary since a PIV measurement will give the wave train not as a function of time, but of space. Figures 3.9a and b show the components and the wave height sums.

This was necessary since a PIV measurement will give the wave train not as a function of time, but of space. Using linear wave theory, the theoretical wave heights

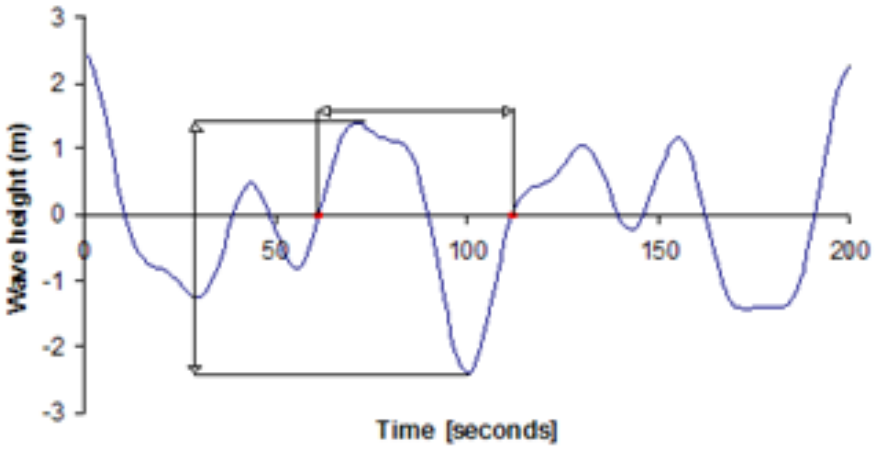

Figure 3.8: Irregular sea time series.

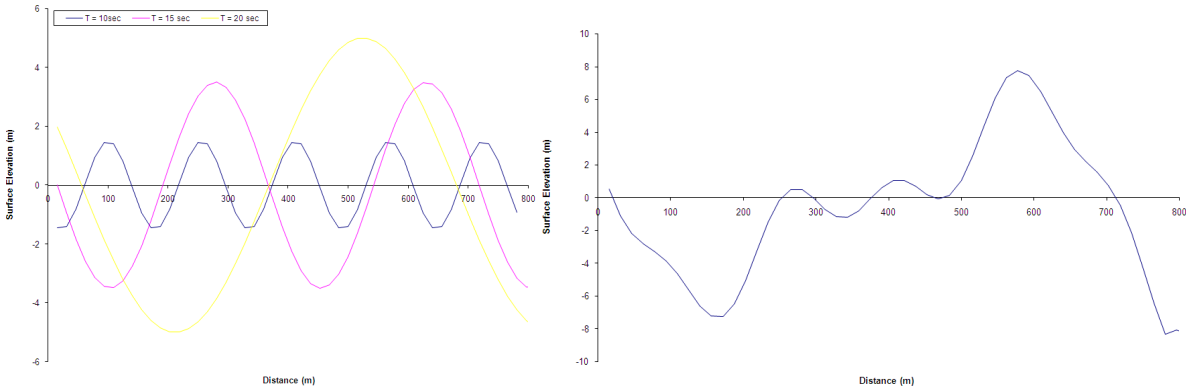

Figure 3.9: Numerically generated irregular seas, a. irregular sea components (left) and b. superimposed wave profiles (right).

Wave	1	2	3
T(sec)	10	15	20
L(m)	156	351	624
H(m)	3	7	10

Table 3.3: Original wave characteristics for the irregular sea components.

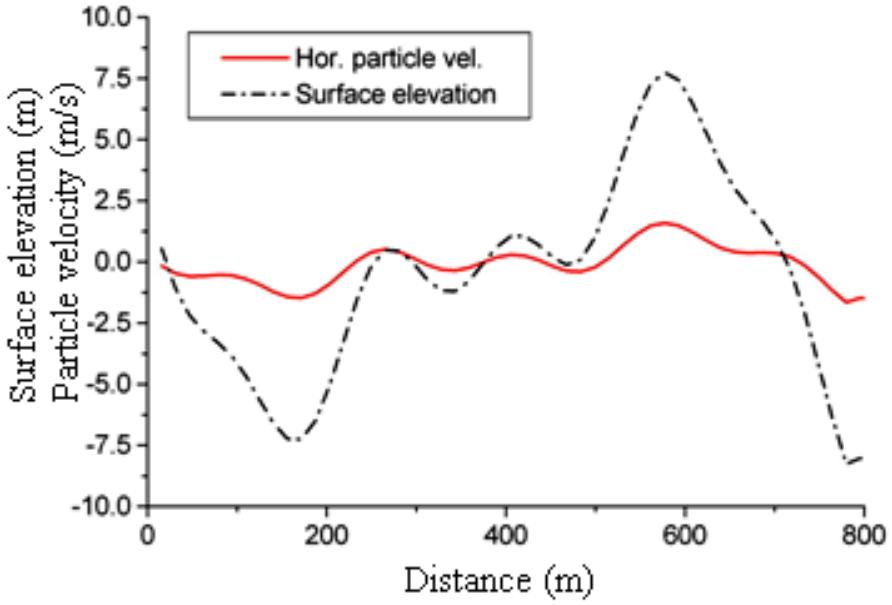

Figure 3.10: Initial surface profile and particle velocities.

can be transformed to particle velocities and plotted over distance. Using the local wave length for each wave crest and trough, wave heights can then be back-calculated from the surface particle velocities using linear wave theory, as described previously.

Figure 3.10 shows the initial wave train and the surface particle velocities; it can be seen that there is a distinct correlation between velocities and wave height, with maximum velocities occurring simultaneously with maximum surface elevation. A check at the points of maximum surface elevation gave good agreement of the back calculated elevations to the initially calculated values for the maximum wave heights; for small wave heights the error increased significantly. PIV therefore has the potential of capturing the wave surface throughout the whole length (and width) of a wave basin at one moment in time (and, if video analysis is employed, as a function of time too).

3.5.3 Experimental results

A series of tests was conducted, and some representative results are presented. Wave heights were recorded using photographs taken through the transparent side walls. The manual motion of the wave paddle assured the generation of irregular waves, but

as a result similar wave conditions were not repeatable. A typical vector map is presented in Figure 3.11. The horizontal velocities calculated (vectors) between two subsequent images were assumed to be the maximum horizontal velocities and used in combination with linear wave theory to estimate wave heights along the whole length of the tank.

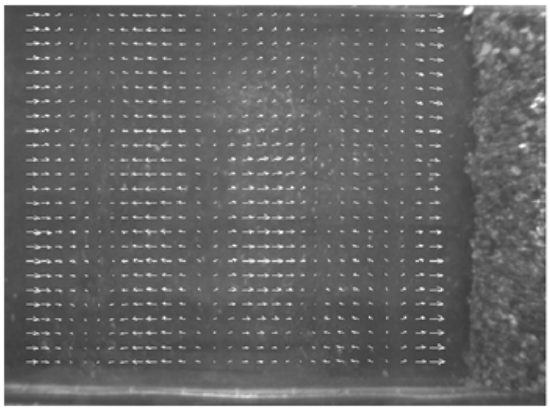

Figure 3.11: Surface velocity field in a irregular sea.

In Figure 3.12, the waves propagate from left to right. Vectors facing in wave direction indicate wave crests, vectors in opposite direction wave troughs, and white dots represent the zero crossing lines. A simple processing of the data can provide a profile of the particle velocities over distance (Fig. 3.12a) which can be easily transformed into a wave height over distance diagram (Fig. 3.12b).

Figure 3.12b can also be compared with the following photograph which represents the side view of the tank through the transparent wall, with the calculated wave

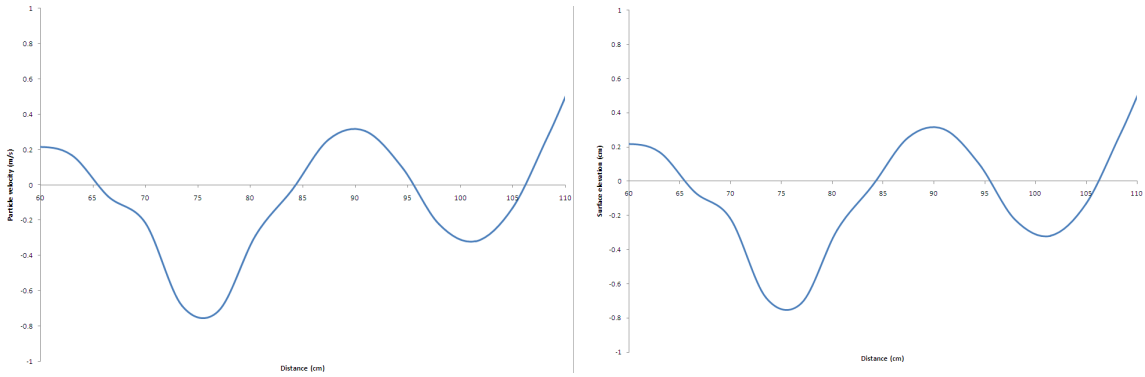

Figure 3.12: Experimental results and inferred water surface elevation, a. horizontal particle velocities (left) and b. water surface elevation (right).

Figure 3.13: Side shot of water surface with added experimental results (blue line).

height projected onto the side wall as a blue line, for the same time instant (Fig. 3.13). Please note that the photograph is reversed and thus the wave paddle is now located on the right hand side and the beach on the left.

Figure 3.13 reveals a reasonable correlation between PIV results and the actual wave train. Although wave troughs appear locally underestimated and thus wave heights overestimated; the method is proven to be capable to depict water surface elevation along the whole length of the tank.

Moreover, the wave length L can be measured from both Fig. 3.12b and 3.13. Figure 3.12 gives L $\approx$ 31cm as the distance between three subsequent zero up-crossing points (66 and 97), whereas Figure 3.13 gives a rough estimate of L $\approx$ 32.5cm.

3.5.4 Discussion on irregular sea measurements

The present work moves wave field mapping a step further by investigating the representation and measurement of a laboratory generated irregular sea. Propagating waves of different characteristics are captured as a function of surface particle velocities, and depicted as a vector map through the whole length and width of the wave basin. A theoretical analysis of irregular seas based mainly on the space domain is presented here for the first time. The comparison of surface elevation profile produced by the PIV process of two subsequent images, with the side photograph reveals a satisfactory correlation between the two and although wave lengths are directly comparable, wave troughs locally appear too shallow, and thus wave heights and are overestimated by the PIV measurements / analysis. This may be attributed to the following two factors:

- the optical distortion introduced by the side camera. A small disorientation (non-parallel) in the cameras position along with the incorporated effects of the cylindrical camera lenses could result in a distorted photograph, underestimating trough depths,
- effective water levels seem to vary between waves in a irregular sea; in order to fulfil the assumptions for the analysis (sinusoidal waves), a shifting MWL should be introduced or a non-linear method needs to be developed

3.6 Conclusions

A novel method for the mapping of wave fields, based on the measurement of surface flow velocities with Particle Image Velocimetry (PIV) has been developed at Southampton University. Using linear wave theory, wave heights could be calculated from the measured velocities and wave lengths for propagating wave fronts. Comparative measurements with resistance type wave probes showed a good agreement, indicating the validity of the method. Experiments with structures (i.e. breakwater gap) showed the capacity of the method to map a complex wave field, including diffraction.

The extension of the PIV method for the visualization and measurement of wave fields, to the analysis and capture of irregular seas is also presented and validated experimentally. Wave heights were overestimated, pointing in combination with visual observations to the existence of a locally increased MWL. Irregular seas are analyzed for the first time in the space domain resulting in the visualization of the developing wave field along the full length and width of the basin, whilst the evolution of the field over time is possible as well. Although further research is required in order to improve the accuracy and non-linear capacity of the method, and investigate its performance with more complex geometries (structures etc) and irregular seas, the method is considered very promising.

Chapter 4

Wave propagation and diffraction in micro-models

4.1 Introduction

The review of the existing literature showed that micro-models have been originally developed and used for sediment transport studies in rivers. Typical model scales ranged from 1:500 to 1:20.000 and distortions of the horizontal to vertical length scale were between 5:1 and 17:1, Davinroy (1994). Given the difficulties of sediment transport modelling even at large scale, is it hardly surprising that such models were heavily criticised and finally discarded as a design tool by authors like Maynord (2006). Earlier, USACE (2004b) applauded the selective use of micro-models and successive micro-model projects were presented by Davinroy (2004) and Brown (2004). Few authors have also reported the use of similarly small scale hydraulic models in port design, Beckett and Marshall (1983) and Rankine (1991), but only tidal flow impacts were investigated with those models and thus waves were not employed. Accordingly if micro-models are to be used for wave studies, their limitations need to be assessed.

Most coastal related investigations require waves travelling over an inclined bed and interacting with defensive structures like breakwaters. The influence of the varying topography on the wave is dictated by the local water depth and the wave

length / wave period. For a water depth to wave length ratio (d / L) smaller than 0.05 the wave is located in shoaling water, and as it propagates from one depth to another, its main characteristics such as the wave height and length will change. If an impervious structure like a breakwater is present part of the incident wave will be reflected or break whereas part of it will move past the tip of the structure and will be the source of a flow of energy in the defended area; a phenomenon known as diffraction, Wiegel (1976).

Hence the minimum requirement for the micro-modelling of wave fields would be the accurate simulation of wave propagation, shoaling and wave diffraction. A prerequisite for all three processes is that the amplitude of the waves generated and travelling inside the model will not reduce in a way disproportional to the prototype. For non-breaking waves gravity, viscosity and surface tension are the dominant factors influencing wave attenuation. Since gravity is the largest and most important force, a Froude scale is chosen for wave micro-models as it is commonly done in any wave related physical model, ASCE (2000). However equality between model and prototype Fr number directly implies that Re and We will be distorted or, in other words, that the influence of viscosity and surface tension in the laboratory will not be similar to the field. LeMehaute (1976) and Hughes (1993) amongst others concluded that the latter is a source of scale effects which depend on the tank / basin dimensions, the water depth and the wave length / period (for $T > 0.35$sec and $d > 0.02$m), and can result in unwanted reduction in the amplitude of propagating waves; an effect occuring also known as wave damping.

Since micro-models refer to very small scales (i.e smaller than 1:50), an increased sensitivity to such scale effects is expected. As a result the lower threshold of wave characteristics and water depth in micro-models for which the effects of viscosity and surface tension are negligible or minimum, needs to be established. The current chapter presents a theoretical analysis along with the results of an experimental series focused on exactly that goal. The PIV method described in the previous chapter is used for the 3D visualisation of the offshore and diffracted waves within the full dimensions of the wave basin. Findings reported are interesting not only for the validation of micro-models but for the overall use of physical models.

Force	Similarity Law	Scale	
		1:10	1:100
Gravity	Froude	1:1	1:1
Viscosity	Reynolds	1:31.6	1:1000
Surface tension	Weber	1:100	1:10000

Table 4.1: Scale requirements for different forces and different similarity laws.

4.2 Theoretical considerations

If wave processes are to be accurately transferred in model scale, then a simultaneous fulfilment of geometrical, kinematical and dynamical similitude is required. For a Froude model, the first two conditions are met if a constant ratio between all lengths in prototype and model is kept and if all time intervals involved are scaled according to $\frac{1}{\sqrt{N_L}}$, were N_L is the prototype to model length ratio. On the contrary dynamic similarity is impossible since a constant ratio between all forces in the field and the laboratory cannot be achieved. In fact as Table 4.1 shows the deviation for surface tension and friction forces increases significantly as the model scale decreases. The limits beyond which the errors resulting from the inability to scale the fluid properties affect the veracity of micro-models are primarily established on a theoretical base.

4.2.0.1 Infuence of viscosity

When laboratory waves travel inside a wave tank / basin and especially over shoaling water part of their energy is consumed through bottom and side wall friction, internal friction and percolation. Nevertheles, the influence of the latter can be ignored since for all micro-models utilised in the current thesis an impermeable bed and slope were used.

Assuming deep water conditions and thus neglecting boundary shear, Keulegan (1950b) presented an expression for the estimation of wave height attenuation due to internal friction:

$$\frac{d}{dt}\left(\pi\rho\frac{H^2C^2}{4L}\right) = -16\pi^3\rho\nu\frac{H^2C^2}{4L^3} \tag{4.1}$$

where,

ρ : is the fluid density,

ν : is the kinematic viscosity,

t : is the time,

L : is the wavelength,

C : is the wave celerity,

H : is the wave height.

By rearranging, cancelling variables and integrating over height and time, 4.1 gives:

$$\frac{H(t)}{H_{t=0}} = e^{-\left(8\pi^2\nu t/L^2\right)} \tag{4.2}$$

where,

H(t) : is the attenuated wave height at time t.

Equation 4.2 can be used for example to estimate the time required for the height of a wave with various offshore wave lengths to reduce by 5% due to the internal friction of the fluid. Accordingly Figure 4.1 shows that the influence of the latter is important for wavelengths smaller than 5cm, but becomes negligible for larger wavelengths and within realistic wave basin geometries. Characteristically it is seen that the wave height of a 0.2m long wave (0.36sec) will reduce by 5% after approximately 30sec. Since, for a wave travelling in deep water, the group celerity is equal to half the wave celerity ($c = \sqrt{\frac{gL}{2\pi}}$) the distance the specific wave will need to travel in order to lose 5% of its height is approximately 8.4m. When in shallow water, e.g. d = 0.01m, the group velocity is equal to the wave celerity ($c = \sqrt{gd}$) and as such the required distance increases to approximately 9.4m.

Furthermore, the dissipation of energy along the bottom and the side wall of the laboratory wave tank / basin can be expressed by the formula given by Hunt (1952):

$$\frac{\frac{dH}{dx}}{H} = -\frac{2k}{d}\frac{\sqrt{\nu}}{\sqrt{2\omega}}\left(1 + \frac{2kd}{sinh2kd}\right)^{-1}\left(\frac{2kd}{sinh2kd} + 2\frac{d}{b}\right) \tag{4.3}$$

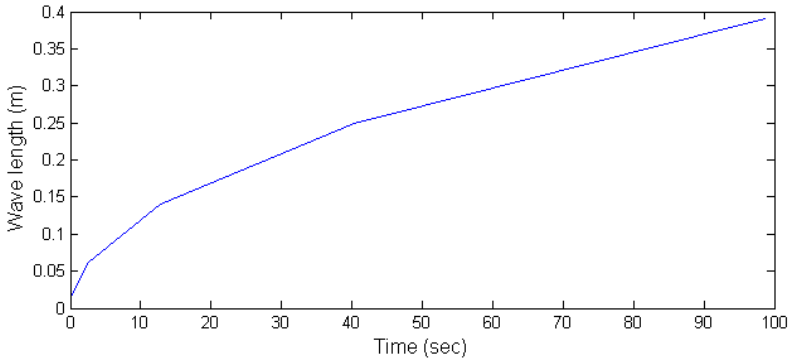

Figure 4.1: Diagram of the offshore wavelength over the time required for the wave height to reduce by 5%.

were,

b : is the width of the wave tank,

ω: is the wave frequency,

d : is the water depth

In equation 4.3 the first term represents the bottom friction and the second term the friction on the side walls. Although Hunt's formula assumes laminar damping, Svendsen (1985) provides measurements of wave height decrease in a wave flume that compare very well with equation 4.3 and hence show that the attenuation is well predicted.

Accordingly Figure 4.2 plots the ratio of the wave height attenuation per meter to the original wave height over the wave period. Solid lines represent wave damping due to bottom and side wall friction in a 0.8m wide wave basin. It is seen that for a water depth of 0.01m the height decay per meter increases dramatically from 10% for a 0.1sec wave to almost 50% for a 0.3sec wave and then decreases as the period increases but remains at a high level even for a 2sec wave (about 25%). As the water depth increases a similar trend is observed but the attenuation values and their decrease rate with T are now drastically reduced. The wave height attenuation decreases to less than 10% per meter for a depth larger than 0.02m and further reduces to less than 5% as the water becomes deeper than 0.03m.

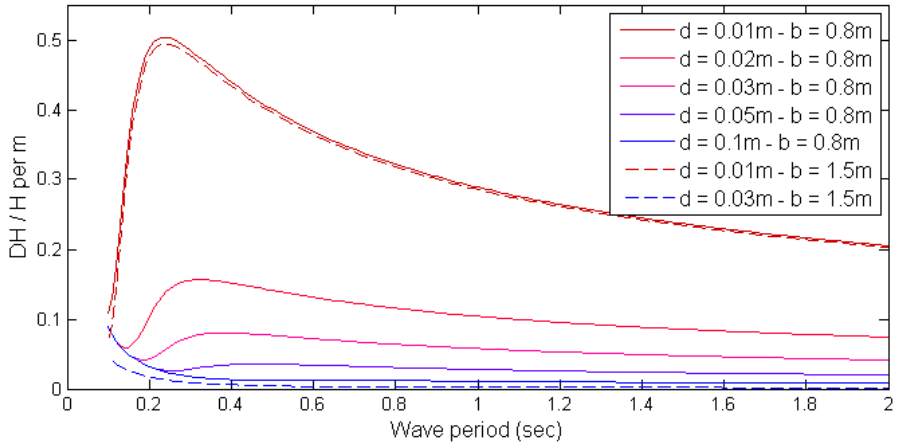

Figure 4.2: Height attenuation due to bottom and side wall friction, of waves propagating in a 0.8m wide wave basin (solid lines) and a 1.5m wide basin (dashed lines).

Moreover, the dashed lines in Figure 4.2 correspond to the attenuation of waves propagating in a 1.5m wide basin. It is shown that for a water depth of 0.01m the influence of the friction force is approximately the same as for the smaller basin but becomes negligible for waves travelling in 0.03m of water.

Hence the cumulative influence of internal, bottom and side wall friction on wave damping can range from insignificant to dramatic, depending on the wave period and the water depth. Figures 4.1 and 4.2 clearly indicate that any wave with period smaller than 0.3sec travelling at a water depth smaller than 0.02m will undergo a significant attenuation of its height. However, since the experimental space of micro-models is restricted to few meters in length (up to 3m for the current project), it can be concluded that if the water depth is larger than 0.02m then the influence of the friction force will range from small to negligible as the wave period increases. Even more, for the same conditions and testing facilities wider than 1.5m the bottom and side wall effect can be ignored without affecting the veracity of the final result.

4.2.0.2 Influence of surface tension

When waves are present on a liquid surface its area is increased. Surface tension is a force acting in a direction tangent to this surface so as to minimize its area and restore the surface to its original state. Since for all the experiments considered here fresh water is used, the scaling requirements refered to in Table 4.1 can not be

fulfield. Even more as the length scale decreases the deviation increases and thus the model will experience wave motion damping, which does not occur in the prototype. The influence of surface tension on wave propagation is expressed by the following equation, given in LeMehaute (1976):

$$c^2 = (\frac{gL}{2\pi} + \frac{2\pi\sigma}{\rho L})tanh(\frac{2\pi d}{L}) \tag{4.4}$$

were,

c : is the wave celerity,

L : is the wave lenght,

d : is the water depth,

σ: is the surface tension,

ρ: is the density

The first term on the right part of equation 4.4 expresses the influence of gravity and the second term expresses the influence of surface tension. Using equation 4.4, LeMehaute (1976) concluded that for d $>$ 0.02m and T $>$ 0.35sec the influence of surface tension on wave propagation is negligible (see also Fig. 2.6).

4.2.0.3 Summary of the theoretical considerations

Previous studies presented above show that the combined influence of friction and surface tension forces on wave propagation is minimised for a water depth larger than 0.02m and wave period larger than 0.35sec. Nontheless the difference in wave attenuation between a narrow flume and a wide basin can be significant. Therefore the above limits refer to micro-model studies taking place in a wave basin at least 0.8m wide. If a wave flume (i.e 0.2m wide) is to be used, then equation 4.3 suggests that for T $>$ 0.3sec an acceptable maximum level of 5% wave attenuation per meter can be achieved for water depths not smaller than 0.05m.

These theoretical limits were investigated through a series of experiments the results of which follow.

4.3 Experimental apparatus

4.3.1 The wave basin

The majority of the experiments presented in the current chapter were conducted in the small size wave basin (1.8x0.8x0.2m) also described in the previous chapter (Fig. 3.4). A rigid flap with a single articulation at the bottom was placed at a distance of 0.3m from the end wall of the tank and used to generate waves. This flap-type wavemaker had and amplitude range from 0.5cm to 3cm and was driven by a 12Volt linear motor made by Motor ParraInx Co. The repeatability of the generated wave climate was tested by conducting subsequent surface elevation measurements at the same location and for the same wavemaker settings. The testing procedure was repeated for water depths ranging between 0.03 and 0.1m and it was found that the motor was able to satisfactory re-generate wave patterns but only for d $>$ 0.05m; wave generation for smaller water depths was either insignificant (very small wave height) or very unstable (very steep).

For these reason tests were also conducted in a 4x1.5x0.2m wave basin at Rostock University, Germany. The basin was equiped with a computer controlled, piston type wavemaker which was capable to generate smooth, high frequency, regular waves for water depths as small as 0.025m. LabView was used to generate and feed the wavemaker with a sinusoidal digital signal, which was starting and ending with a rump up / down part. This was necessary in order to achieve a smooth transission for the rest position of the motor to a fully developed oscillation and vice versa.

4.3.2 Measuring equipment

Originally the surface displacement was measured with resistance type wave probes (Fig. 4.3). A pair of stainless steel rods (1.5cm apart) with a diameter of 1.5mm was used for the construction of each of these small size gauges (length 20cm), which were then plugged into a Churchill Controls Wave Monitor Module, Ltd (2001). According to the principle of operation explained in the manual, each submerged

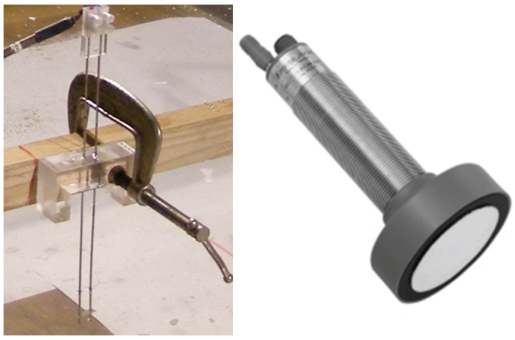

Figure 4.3: Pictures of the resistance type wave probe (left) and the ultrosonic sensor (right), used in the current thesis.

probe is energised with a high frequency square wave voltage to avoid polarisation effects at the rod's surfaces. The current flowing between the two rods is proportional to the depth of immersion and is sensed by an electronic circuit, which provides an output voltage proportional to the instantaneous depth of immersion, i.e. wave height. Potential noise from external sources was further reduced by the use of multilayer telecommunication wires; for the same reason the length of the wires was also kept as small as possible (i.e. 3-5m).

Before every test the wave probes were calibrated in the same water used for the experiment, and the final calibration graph was parted from at least five different calibration points. The calibration procedure was repeated until $R^2 > 0.999$. Side photographs of the propagating waves were also used for the validation of the wave probe signal (256 samples per wave) and differences in the estimated wave heights did not exceed 5%; the analysis of the photographs gave slightly smaller H.

For the experimental series conducted in Germany ultrasonic-sensors were employed to measure wave heights (Fig. 4.3). The sensors were made by Pepperl & Fuchs and had a sensing range from 350mm to 6000mm, a transducer frequency of 65kHz and an accuracy of approximately 0.2%. The sensors were again calibrated before each experiment following the method suggested by the manufacturer.

Finally, surface elevation was mapped and measured with the PIV based technique described in chapter 3, but the SONY camera was now replaced by a black and white Basler video camera. A PC was used to control the camera and videos were recorded

with 60fps and a 640x480pixels resolution and stored directly into the hard drive. By increasing the temporal resolution of the method (increased fps) the error on the calculation of the wave height is reduced because the assumption for constant particle velocity now refers to a smaller area. However, the particles need to move between two interogation cells within two subsequent images and thus an upper limit on the increase of the fps is set; 60fps were found to be enough for wavelengths as small as 0.15m.

The freeware Photron FastCam Viewer 3 was used to separate the videos acquired into frames and whenever necessary to improve the quality of each image (i.e. contrast adjustments), whilst all the numerical work required (i.e. calibration, wave height extraction, diffraction coefficient calculation etc) was done with MatLab.

4.4 Results

4.4.1 Wave propagation in micro-models

The attenuation in height of waves propagating inside the small wave basin (see previous section), has been previously measured in Stagonas (2005) for water depths and wave periods larger than 0.04m and 0.3sec respectively. For these conditions the author did not observe any wave damping even when the waves were shoaling over a slope.

However in order to investigate the validity of the theoretical limits for negligible surface tension and viscosity influence on wave propagation, further experiments were conducted in a 4x1.5x0.2m wave basin located in Rostok University, Germany. The basin was equipped with a computer controlled piston type wavemaker and was favoured over the equipment available in the University of Southampton due to its ability to generate smooth and stable, large frequency (small T) waves, even at water depths as small as 0.025m.

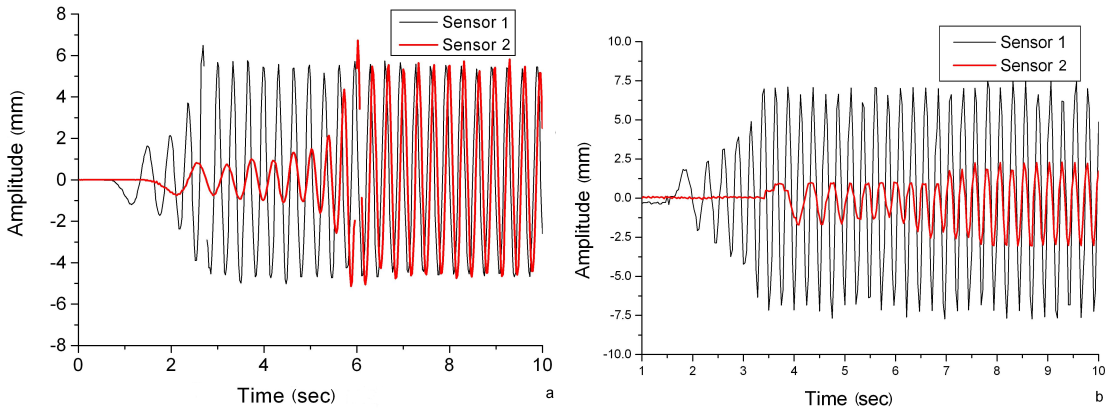

Figure 4.4: Wave height attenuation in a micro-model for a 0.35sec wave (a) and a 0.15sec wave (b), and a water depth of 0.025m.

Accordingly a pair of ultrasonic sensors was used to measure wave heights at 2 different locations inside the basin; the first sensor was placed 1.5m from the wavemaker and the second 0.7m apart. Results presented in Figure 4.4 correspond to surface elevation measurements for 0.35sec (a) and 0.15sec (b) waves travelling over 0.025m of water.

Figure 4.4a shows that for a period of 0.35sec, waves suffer no attenuation of their height over time. On the contrary the height of a 0.15sec wave (Fig.4.4b) reduces to almost 1/3 of its original value within a distance of 0.7m.

These findings are in good agreement with theory (see previous section), which suggests that for water depths and wave periods smaller than 0.025m and 0.35sec respectively, laboratory (side wall and bottom friction) and scale effects (viscosity and surface tension effects) are important and cannot be neglected.

4.4.2 Wave diffraction in micro-models

Diffraction is the wave phenomenon resulting from the interaction of propagating waves with immersed obstacles such as breakwaters, and which in a large extent determines the amount of energy entering a harbour. According to Wiegel (1976) the diffraction coefficient is defined as the ratio of the wave height in the area affected by diffraction to the wave height in the area unaffected by diffraction. The latter ratio is

in a most general way an expression of the disturbance level at a point inside a harbour. Because the principal aim of a harbour designer is to provide an optimum level of usability for every region within the harbour it yields that the determination of the diffraction coefficient is of crucial importance.

Several researchers like Penny and Price (1944); Morse and Rubinstein (1938); Johnson (1952) and Wiegel (1962) have theoretically studied wave diffraction around a semi-infinite breakwater and through a breakwater gap and published wave diffraction diagrams (see Chapter 2). Putnam and Arthur (1948); Blue and Johnson (1949) and Carr and Stelzriede (1952) presented experimental results, which verified the general theoretical outcomes despite the fact that the measured values did not coincide with the theoretical values. Carr and Stelzriede (1952) for example recorded experimental values 20% lower than theoretical and Blue and Johnson (1949) observed zones of considerably reduced wave heights.

Since wave micro-models are meant to model, amongst other things, proposed harbour layouts and provide preliminary evidence on the effectiveness of defence structures, the accurate modelling of wave diffraction is a necessity. Nevertheless, this new tool in combination with the full field measuring method described previously can provide information which up to present was only available by numerical models.

Consequently experiments on the diffraction of waves around a single breakwater and through a breakwater gap were conducted in the 1.8×0.8×0.2m wave basin. Wave fields were mapped using the PIV method, which also resulted on the calculation of the diffraction coefficient within the full dimensions of the working area. Minimum water depths and wave periods were restricted to 0.025m and 0.03m, and 0.3sec and 0.5sec, so as to avoid wave damping due to viscosity and surface tension effects.

4.4.2.1 Wave diffraction around a single breakwater

Figure 4.5 presents the velocity vector field (on the left) and the extracted 3D surface elevation field (on the right), for 0.35sec waves travelling in the wave basin, over a water depth of 0.03m, and being diffracted around a single breakwater. Waves

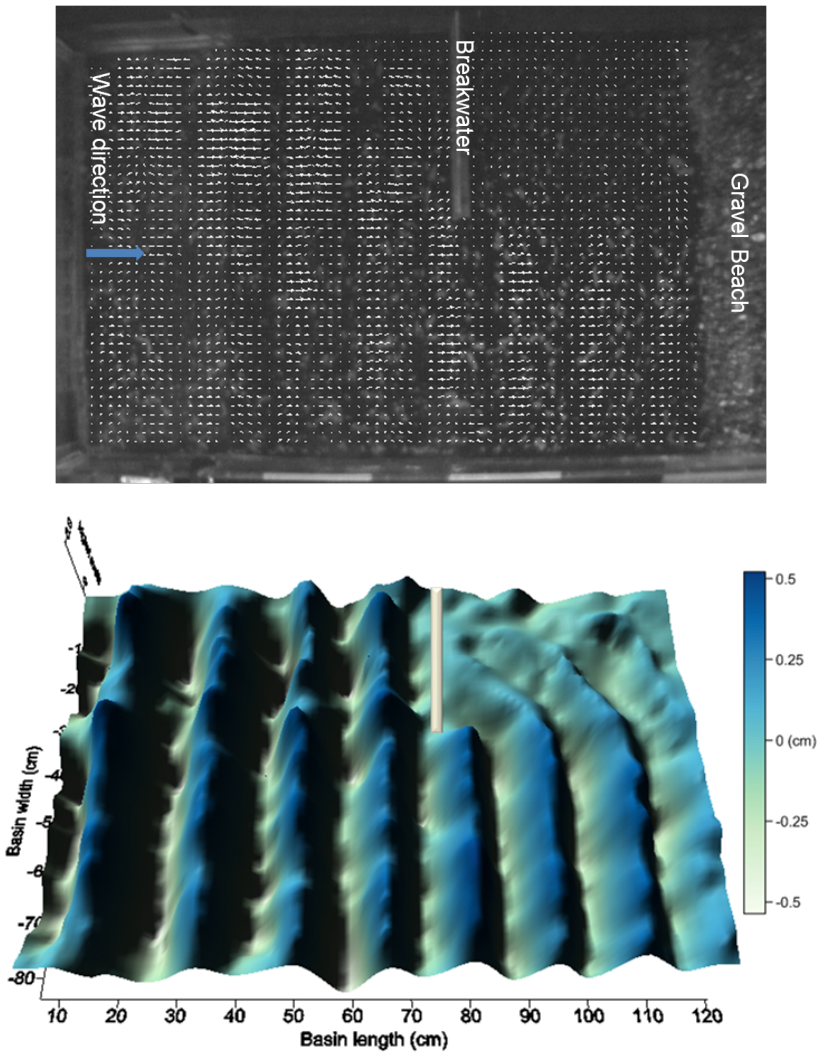

Figure 4.5: Velocity vector field (above) and 3D surface elevation field (below) of waves diffracted around a single breakwater for d = 0.03m and T = 0.35sec.

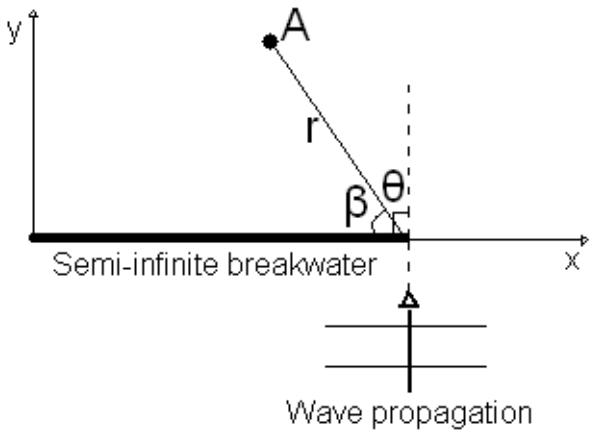

Figure 4.6: Wave diffraction symbols.

generated by the paddle, propagate from offshore into the protected area and curve over the structure. No reduction in the wave height is observed between the 'open sea' and the un-sheltered area behind the breakwater but the wave height reduces on the lee of the structure at a rate which increases with the distance from it.

Since the surface elevation is known for every point within the basin the value of the diffraction coefficient can be calculated at a given position A (Fig. 4.6) as the ratio of the incoming to the transmitted wave height. Point A is located at a distance r from the structure and ϑ, and β are the wave propagation angle and the angle formed between the edge of the breakwater and r or else the deviation angle (Fig. 4.6).

Table 4.2 summarises the diffraction coefficients calculated for the set-up of Figure 4.5, at two different locations (r = 20cm and r = 50cm), for $\beta = 45^o$, $90^o$and 135^o, $\theta = 90^o$, for two water depths of 2.5cm and 3cm, and for wave periods ranging between approximately 0.3sec to 0.5sec. The experimental results are compared with the theoretical diffraction coefficients calculated using the Penny and Price (1944) method. For this reason a Fortran routine was used, which solves analytically the Helmholtz equation, as described in Karambas (2004).

In general a very good agreement is observed between the micro-model and theory. Experimental and analytical values are almost identical for the largest wave period (approx. 0.45sec) regardless the water depth but differences are seen as T reduces. For T = 0.35sec the experiments coincide with theory near the breakwater for both

Water depth (cm)	Wave period (sec)	Distance from break-water (cm)	Deviation angle					
			45^o		90^o		135^o	
			Exp.	Th.	Exp.	Th.	Exp.	Th.
2.5	0.48	50	0.27	0.26	0.46	0.56	1.03	1.06
3	0.45	50	0.22	0.24	0.51	0.55	1.1	1.06
2.5	0.33	20	0.21	0.27	0.69	0.56	0.85	1.09
2.5	0.33	50	0.05	0.18	0.39	0.54	0.7	0.97
3	0.35	20	0.35	0.28	0.64	0.56	0.99	1.09
3	0.35	50	0.06	0.19	0.37	0.54	0.49	0.53
2.5	0.29	20	0.10	0.25	0.46	0.56	0.66	1.02
2.5	0.29	50	0.05	0.18	0.41	0.53	0.59	0.95
3	0.29	20	0.19	0.3	0.56	0.57	0.98	1.09
3	0.29	50	0.13	0.20	0.55	0.54	0.85	0.94

Table 4.2: Experimental and theoretical values of the diffraction coefficient for waves diffracted by a single breakwater.

water depths but a deviation is observed for an increased distance from the structure where experimental results appear to be smaller. Nevertheless, in most cases this deviation is less than 20%.

A similar trend is observed for the smallest wave period (T = 0.29sec) but only for a water depth of 3cm. When d = 2.5cm and despite the distance from the breakwater, laboratory values are in principal smaller than the theoretical values by more than 20%. It is no surprise that the latter experimental conditions lay on the limits of increased influence of surface tension and viscosity forces.

As an overview it can be concluded that experimental results about the diffraction of waves around a single breakwater in micro-models are encouraging. Although some differences were observed between the model and theory, those are within the limits suggested in the existed literature, e.g. Carr and Stelzriede (1952), except when d = 2.5cm and T = 0.29sec. For the latter case although the decrease of the transmitted wave height presents the same trend as in theory, the diffraction coefficients measured are significantly smaller and thus errors on the final result should be expected.

4.4.2.2 Wave diffraction at breakwater gap

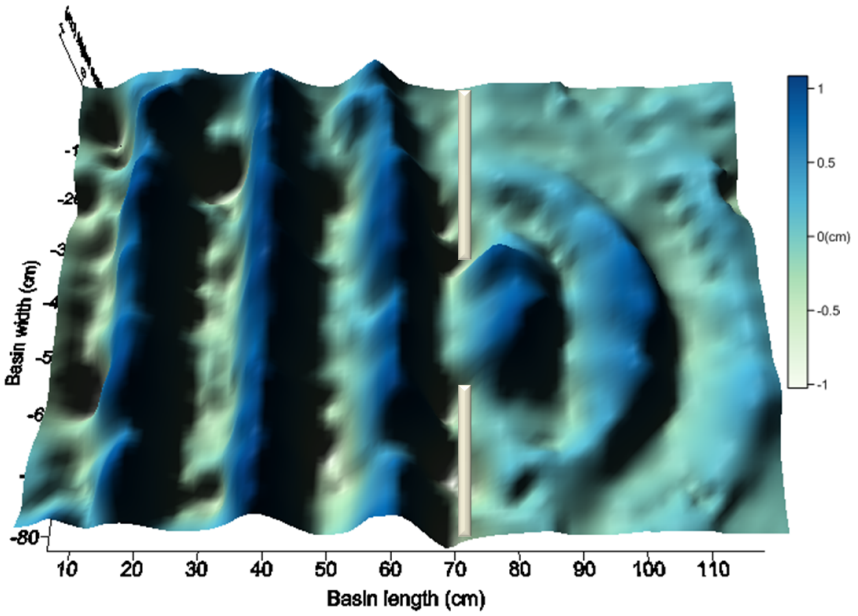

Figure 4.7: 3D surface elevation map for wave diffracted through a breakwater gap in a micro-model; d =3cm, T =0.35sec, B ≈ L.

In a similar way, the diffraction of waves through a breakwater gap was also investigated for water depths ranging from 2.5cm to 4cm and wave periods larger than 0.3sec. Accordingly, the 3D surface elevation map of the wave field inside the basin is presented in Figure 4.7; the gap length is equal to approximately one wave length (B = L). Based on these measurements a contour plot depicting the distribution of the diffraction coefficient was created (Fig. 4.8a) and is compared with the theoretical diagram of Johnson (1952) (Fig. 4.8b).

The most striking difference between the two diagrams of Figure 4.8 is the size of the area under investigation. For his theoretical graph Johnson (1952) assumes a 20x20L area without any solid boundaries, whilst the size of the experimental area presented is 2x3L and is surrounded by the basin walls and concludes on the limits of the energy absorbing gravel beach. The latter implies that all the residual wave-boundary interactions, like wave reflection, are not considered for Figure 4.8b.

Nonetheless, the overall distribution of the contour lines is similar for both diagrams but the measured values of the diffraction coefficient reduce much faster along the

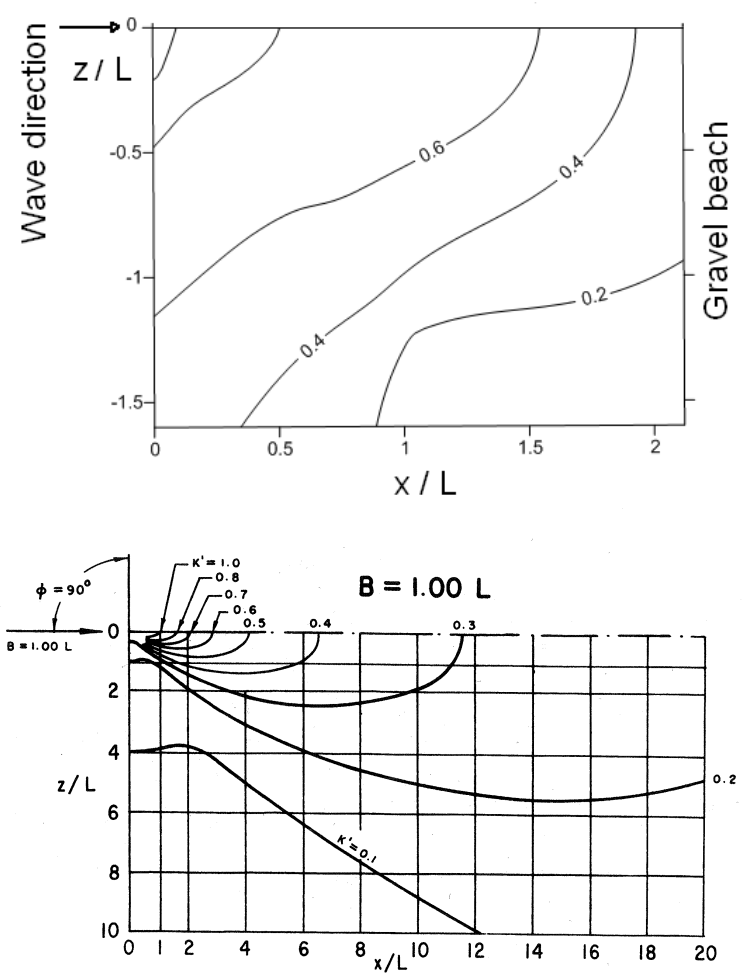

Figure 4.8: Above, experimental contours of equal diffraction coefficient at breakwater gap and below theoretical contours after Johnson (1952); d = 3cm, T = 0.35sec, B ≈ L.

area's length than the theoretical. For example, within a distance of 2L the experimental coefficient has reduced to approximately 0.4, while its theoretical value is 0.7. However the chosen water depth and wave period entails a negligible influence of viscosity and surface tension, whilst in their experimental results Blue and Johnson (1949) also recorded lower than theoretical diffraction coefficients. The authors observed zones of considerably reduced wave heights in the lee of the breakwater, without however providing an explanation.

Overall it can be concluded that wave diffraction through a breakwater gap is modelled to an acceptable level in micro-models. Nevertheless the final result can be biased by laboratory effects due to the small dimensions of the wave basin and hence similar investigations are better facilitated in a larger and wider basin. However, it is apparent that the combination of micro-models with the PIV mapping method can

provide, for the first time, the temporal and spatial history of the evolution of a wave field within the full dimensions of a physical model.

Furthermore, during the current experimental series an additional laboratory effect was observed. Although waves transfer energy they can also, depending on their steepness, transfer mass (i.e. water and PIV particles) towards the end of the basin. As a result, and when at least one breakwater was present, a surface flow pattern was developed, as depicted in Figure 4.9. Although the development of such a drift is enhanced by the small size of the current basin it is possible that a similar flow pattern will develop in any large scale 3D facility and locally increase the water level.

Obviously the presence of such a surface drift constitutes a laboratory effect that affects the final result of any measurement conducted within the basin and thus limits the experimental time to prior its development.To the author's knowledge, the present literature has mainly focused on the development of laboratory induced flows in wave flumes (2D) and seldom in wave basins, i.e. Huang (2007) and Swan (1990).

On the other hand, the PIV method proposed here is able to visualise surface flows, which are otherwise ignored by all existing surface elevation techniques, e.g. wave gauges. As a step further the present mapping method combined with micro-models highlights potential errors that can affect large scale experiments as well. Accordingly wave micro-models could also be developed as a valid tool for the pre-design of large scale experiments.

4.5 Conclusions

The principal goal of the work presented in the current chapter was to establish the operational limits of wave micro-models and investigate the veracity of micro-modelling basic wave features like wave propagation and wave diffraction. Indeed the review of the existed literature showed that the propagation of waves in laboratory conditions is affected by the viscosity and surface tension forces. Such scale effects cause wave damping and their influence increases in importance for water depths smaller than 0.03m and wave periods smaller than 0.35sec.

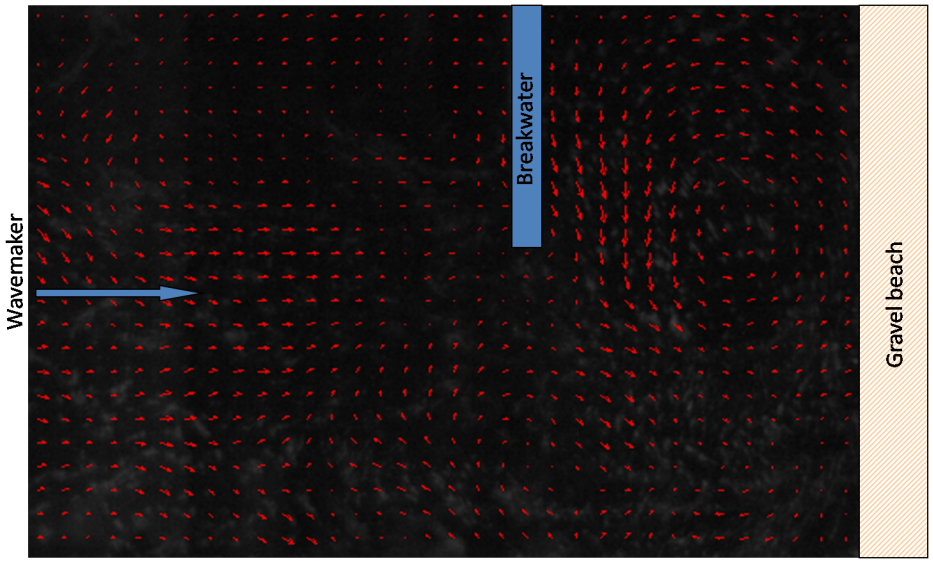

Figure 4.9: Vector map of surface particle velocities; a surface flow pattern is observed within the wave basin; d = 0.025m, H / L = 0.1.

Accordingly an experimental work plan, focused on verifying the above limits, was carried out. Two wave basins (1.6x0.8x0.2m and 4x1.5x0.2m) were used to observe and measure the surface elevation of small period waves propagating at the water depths suggested by the literature. Moreover the diffraction of such waves by idealised breakwaters was investigated with the use of the novel mapping technique, described in the previous chapter. The overall conclusions are:

1. The minimum experimental conditions below which significant wave damping occurs in micro-models of wave fields, are set for a water depth of 0.03m and a wave period of 0.35sec. However if a wide (i.e. $\geq$ 0.8m) and relatively short (i.e. $\leq$ 4m) wave basin is used then the aforementioned limits can be further reduced to d = 0.025m and T = 0.3sec since the overall attenuation of wave height will be negligible. Indeed the latter has been experimentally verified here (Fig. 4.4).

2. Wave diffraction around a single breakwater is accurately modelled in micro-models. Once more the minimum operational limits are the same as above, since for d = 0.025m and T = 0.3sec the experimental diffraction coefficient values were significant smaller than the theoretical.

3. Wave diffraction through a breakwater gap is modelled to an acceptable level for the above limiting conditions. The experimental contour plot presented here was

found to be qualitatively similar to the theoretical diffraction diagram. On the contrary the rate of energy reduction inside the protected area is much larger in the micro-model. However the quantitative comparison of the physical model and theory is subjected to errors introduced due to the presence of solid boundaries in the model, which result in unwanted interactions with the diffracted waves such as wave reflection. Differences between experimental and analytical diffraction coefficients have also been previously reported in the literature.

4. The formation of an unwanted surface flow drift was observed. The presence of the drift was attributed to the combination of, 1. the movement of mass by steep waves, 2. the presence of a structure inside the basin and 3. the small size of the basin. Such a flow pattern affects the quality of the final result, limits the experimental time and could be developed in any 3D wave facility.

5. The PIV method proposed here is able to visualise surface flows, which are otherwise ignored by all existed surface elevation measuring techniques. The combination of such a mapping method with micro-models could be developed to a novel pre-design tool for large scale experiments.

6. The dimensions of the small wave basin used here are on the lower operational limits for micro-models since a limited range of waves can be used without generating unwanted laboratory effects; thus the use of a larger wave basin is suggested. Nonetheless, the work presented here as well as in the previous chapter suggests that such a small basin can be useful for the preliminary development and investigation of novel ideas, e.g. wave mapping techniques.

Chapter 5

Wave breaking in micro-models

5.1 Introduction

Wave breaking is one of the most violent, impressive and important phenomenon as it is the predominant mechanism involved in air-sea interactions and energy dissipation in the coastal zone, momentum transfer from wave to currents as well as in turbulence generation and turbulence-wave interactions. Upon breaking energy is consumed during air entrainment, bubble and turbulence generation, splash, and noise production. As described by Dean and Stokes (2002) the evolution of a plunging breaker consist of two processes; (1) the overturning wave crest (jet) struck the wave face prior to the fragmentation of the trapped air and (2) about 1sec later, a shear flow on the wave face is formed, and the entrained air is split into filaments and bubbles. While studies related to all the aforementioned factors are being conducted over the past years, our knowledge on the detailed nature of each mechanism and its relative contribution to the total energy dissipation is yet incomplete. As a result no comprehensive numerical model of energy dissipation during breaking is currently available and a significant part of the ongoing research and development is based on large scale physical models.

Even though all the principal mechanisms are by default modelled in laboratory breaking waves, scale effects can bias the final result. Similarity laws dictate that instantaneous geometric and dynamic similitude can only be achieved in a 1:1 model,

or in other words only nature can accurately model nature. Wave breaking is mainly dominated by gravity and surface tension forces (Hughes, 1993). Nevertheless, most wave motion studies are base upon Froude similitude, whereas air entrainment, bubble break up and coalescence are dominated by surface tension effects implying the need for a Weber similitude (Chanson, 1997). The wave's geometry and the crest structure are also affected by the length scale and surface tension, the significance of which is unproportional to the to model's size (Tulin, 1996; Duncan, 2001).

Hence it would be rational to assume that due to their very small size (i.e L $<$ 0.5m, H $<$ 0.1m) micro models will be strongly affected by scale effects. For example, for waves breaking in a Froude scale of 1:100 the surface tension force will need to be 10^4 times smaller in the model than in prototype. Since freshwater is however, mainly used in most physical models the values of all the fluid's properties will be approximately the same as in nature. Nevertheless, the same principal mechanisms will contribute to the phenomenon's evolution almost all its individual features, such as the jet formation, the entrainment of air, the bubble size and rise velocity will strongly deviate from reality. In a similar manner energy dissipation significantly reduced between model and prototype, since it is linked to all the aforementioned processes.

Consequently the focus of the work carried out in this chapter was to investigate the amount of energy dissipated during wave breaking in micro models and how this varies with the reduction of surface tension. Energy dissipation values were measured for waves with maximum period of 3sec and height of 8cm. In order to assess the sensitivity of the micro-model to surface tension effects, the experiments were originally conducted with freshwater, which was subsequently replaced by a surface tension reduced solution of 10% isopropyl alcohol in distilled water; it is shown that more energy is consumed by waves breaking in the latter than the former fluid. The results are compared with previously published studies from larger scale physical models and their similarities and differences are discussed. A global approach is adopted in order to assess the findings presented herein, and thus it is beyond the scope of this investigation to accurately quantify either the effects the reduction of

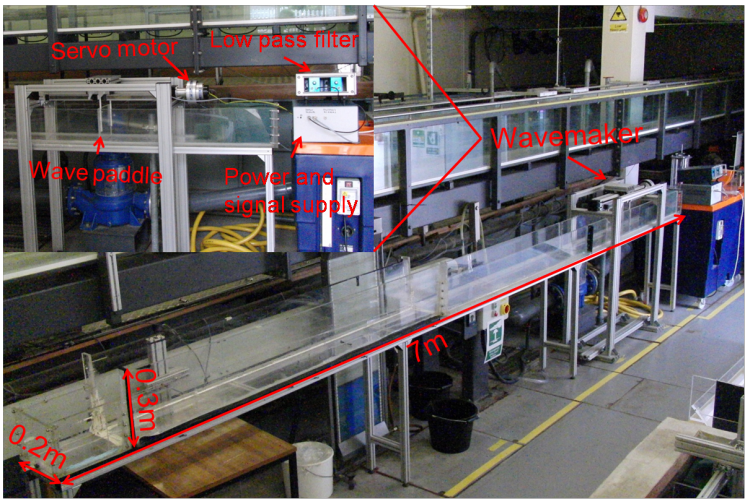

Figure 5.1: The small scale wave flume in the Hydraulics laboratory.

surface tension has in each process, or the contribution to the overall dissipation of the wave's energy.

The data presented herein is of great interest on it own right as they might have implications in every physical study involving strong turbulent flows and air entrainment like hydraulic jumps, and spillways.

5.2 Experimental apparatus

5.2.1 The wave flume

All the experiments presented in the current chapter were conducted in a 7m long, 0.2m wide and 0.3m deep wave flume, specifically built in the hydraulics laboratory (Fig. 5.1). Regular waves were generated by a piston type wavemaker and absorbing material was placed on both ends of the flume in order to dissipate the incoming wave energy. A PC was used to create a digital sinusoidal signal including a rump-up and down part, which was than converted to analogue, passed through a low pass filter to the power and signal supply box and was ultimately fed into the wavemaker. Wave transformation and breaking were observed for two different slopes, one steep 1:10, and one smoother 1:20 followed by a plateau. The latter slope was preferred for the calculation of the energy dissipation by breaking waves in the micro-model

because it was less reflective and mainly allowed for the measurement of the incoming (pre-breaking) and the transmitted wave height (post-breaking); measurements were conducted at a distance of 1m and 2.5m (over the slope) from the wavemaker and 0.5m away from the end wall.

5.2.2 Measuring equipment

Wave heights were measured with resistance type wave gauges for both freshwater and the Isopropyl-Alcohol and distilled water solution (IPA). However, due to the very high resistance of the IPA solution the current flowing between the two rods was very weak and could not be detected by the electronic circuit of the wave monitors (see Chapter 4). Alternatively, three wave probes were plugged into a DT800 Datataker able to record down to 10mV with a scanning frequency of 20Hz. In order to reduce the instruments sensitivity to external noise the same cable as before were used but also the output voltage of the instrument was set to 10V; 3V was the default value for the datataker and 12V is the maximum voltage allowed by the School of Civil Eng. and the Env. health and safety regulations for exposed hardware (wave probes in this case).

The wave sensors were calibrated before each experiment but this time the calibration graph was created from at least 10 points and the calibration procedure was repeated several times for the same test run; the spatial distance between each point was 1cm. This was necessary because the wave monitor is equipped with a series of amplifiers and resistors used to balance the energisation voltage, measure the input current, compensate for the resistance of the connecting cable and in general ensure that a high linearity of measurements is achieved, but unfortunately such a circuit is not available in the Datataker.

Indeed the voltage-depth of immersion relation was found to follow a power law curve instead of being linear and once more the measured wave heights from each probe were compared with those calculated from side photographs. The wave probes were found to underestimate surface elevation by approximately 25% and as such an

extra calibration factor was applied in order to improve the final data. For this reason, the incoming and transmitted height of every wave used in the present chapter were recorded simultaneously with the probe measurements, which were then corrected accordingly. Although extracting distance from an image can be erroneous (i.e. distortions, measuring point allocation etc) the surface elevation measurements of chapter 4 showed that the final error induced is much smaller than the one observed here.

Control over the Datataker was provided through the same PC employed to control the wavemaker. The editing suite of TestPoint was utilised in order to alter the graphical user interface platform (written by Prof. J.Chaplin), which was originally used to drive the wavemaker and operate the wave gauges. Furthermore, MatLab was again preferred to conduct all the necessary numerical work (i.e. calibration) and for the signal processing. Energy dissipation was estimated for the third wave within each surface elevation time series because it was the first fully developed wave and was also considered to be the less affected by the reflection components of the previous waves.

5.2.3 Wave tracking

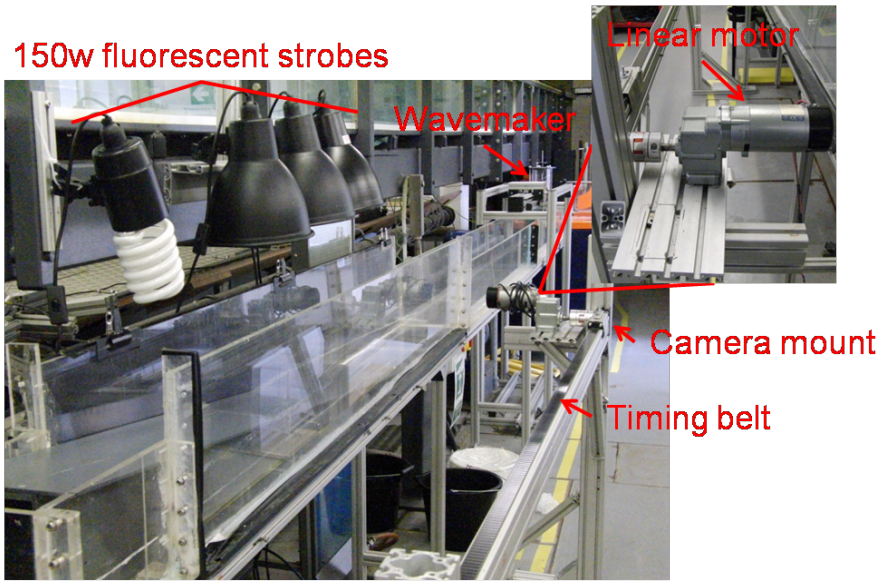

Figure 5.2: The wave tracking system.

Figure 5.2 depicts the mechanism especially built in order to follow the wave evolution within the flume. Video records of the breaking phenomenon were captured with a Casio EX-F1 camera at 300fps (512x384p), 600fps (432x192p) and 1200fps (336x96p), whilst the high intensity lighting conditions required were provided by 4x85w fluorescent strobes. The camera was mounded on a timing belt, driven by a linear motor. Unfortunately the motor was manually controlled and as such each wave was recorded several times in order to achieve for the crest to be located in the middle of the footage. This turned out to be a very laborious process, which finally resulted in the collection of approximately 15Gb of video data.

5.2.4 The isopropyl-alcohol and distilled water solution (IPA)

In order to estimate the effects of surface tension in small scale breaking waves the freshwater was replaced by a 10% isopropyl-alcohol and distilled water solution. McDonald (2005) was the first one who proposed the idea of using such a fluid in the study of small scale plunging breakers. However his research differs from the present because it was focused on the visualisation and study of the air-water interface and not on the investigation of the surface tension influence in micro-models.Other authors like for example Liu and Duncan (2003) have used surfactants (e.g. sodium dodecyl sulphate) in order to reduce surface tension and explore the evolution of spilling breakers. However, the use of such agents requires detailed volume calculations and constant in situ measurements of the mixture's surface tension and viscosity. Unfortunately during the current project neither could be measured.

On the contrary the IPA has a low surface tension ($\sigma_{alcohol} = 0.022 N/m$, $\sigma_{water} = 0.073 N/m$), is completely soluble in water at all concentrations and also forms an azeotropic mixture with it; in such mixtures alcohol does not evaporate. Moreover, distilled water was preferred over freshwater since the composition of the latter can vary over time and result in poor mixing of the two liquids and a final stratified fluid. In order to further assure proper mixing, the solution was stirred prior to each test and was subsequently let to return at a state of calm. The solution was then visually inspected to make sure that no bubbles and / or foam remained in the water column.

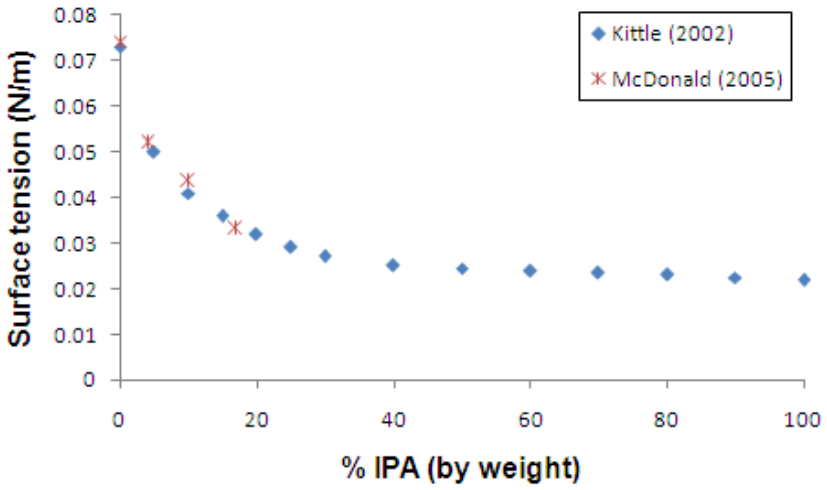

Figure 5.3: Surface tension values of an IPA-distilled water solution over the IPA percentage by weight, after Kittle (2002) and McDonald (2005).

The volume of the IPA in the solution was decided based on Figure 5.3 and the overall effect of the IPA concentration on the solution's viscosity and density. The empirical equation 5.1, proposed by Hirschfelder (1954), was used to derive the viscosity value and the density was calculated with equation 5.2:

$$logv = x_1 logv_1 + x_2 logv_2 \tag{5.1}$$

where,

$v_{1\,and\,2}$: are the viscosities of the IPA and the distilled water respectfully,

$x_{1\,and\,2}$: are their mole fractions

$$\rho_{sol} = 0.1\rho_{IPA} + 0.9\rho_{dwater} \tag{5.2}$$

where,

$\rho_{sol,IPA,dwater}$: are the density values of the solution, the IPA and the distilled water

Accordingly it was decided that a 10% IPA concentration reduces sufficiently the surface tension to 0.0436N/m instead of 0.073N/m (at 20°C) but without significantly altering the mixture's kinematic viscosity and density, $1.027*10^{-6}m^2/s$ instead of $1.005*10^{-6}m^2/s$, and $976kg/m^3$ instead of $998kg/m^3$. The latter entails that except from the surface tension the other properties of the solution remain

similar to freshwater, which is considered a valid surrogate of seawater, see Blenkinsopp and Chaplin (2007).

5.3 Results

5.3.1 Waves breaking in freshwater

The primary goal of this chapter is to provide information about the amount of energy dissipated by waves breaking in a micro-model. Accordingly the experiments described in the current section were designed to investigate the proportion of the incident wave energy consumed as waves shoal over an 1:20 slope and finally break over a plateau. For different initial conditions both plunging and spilling breakers were created, the incident and transmited wave heights were measured in prior and post breaking locations, and estimates on the energy dissipation were made according to linear wave theory and:

$$E_d = E_i - E_t \tag{5.3}$$

where,
E_d : is the energy dissipated during breaking
E_i : is the incident wave energy
E_t : is the transmitted wave energy

In these tests more than 100 different wave cases were examined with the final incident wave steepness varying in the range $0.0132 < H_i/L < 0.0868$; very steep waves that broke near the wavemaker were excluded from the final measurments. The wavemaker frequencies were chosen as such in order for the generated wavelengths ($2.8m < L < 0.35m$) falling within the limits of surface tension effects in breaking waves as referred to in Tulin (1996). The tracking system previously described was used to capture the evolution and deformation of plunging and spilling breakers which were chosen based on preliminary observations.

Due to the small water depth in the wave flume (d=0.13m) all the waves with L > 0.26m were propagating either in intermediate or in shallow waters. Linear wave theory was used for the transformation of the wave properties (Hi, L) measured in the deepest section of the tank to their deep water equivalent:

$$\frac{H_i}{H_o} = (tanh(kd(1 + \frac{2kd}{sinh(2kd)})))^{-0.5} \tag{5.4}$$

where

H_i : is the wave height measured near the wavemaker

H_o : is the deep water wave height

k : is the wave number

d : is the water depth

Figure 5.4 presents the energy loss due to breaking as a function of the non-dimensional surf similarity parameter and the incident wave steepness as measured near the wavemaker. It is shown that the proportion of the incident wave energy consumed during breaking varied in the range of 17% to 78% for plunging breakers and 25% to 88% for spilling breakers. Dissipation values for plunging waves agree reasonably well with those presented by Chanson and Lee (1995) for waves breaking over a submerged reef and are within the same range as those measured by Yuksel and Kapdasli (1994); Kapdasli and Turker (2002).

Moreover, waves which according to the classification of Battjes (1974) would be expected to break in a more spilling way consume more energy than the more intense plunging breakers. One possible explenation for that would be that although plunging waves are more energetic during the initial phase of breaking, spilling breakers transport turbulent kinetic energy seawards and dissipate energy for longer and over a larger area. Further support to that is provided by Lamarre (1993); Yasuda et al. (1999) who suggested that the plunging wave's energy is mainly dissipated for the generation of turbulence, splash and air entrainment at the point of impingement and also by the measurments of the turbulent kinetic energy under breaking waves by Ting and Kirby (1995, 1996).

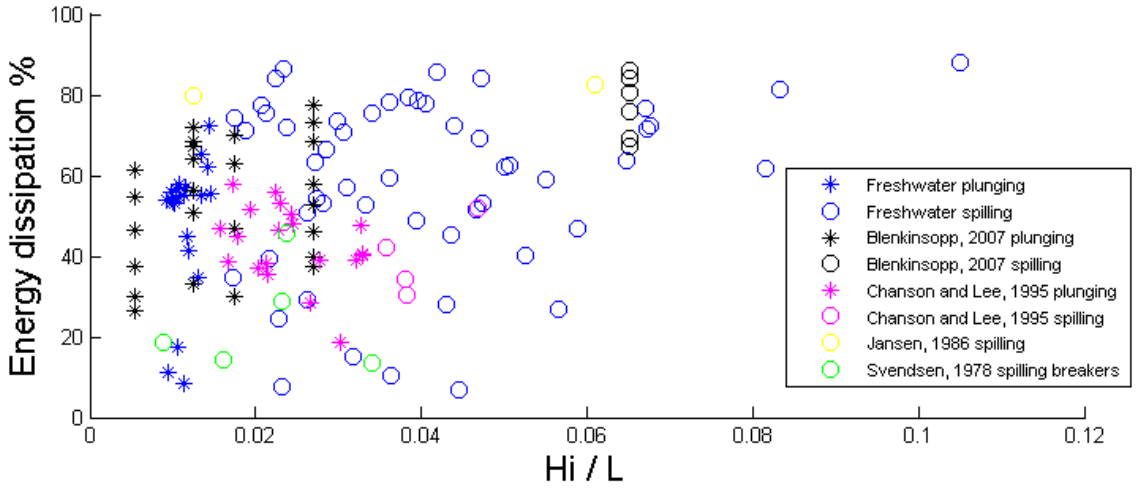

Figure 5.4: Wave energy dissipation as a function of the surf similarity parameter

Nevertheless, Blenkinsopp (2007) and Jansen (1986) also presented similarly high dissipation values (67%-87%, 82%) for waves spilling over a reef and a 1:30 smooth slope respectively, but Svendsen et al. (1978) recorded significantly smaller rates (13%-43%) for spilling breakers on a 1:34 slope.

Although encouraging, results presented so far do not describe the mechanics of the breaking phenomenon in micro models. For this reason the evolution and deformation of waves inside the tank were visualized and the results are now presented.

5.3.1.1 Characteristics of waves breaking in freshwater

Experimental and numerical results by researchers like Duncan (2001) and Banner and Peregrine (1993) have thus far indicated that for long waves the initial stage of breaking is unaffected by surface tension and a small jet is freely formed at the crest. On the contrary, for small wavelengths (i.e L $<$ 2m), the jet is replaced by a bulge, on the lower edge of which a toe is formed, capillary waves are generated on the shoreward face of the breaker and as the phenomenon progresses ripples are formed between the toe and the bulge. Perlin and He (1996) and Duncan et al. (1999) have visualised such surface pattern for both plunging and spilling breakers generated by a packet of waves with central frequency of 1.4Hz and 1.42Hz respectively.

In the current work the tracking system discribed previously was used to capture the breaking event; wave frequencies ranged from 0.3Hz to 2Hz and wave heights from 0.028m to 0.06m. The experimental series involved tests for a 1:20 slope followed by a plateau, with water depths of 13cm and 10cm and also a 1:10 slope with d = 13cm.

Figure 5.5 presents a frame shot sequence of a plunging breaking event inside the small wave tank. In the following description the upstream direction is defined as toward the left and the forward face of the wave is on the left as well. As can been seen for a wave with T = 1.5sec and H_i = 0.05m the breaking process starts with an asymmetric wave profile (t = 0sec). For t = 0.024sec the wave front steepness further increases and its uppermost part becomes rounded and projects out. This rounded tip has been previously highlighted by other researchers, like Duncan et al. (1994a) and Dommermuth et al. (1988), and is commonly referred to as the bulge. On the upstream edge of the bulge a discontinuity of the front face, called the toe, is also observed (small darker area). As the process progress the bulge increases in diameter and the toe moves further down the upstream direction (t = 0.1241sec).

The breaking procedure described thus far agrees well with the numerical results of Longuet-Higgins (1997) for a 1.32m long wave with σ = 0.073N/m. For t = 0.1717sec the bulge is further projected out and gradually reshapes to a jet-like structure, the toe is no longer visible, while the spilling phase observed on the front face of the wave was confirmed to be a side wall effect. Indeed placing the camera with an angle to the wave direction verified that this spilling phase was restricted near the side wall, did not exist prior to the commencement of the overturning motion and it was soon after the impact consumed by the subsequent splah up. Almost 0.12sec later the jet grows larger, curves down towards the underlying surface of the crest, and a small pocket of air is created. At t = 0.3366sec the elongated jet impacts on the leading wave face. At the point of impingement a cavity of air with an anti-clockwise circulation is created between the jet and the wave face.

Soon after that (t = 0.3825sec) a plume is formed due to the reactionary splash-up caused by the jet impact, the fragmentation of the air cavity evolves, and air bubbles

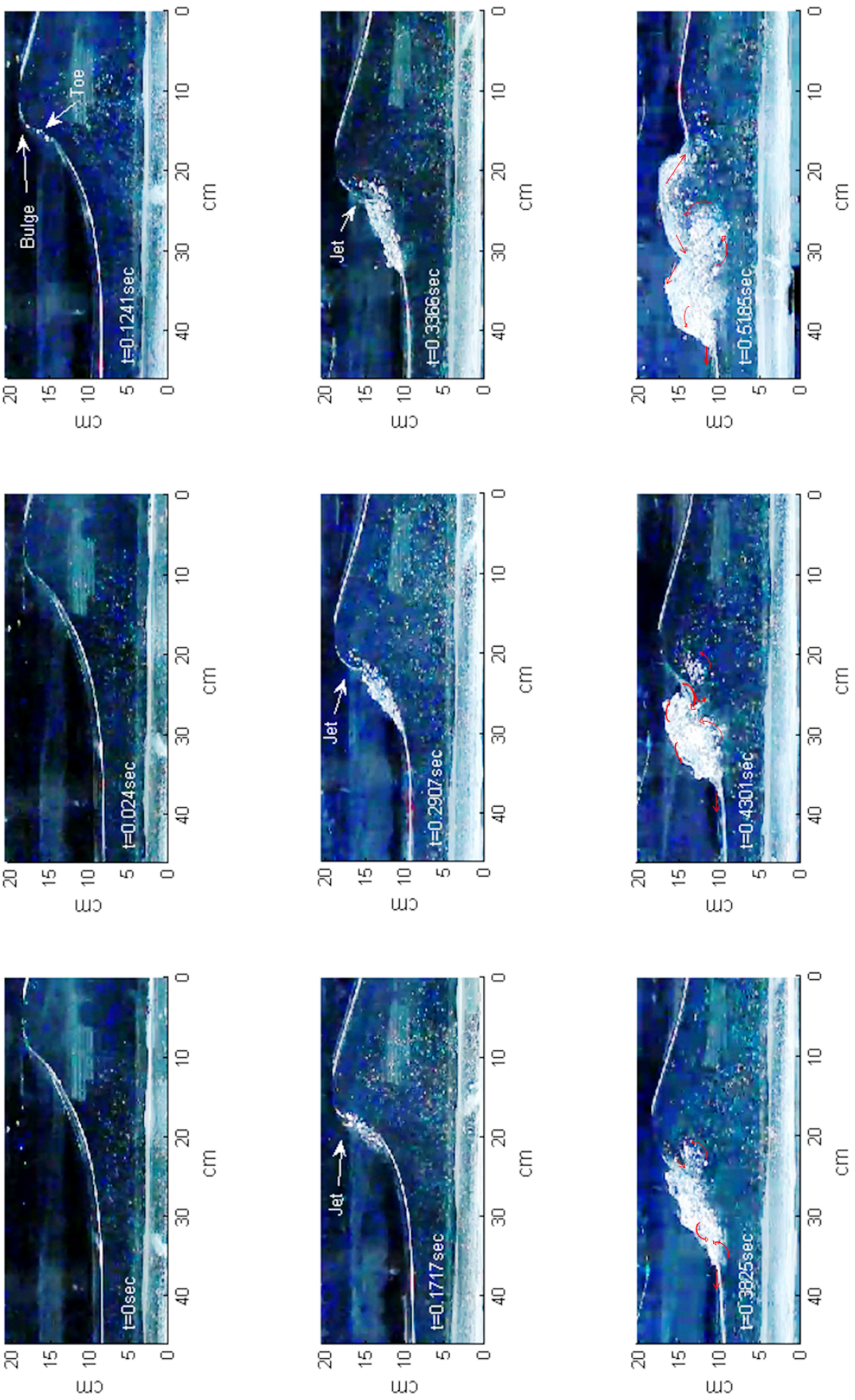

Figure 5.5: Profile history of a plunging breaker with T = 1.5sec and H_i = 0.05m, part a

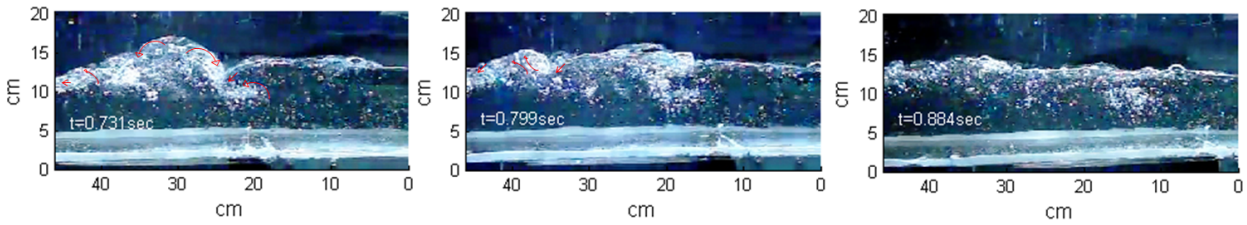

Figure 5.6: Profile history of a plunging breaker with T = 1.5sec and H_i = 0.05m, part b

are created. As the red arrow indicates, the anticlockwise circulation of the cavity advects the entrained bubbles and ultimately a small portion of them is re-circulated through the jet. The plume propagates shoreward along with the wave and two major, opposite moving, eddy structures are observed. After approximately 0.05sec (t = 0.4301sec) the jet motion develops further and creates a shear zone, the plume increases (mainly) in width and part of it is now moving downstream. The air cavity has almost disappeared and replaced by a second plume, which retains the anti-clockwise circulation pattern but appears to be detached from the free water surface. At t = 0.5185sec the plunging jet has fully collapsed, the secondary plume has dissolved, the splash-up continues and the primary plume evolves through a very complicated turbulent regime.

The profile history of a plunging breaker in a micro model is concluded in Figure 5.6. At t = 0.731sec the plume still moves shoreward but it reduces in size, the splashing intensity also decreases significantly, and air bubbles are mainly detrained, float towards the surface and burst. A similar pattern is observed for the last two images were the splash-up stops and air detrainment mainly takes place. In general though it is seen that since t = 0.5185sec the large scale deterministic flow breaks up into small scale details of turbulent nature, which remain almost until t = 0.0884sec. A similar behavior has been observed by Svendsen et al. (1978) for waves breaking on a smooth slope (1:34), and is commonly resembled to a moving bore or a hydraulic jump. The same plunging process was repeated with reduced surface tension and the results are presented and compared later in this chapter.

Nevertheless, the effects of surface tension were found to increase in significance as the wavelength and wave height decreased. The latter is better displayed in 5.7 were

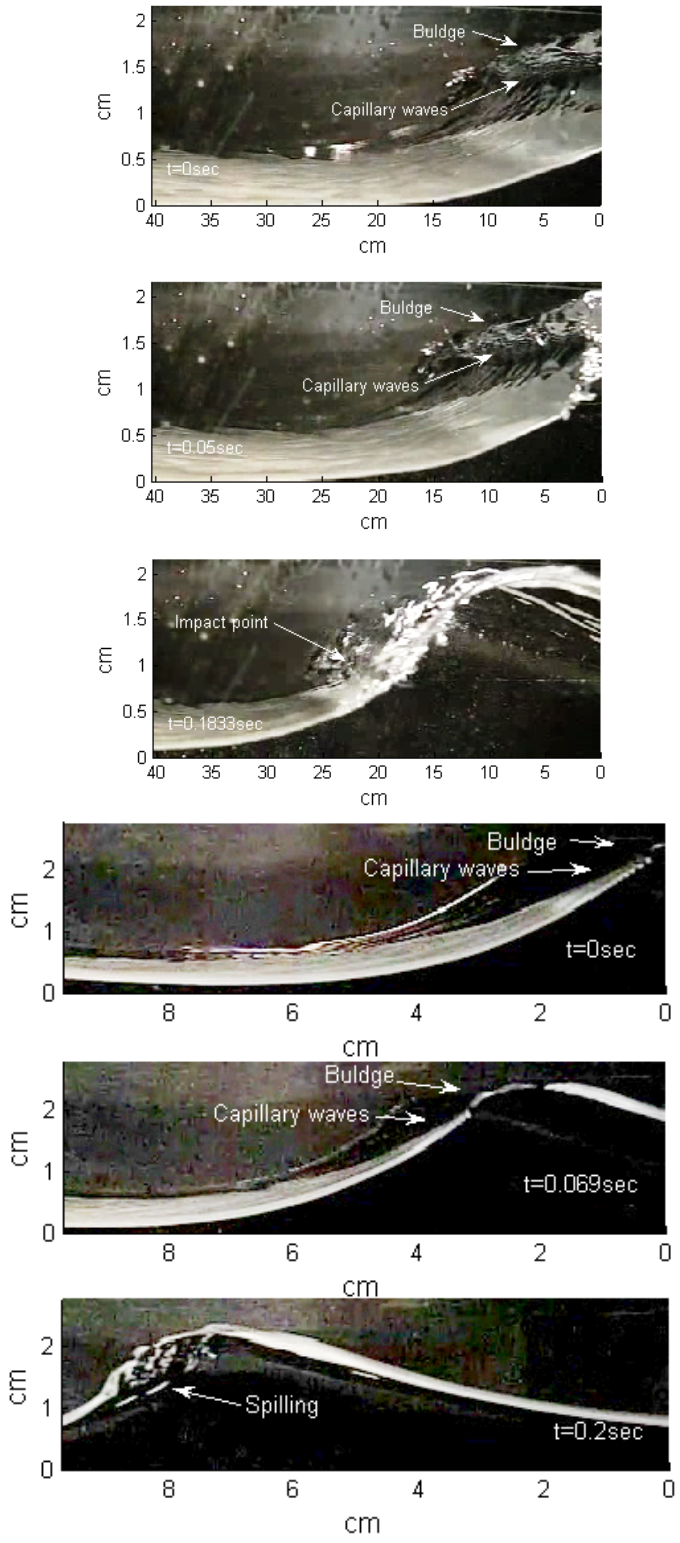

Figure 5.7: Profile hystory of a. a plunging breaker with L = 0.6m and H_i= 0.015m and b. a spilling breaker with L = 0.47m , and H_i= 0.022m

the profile history of a plunging breaker with L = 0.6m is presented. The breaking event starts with the development of a bulge (t = 0sec), which increases in amplitude (t = 0.05sec), curves over and finally impacts on the underlying water surface (t = 0.1833sec) without forming a jet at any time instant. This observation confirms previously published studies which suggest that for L < 0.5m, the plunging jet is replaced by the bulge.

The existence of capillary waves upstreem of the leading edge of the bulge is verified in Figure 5.7 for both a plunging and a spilling breaker. These surface tension waves traveled downstream, with increasing amplitude while their number dicreased with time. Although small in size such structures should have an effect on the energy regime of the gravity wave, since energy is required in order for them to form and grow in amplitude. In a laboratory environment were no wind is used, this energy can only be substracted from the gravity wave. Even more, it can be seen in the work of Longuet-Higgins (1994) and Longuet-Higgins (1996) that the presence of such patterns in conjunction with the toe movement can start the spilling process without the overturning of the water surface. Further support to that is provided by Qiao and Duncan (2001), who measured the horizontal fluid velocities near the surface, under the toe and found them to be up to 1.4 times larger than the crest speed. They also found that these features are unreleated to the wave period (T) and their length scale with $\sqrt{\sigma/\rho g}$ (where, σ is the surface tension and ρ is the water density).

In summary results presented thus far indicate that the micro modelling of breaking waves ($2.8 <$ L < 0.35m and H < 0.08m) can be significantly biased by surface tension effects. It has been shown that although energy dissipation measurements agree well with previously published values, the breaking phenomenon inside the small scale tank can be dictated by processes different than those observed in nature (bulge formation, capillary waves etc). If for example a 2m long wave is scaled to a 0.2m wave the surface patterns observed during this study will remain at about the same physical size (assuming similar σ) and therefore cover a larger fraction of the wave. Furthermore, surface tension can significantly alter air entrainement, bubble formation and break up, and vortex speed.

5.3.2 Waves breaking in the IPA solution

The dramatic effects of surface tension in short waves and / or weak breaking events in clean water (i.e bulge and toe formation etc) have been numerically and experimentally investigated by previous researchers like Ebuchi et al. (1987), Ceniceros and Hou (1999) and Wang and Tulin (1996). Later, Liu and Duncan (2006, 2003) and Ceniceros (2003) observed that for waves spilling in the presence of surfactants and for $\sigma = 0.037$N/m a bulge still forms, but without a toe and without capillary waves, and after a short time period a jet emerges from the bulge. The jet ejects forward and re-enters the front face of the wave, causing a more violent surface motion. Although very useful these studies are mainly focused on spilling breakers and do not refer to the energy consumed by the broken wave.

On the other hand McDonald (2005) used an IPA solution and measured the energy dissipated by small scale (L $<$ 0.7m) plunging and spilling breakers in a wave flume. The author reported the absence of capillary waves and recorted energy dissipation values that ranged between 92% and 98%, for both breaker types. McDonald (2005), however, did not seek to spot out the differences between the IPA solution and freshwater, and he mainly focused on the visualisation of exchanges on the air-water interface. Furthermore, Dimas (2007) provides numerical evidence that energy dissipation by spilling breakers increases with increasing We, whilst the peak strength of the sub-surface vortex in the spilling region decreases. Thus it is seen that although the importance of surface tension in small scale waves has been previously studied the concept of using fluids with reduced σ in small scale physical models has never been realised before.

Consequently, the same experimental procedure as before was repeated but the freshwater was replaced by a 10% isopropyl alcohol and distilled water solution (IPA) ; the new fluid had a reduced $\sigma_{IPA} = 0.0436$N/m instead of $\sigma_{water} = 0.073$N/m for freshwater. As mentioned previously the relative importance of surface tension is expressed by the non-dimensional Weber's number (We). For the current experimental series We was calculated at the breaking point according to:

$$We = \frac{\rho C d_b}{\sigma} \tag{5.5}$$

where:

ρ : is the fluid's density

σ : is the fluid's surface tension

C_b : is the celerity of the particle located at the top of the crest at the break point

d_b: is the water depth at the break point

The breaking point was defined based on the description provided by Iversen (1952) as the location where any portion of the front face of the wave becomes vertical. The d_b was selected as the representative length for We since particle parameters are mainly affected by it, and it was measured in still frames as the vertical distance between the SWL and the slope. Originally, linear theory was used for the estimation of the wave's velocity at the break point ($C_{wb}=\sqrt{gd_b}$) and C_b was calculated according to:

- Dimas (2007), who for spilling breakers found the instantaneous speed of the breaker crest (assumed here to be the particle's velocity as well) at the break point to be $1.03C_{wb}$ and independent of We,
- Perlin and He (1996), who measured the horizontal speed of the plunging jet to be 30% greater than the phase speed of the wave.

Thus, We ranged from 1207 to 4010 for the IPA instead of 582 to 969 for the freshwater. For the same input conditions in the wavemaker, Figure 5.8 presents the percentage of energy dissipation over the incident wave conditions. It is seen that plunging breakers are now almost as dissipative as spilling breakers and dissipation values range between 69% and 97%. When compared with the freshwater case, energy dissipation values are highly increased (i.e. 93% for the IPA instead of 58% for the freshwater), while the scatter of the data is significantly reduced, indicating possibly that energy consumption is now less sensitive to Hi and L. In every case plunging breakers dissipate more energy when the surface tension is reduced, and the energy dissipation is more consistently high with spilling breakers in the IPA solution.

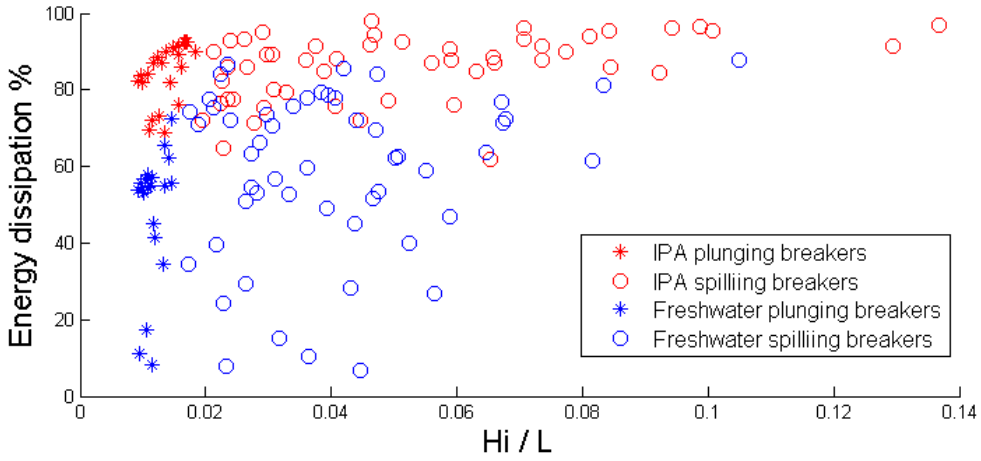

Figure 5.8: Wave energy dissipation in the IPA solution as a function of incident wave steepness

As mentioned previously, several mechanisms act during the breaking process and extract energy from the gravity wave; these mechanisms mainly refer to entrainment of air, formation of bubbles, splash-up, trasformation of potential energy to turbulent kinetic energy etc. Unfortunately for the current project distinct flow features like void fraction, bubble size etc could not be accurately measured, hence the comparison between the IPA and freshwater results was based on the qualitative analysis of a series of videos and the information extracted by still frames. Nevertheless, as it is later shown the differences between the two liquids are so pronounced that the final conclusion can not be disputed by the lack of highly accurate measurments.

5.3.2.1 Characteristics of waves breaking in IPA and comparison with freshwater

The profile history of a plunging breaker in the IPA solution is presented in Figure 5.9. Once more the wave is pictured to shoal (t = 0sec), but for t = 0.024sec, a bulge is not formed. Although the upper most point of the crest is rounded for t = 0.1241sec, a toe is not seen, while almost 0.05sec later a jet is clearly developed and projected upstream of the wave crest. At t = 0.2907sec the jet elongates, curves over the underlying water surface and a larger pocket of air is formed between the plunging jet and the wave face; the spilling phase is again a side wall effect. 0.045sec later the jet struck the free water surface, a well pronounced cavity of air develops,

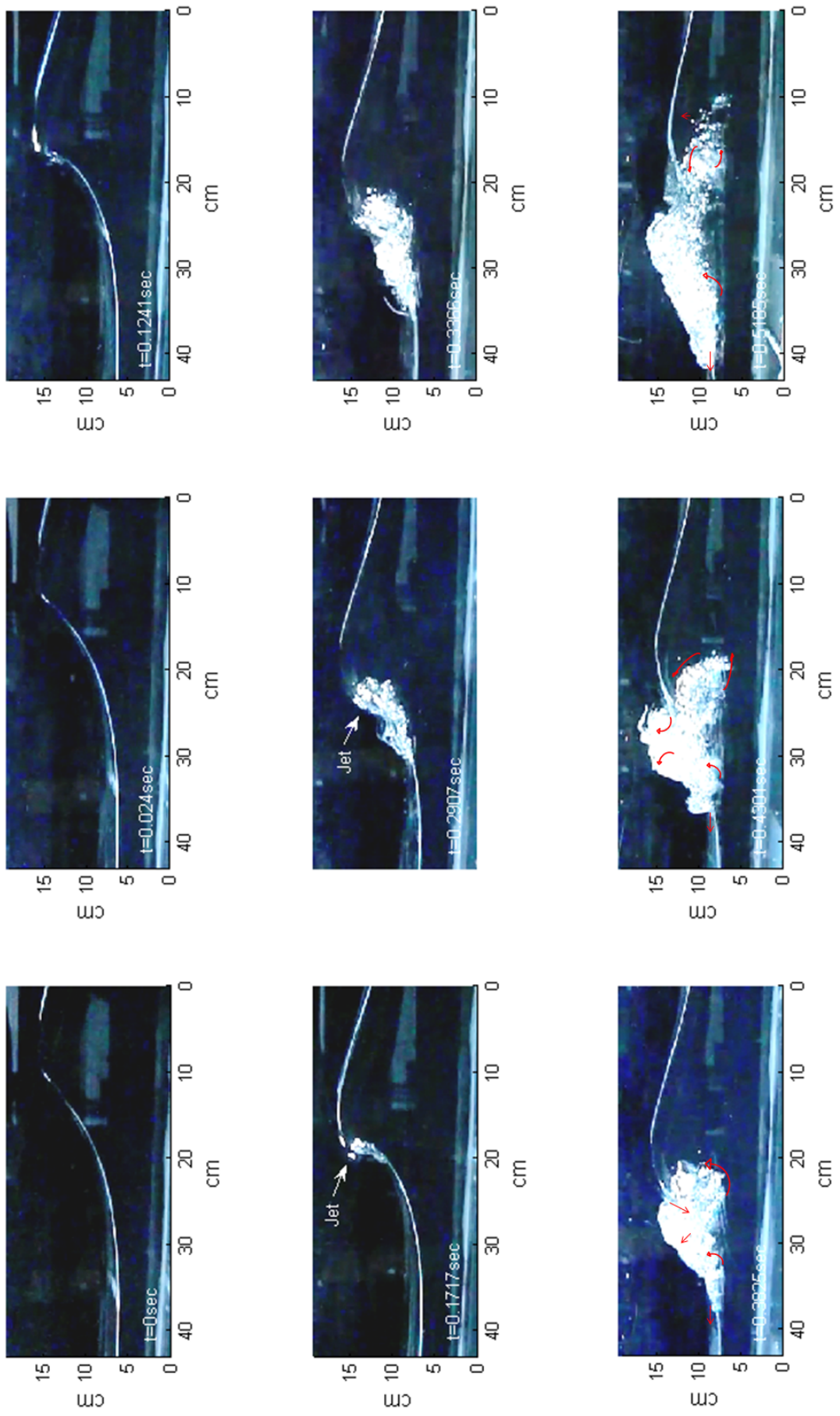

Figure 5.9: Profile history of a plunging breaker with T = 1.5sec and H_i = 0.05m, part a

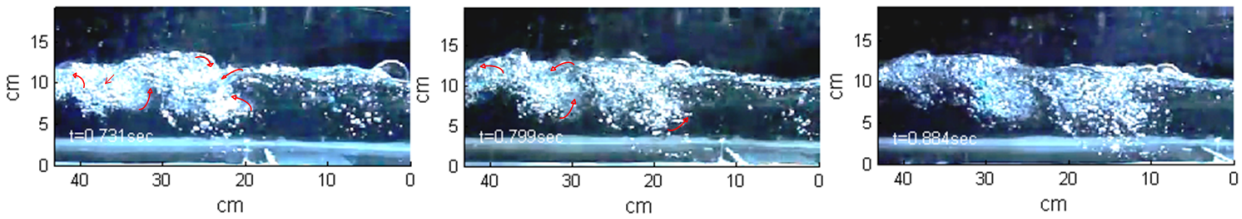

Figure 5.10: Profile history of a plunging breaker with T = 1.5sec and H_i = 0.07m, part b

and the reactionary splash-up causes again the generation of a plume. The bubbles which surround the air cavity move in an anti-clockwise motion, a feature which is better depicted for t = 0.3825sec.

Meanwhile, the jet motion continues, the plume size increases, and more bubbles are created from the fragmentation of the air cavity; red arrows indicate the instantaneous flow circulation. At t = 0.4304sec the width of the primary plume exceeds in size the residual wave height, whilst the cavity remnants are gradually transformed into a secondary plume which retains its anti-clockwise rotation. A similar flow patern is depicted for t = 0.5105sec, but bubbles are now start to detrain from the secondary plume and to float freely towards the surface. The breaking event is concluded in Figure 5.10 were the plunging jet has fully collapsed, splash-up motions reduce in intensity (from t = 0.731sec to t = 0.799sec) and finaly stop at t = 0.884sec. At this latter stage the quiscent phase of the plume starts and the bubbles rise to the surface.

5.3.3 Observation on breaking intensity

Throughout the whole experimental procedure it was observed that the waves were breaking in a more plunging manner in the IPA solution while the characteristic noise produced during breaking was stronger than the corresponding noise for the freshwater case; in other words the intensity of the breaking event was increased. Several authors like Yasuda et al. (1999), Fairley and Davindson (2008), and Govender et al. (2002), have linked breaking intensity with energy dissipation. They suggested that as oceanic waves become more plunging, the amount of turbulence

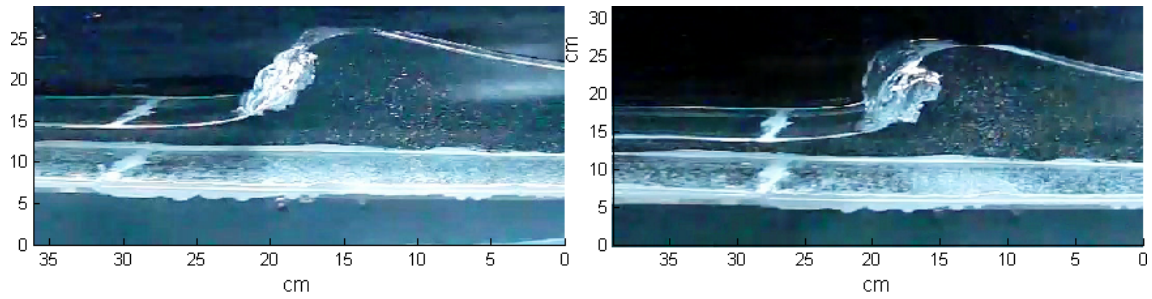

Figure 5.11: Plunging breakers in freshwater (left) and in the IPA solution (right); T = 1.5sec

increases, along with the splach-up and air entrainment, all of which contribute to the energy dissipated. Mead and Black (2001), analysed crest parallel images of plunging breakers in nature and related the breaking intensity with the size of the air 'pocket' formed in between the overturning jet and the wave face. The authors used the parametric solution of the equations of motion provided by Longuet-Higgins (1982) to estimate the tube's length and width. They concluded that when the vortex was larger the wave broke in a more violent way.

Consequently it is seen that the existed literature suggests that breaking intensity is an important feature of breaking wave and it needs to be considered in every physical model, including micro-models. Nevertheless, the frameshots for t = 0.3366sec in Figure 5.9, and Figure 5.5 indicate that a larger and more pronounced vortex is formed when the surface tension is reduced. The latter is better depicted in the following image, were the input to the wavemaker was the same as for Figure 5.9, but the water depth in the deep section of the flume was reduced to d = 0.1cm. This experimental series (reduced water depth) was prefered for the measurements presented in the current section since it was observed that waves were breaking more intensely and a vortex with a more open shape was formed; similar field observations from surfers have been reported in Sayce et al. (1999).

Accordingly vortex length (l_v) and width (w_v) were measured for selective cases. Frameshots depicting the time instant prior to impact were extracted from the video sequenses and a cubic curve was fitted to the vortex using a MATLAB routine described in Gorman (1999), (Figure 5.11). In most pictures (and especially for the freshwater), due to the friction with the side wall, water had been entrained in the

Frequency (Hz)	Amplitude (V)	l_v (cm)	w_v (cm)	l_v/w_v	Area ($= \frac{1}{5}\sqrt{2}\sqrt{6}l_v w_v$, after Mead and Black (2001))	Energy dissipation (%)	Fluid
0.4	2.8	2.1	1.1	1.9	1.6	72.4	Freshwater
0.55	2.6	2.8	2.1	1.3	4.1	77.5	Freshwater
0.75	2.8	2.8	1.5	1.9	2.9	70	Freshwater
1	1.6	-	-	-	-	62	Freshwater
0.4	2.8	5.7	2.7	2.1	10.6	86.1	IPA
0.55	2.6	6.6	3.1	2.1	14.3	92.9	IPA
0.75	2.8	4.3	2.3	1.9	6.8	82.3	IPA
1	1.6	2.8	1.2	2.3	2.33	85	IPA

Table 5.1: Vortex characteristics for freshwater and IPA; the first two columns includes the wavemaker input parameters

vortex and made the determination of the tube's boundaries difficult. In order to overcome this, the images were processed (increased contrast, brightness adjustment) prior to the fitting of the curve and the procedure was repeated 3 times for every wave; l_v measurements differed by approximatelly $\pm 7\%$ and w_v by approximatelly $\pm 12\%$. However it should be made clear that the purpose of these measurements was not to accuratelly measure vortex sizes but to highlight the observed differences between the freshwater and the IPA solution. For more detailed laboratory measurements on the intensity of shallow water breaking waves, the keen reader is referred to the work of Blenkinsopp (2007).

Table 5.1, presents the measured vortex length, width, area and energy dissipation values for both liquids. It is seen that for the IPA solution the vortex characteristics increase significantly, with maximum differences for l_v and w_v to be 3.8cm and 1.1cm respectively. These values are in accordance with observations made in Figure 5.5 that the formation of the bulge on the top of the breaking crest results on the formation of a smaller air tube. Moreover, although l_v / $w_v$ratios increased for reduced surface tension, they remain within the range of values presented by previous researchers like Mead and Black (2001) (max. 3.43 and min. 1.42) and Couriel et al. (1998) (max. 3.4 and min. 1.5) suggesting that the breaking conditions remain realistic.

Furthermore for the freshwater experiments and L $<$ 0.7m (1Hz and 1.6V) the jet

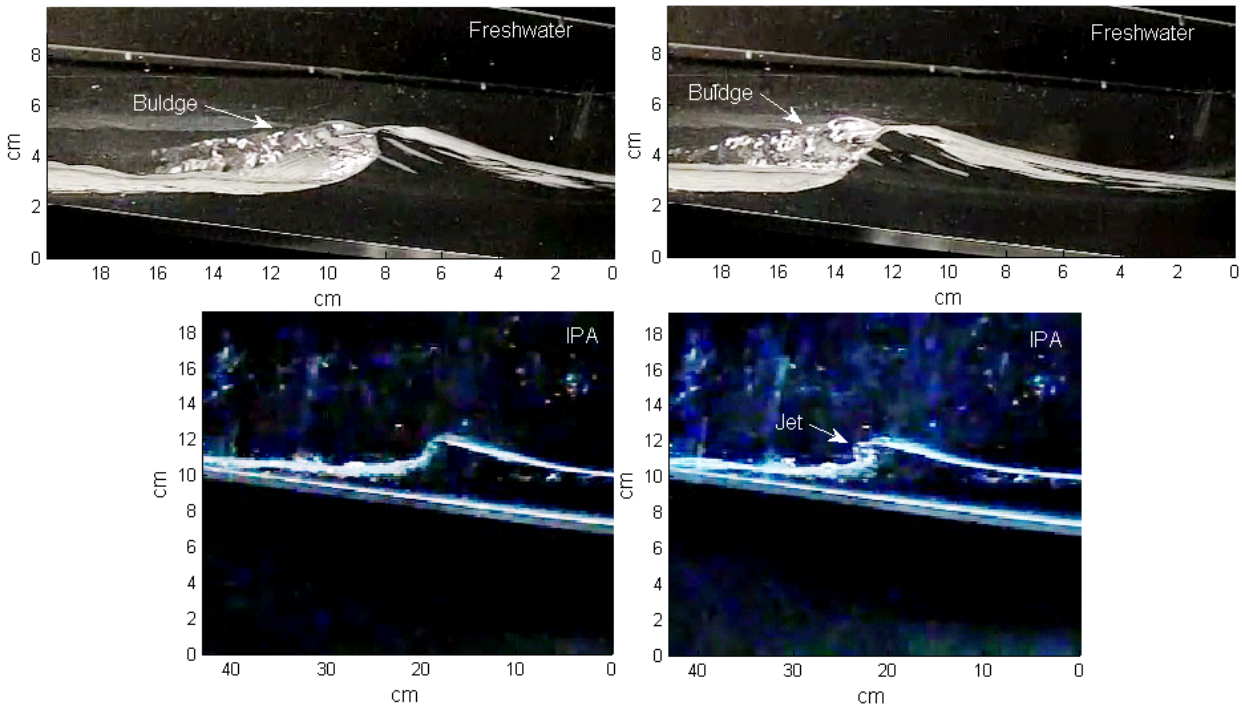

Figure 5.12: Plunging breaker in freshwater for L = 0.5m and H_i= 0.02m (above) and in the IPA solution for L = 0.38m and H_i= 0.025m (below)

structure was gradually replaced by the bulge. For example, in Figure 5.12 it is shown that the bulge structure is not transformed to a jet and it appears to surf on the crest face instead of plunging on it. In this case a vortex is not formed and air is entrained (not shown here) possibly due to the shear developed between the bulge and the free water surface. On the contrary in the IPA solution clear plunging breakers were created even for L = 0.3m and H_i = 0.022m (Figure 5.12). Unfortunately, the small size of the waves in conjuction with the low camera resolution prevented the measurements of the vortex size for these waves.

Even more, it is seen in Table 5.1 that energy dissipation is strongly related to the area of the vortex. Waves in the IPA solution form a larger vortex, break more intensely and dissipate more energy. This is not suprising since similar and more detailed results have been previously reported by Blenkinsopp (2007) for waves breaking in a large wave flume. A possible explenation is that more air is trapped and thus more of the gravity wave's energy is spend to entrain it.

Findings presented here are of importance not only for micro-models but for larger physical models as well. It is shown that surface tension significantly affects the

breaker geometry even for waves with L = 1.5 m and H_b = 0.1m (H_b is the wave height at breaking), which entrain less air and break in a less violent manner. This contradicts Couriel et al. (1998), who suggested that the breaker geometry is unaffected for waves heigher than 0.05m; an argument often used in physical model studies.

5.3.4 Observations on air entrainment

In the previous section it was shown that in micro-models, waves with the same initial conditions brake in a more intense manner for larger We and a larger amount of air is trapped under the plunging jet. Moreover, the formation of clean plunging breakers was also made possible for the smallest wave parameters employed in the current project.

However in order for similarity to be achieved between a micro-model and the prototype several aspects of the breaking event need to be in similitude. These aspects contribute to the dissipation of energy and include the mechanisms evolved during breaking, the amount of entrained air, the formation and distribution of bubbles etc. Although research focused on scale effects in turbulent air water flows (i.e hydraulic jumps) and especially in air entrainment by breaking waves has been contacted in the past, the information available is contradictory, see for example Blenkinsopp and Chaplin (2007).

A detailed reference to key research findings by previous authors can be found in appendix A, but in summary the existed literature suggests that the veracity of a physical model strongly depends upon its size/scale, the effects of which are more important than the influence of the water type. Even when the same mechanisms are evolved (i.e. plunging breakers of Blenkinsopp (2007)) important flow features like the plume evolution, cannot be accurately reproduced if the scale selected is not sufficiently large. Consequently it is seen that all previously published studies prohibit the modelling of breaking wave in micro-models due to their very small size and mainly due to the increasing importance of surface tension. However,

observations are now presented which show that if the surface tension effects are mitigated then the micro-modelling of breaking wave might be possible.

5.3.4.1 Observations on air entrainement: Amount of entrained air and air cavity fragmentation

In 2D models it is commonly accepted that all of the air trapped by the overturning jet is subsequently entrained in the water column. Originally Oguz and Prosperetti (1989) studied the effects of surface tension in the contact areas of liquid surfaces and later Prosperretti and Oguz (1997), assumed the effects of surface tension and viscosity to be negligible and concluded that the volume of air entrained by a single jet impact depends only on the jet's Froude number. This clearly implies that the amount of air trapped by the plunging event should scale geometrically.

However, Table 5.1 and Figure 5.11 suggest that in micro-models even for long and relatively high waves (i.e L = 1.5m and H_b = 0.1m), surface tension effects are important and they can not be neglected. The presence of the bulge followed by the toe, alters the breaking event and the breaker geometry and suppresses the size of the vortex which finally diminsh for L < 0.5m (Figure 5.12). On the contrary for the IPA solution a vortex is clearly formed for all cases investigated in the current project, and its size compares directly with previous studies. All that sugest that the amount of entrained air can scale geometrically in micro-models but only when the surface tension is reduced.

Thus far evidence has been presented, which indicate that more air is entrained by plunging breakers in the IPA solution. Accordingly it is not surprising that the plume formed under the collapsing cavity is significantly larger than that for freshwater (Figure 5.5, Figure 5.9 for t = 0.3366). Moreover the temporal evolution of the plume is also larger as it is seen that for t = 0.5185sec a small number of bubbles rise back to the surface but the circular motion persists in the main bubble cloud. On the contrary in the freshwater case the plume has been fully dispersed. Although the measurement of the bubble size is not favoured by the small resolution

of the images (max. 512×384p, for 300fps) observations indicate that when the surface tension was reduced the size of bubbles reduced as well.

Bubbles burst when the differential pressure forces exceed the restoring force of surface tension, or else, when the critical value of the bubble's Weber number is exceeded (see equations A.1 and A.2, in appendix A). Assuming the same bubble radius d_b= 7mm in seawater and freshwater and if the peak vorticity values inside the plume are the same as those given by Dimas (2007) under the turbulent surface of spilling breakers, for We = 10, $|\omega|_{max} = 0.1741$ and We = 5, $|\omega|_{max} = 0.1783$, and by substituting ρ, σ, and ν in equations A.1 and A.2, it is easily calculated that the bubble burst limit for both $We_b$and $Re_b$is met only when the IPA solution is used. In other words because the ratio of inertia forces to surface tension and viscosity is larger for the IPA, larger bubbles break up easier into smaller ones.

Furthermore, the examination of all the available videos revealed that regarding the cavity fragmentation, qualitative similarities exist between all the wave parameters / sizes employed in the current project. This is better illustrated in the following Figure were image a. presents the breaking wave crest for L = 1.4m and H_i = 0.07m, b. for L = 0.6m and H_i= 0.03m, and c. for L = 0.3 and H_i= 0.022m. All three frameshots compare very well with Figure 2b (page 840), in Dean and Stokes (2002), for a 2.3m long wave in a 33m long, 0.5m wide and 0.6m deep wave tank. On the contrary when freshwater was used the bulge structure dominated the wave crest and eventually surfed over it without forming an air cavity.

Observations presented thus far, show that when the freshwater is replaced by the IPA solution, waves break in a more violent manner, more air is entrained, and a greater number of finer bubbles is formed by the cavity fragmentation which has a longer temporal evolution. All that can partly explain the differences in energy dissipation between the two fluids. Although to this authors knowledge the size of the plume has not been linked before to the amount of energy dissipated during breaking, it is generally acceptable that 1. energy dissipation increases with the vortex area, 2. energy is transformed to turbulent kinetic energy under the plunging jet, 3. is spent against the buoyancy force of the bubbles.

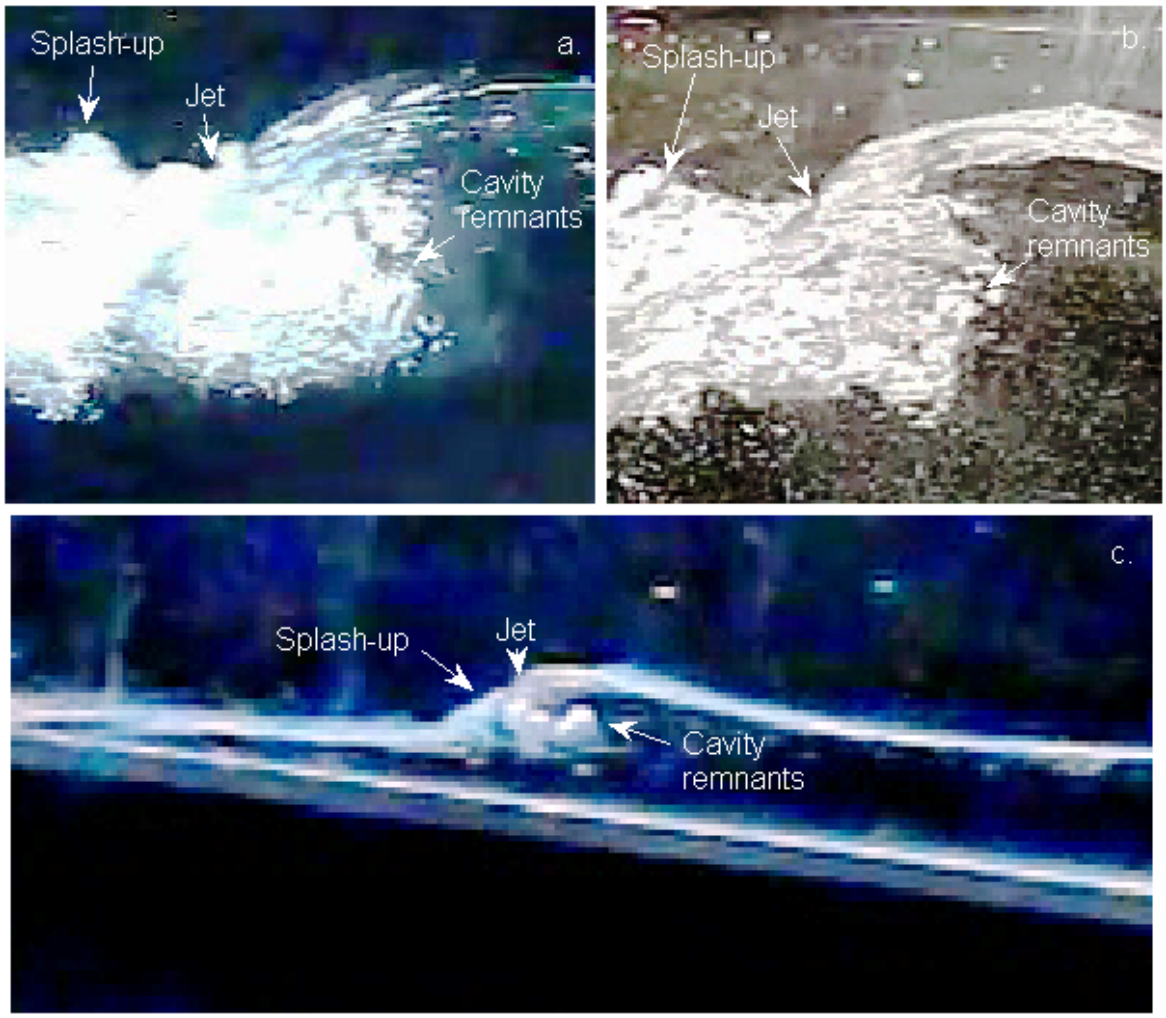

Figure 5.13: Frameshots of the bubble plume for three different incoming wave conditions, a. for L = 1.4m and H_i = 0.07m, b. for L = 0.6m and H_i= 0.03m, and c. for L = 0.3 and H_i= 0.022m.

5.3.4.2 Observations on air entrainment: Jet impact and splash-up

As the plunging jet impacts the water face it causes the reactionary splash-up. which in turn results on the formation of a secondary plume. Air is originally trapped in large cavities which break up into smaller bubbles under the action of the strong shear flow developed by the interaction of the impinging jet with the water column. Frameshots depicting all that are presented in Figure 5.5 for freshwater and in Figure 5.9 and Figure 5.13 for the IPA solution. It is clearly seen that when the surface tension is reduced the splash-up shoots-up heigher and for t = 0.4301sec it surpasses the residual wave crest height, whilst the secondary plume formed is again larger than the one in freshwater; the differences in the plume size and bubble

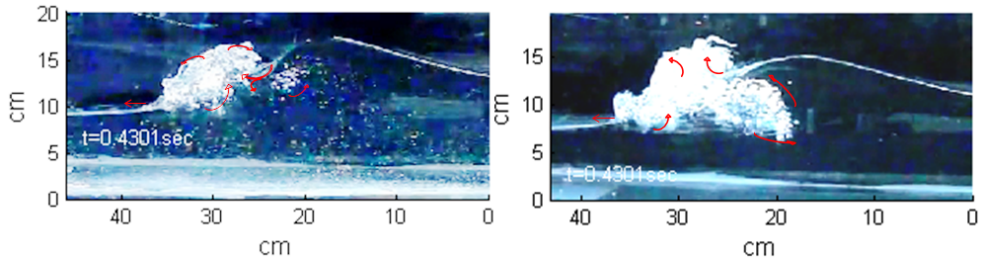

Figure 5.14: Frameshots of the breaking event for a wave plunging in fresh-water (left) and in the IPA solution (right).

formation between the freshwater and the IPA fluid are better illustrated in Figure 5.14.

Moreover, Figure 5.13 shows that this secondary plume is surrounded by a population of smaller bubbles which exist even for L = 0.6m (b.); unfortunately the low image resolution did not allow for similar observations to be made on the smaller waves used. From t = 0.731sec and on (Figure 5.6 and Figure 5.10), the splash-up intensity reduces and finally seize along with the injection phases of the secondary plume evolution, and for t = 0.884sec the bubbles begin to rise back to the surface.

At this later stage it is verified that for IPA solution case significantly more air is entrained in the water column in the form of bubbles, the detrainment of which occurs faster in freshwater. It is also seen that the IPA bubble plume penetrates almost twice as deep in the water column as the freshwater, while a population of fine bubbles was observed to spread throughout the inner breaking region and to accumulated over repeated breaking events; regardless the length scale of the incoming wave. The latter is depicted in Figure 5.15, for two waves with the same characteristics (T = 0.5sec, H_i = 0.04m), plunging in both fluids. A similar behaviour was also observed for the smallest waves employed in the current project (i.e Figure 5.12) but the number of remaining bubbles was very small (i.e. < 10).

Similar accumulation of small bubbles was previously reported and measured by Blenkinsopp (2007) and Chanson et al. (2006) who concluded that due to their small number these bubble remnants do not have an important contribution to the distribution of void fraction. Nevertheless, Bullock et al. (2001) found that the

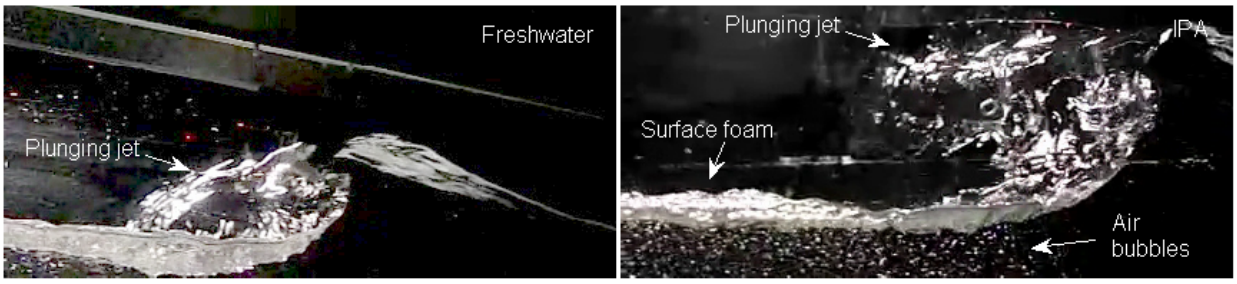

Figure 5.15: Bubble could accumulation over reapeted breaking waves in the IPA solution (right), and freshwater (left).

smallest change in void fraction (i.e 0.01%) can significantly alter the elasticity properties of the fluid. Accordingly results presented here encourage the use of the IPA solution in studies like those presented in Muller (2003), about pressure propagation in cracks and wave impact forces.

In addition to the differences in bubble remnants, Figure 5.15 also provides evidence that foam is formed in the case of the IPA solution. The foam structure was farraginous and was not observed to be confined in a certain location. Throughout the current experimental series, it was also noted that the formation of foam and the bursting of air bubbles at the free water surface was accompanied by a characteristic fizzing sound.

In summary observations presented so far show that the micro-modelling of breaking waves is not valid, since surface tension effect appear to dominate the breaking event at small scales, even for long waves (i.e. L = 1.5). However, when the freshwater was replaced by the IPA solution, and thus the surface tension was reduced, more realistic plunging breakers were formed even for the smallest wave lengths and heights employed here. For most cases the breaking event was also observed to be stronger in the IPA solution than the freshwater. Air entrainment was also significantly increased, splash-up intensity was enhanced and larger bubble plumes were created. Furthermore the air bubbles generated were seen to penetrate deeper in the water column and accumulate over repeated breaking waves, while surface foam was also formed regardless the length scale. At this point it should also be mentioned that capillary waves did not form on front face of the crest, an observation which is also supported by the observations of McDonald (2005).

Finally, the findings presented in the current chapter encourage the use of the IPA solution for other air-water related experiments / investigations, such as hydraulic jumps, flows over stepped spillways, dambreak problems etc.

5.4 Summary

The experiments presented in the current chapter have examined various aspects of the micro-modelling of breaking waves. The energy dissipated during the breaking event was measured for a large range of waves generated in freshwater which was later replaced by a 10% isopropyl alcohol and distilled water solution. The analysis was focused on plunging breakers and results obtained are of interest to the engineering community since they entail that the IPA solution could be used for more accurate modelling of highly aerated flows.

The reduction of surface tension resulted in the formation of more realistic and violent plunging breakers for all wave lengths used here ($2.8 > L > 0.35$m). The measured vortex sizes were found to agree reasonably well with previously published

values for laboratory and oceanic waves, whilst the amount of entrained air was observed to be significantly increased for the IPA fluid. Moreover, frameshots of the breaking phenomenon showed that air bubbles penetrate deeper in the water column and a population of finer bubbles was seen to accumulate over repeated breaking waves. Surface foam was also formed.

Overall, a large amount of experimental effort has been presented in the current chapter and the main conclusions drawn from it are now presented.

1. The micro-modelling of breaking waves is not valid when freshwater is used.

2. Tests with reduced surface tension provided encouraging results and thus the IPA fluid needs to be used in the micro-modelling of breaking waves.

3. Surface tension effects in wave breaking were found to be important even for waves that fell outside the limits set by studies of previous authors (i.e H $>$ 0.05m).

4. Energy dissipation values for the IPA solution were found to be significantly increased, from approximately 60-70% (freshwater) to 85-90% (IPA) for both spilling and plunging breakers.

5. Energy dissipation values for the IPA solution were found to be increased compared to previously published values from large scale physical models (e.g. Chanson and Lee (1995) and Blenkinsopp (2007)) but agree with the those given by McDonald (2005).

6. An excellent qualitative agreement was found between the IPA micro-model and previously published studies at large scale. Photographs presented in this chapter show that the mechanisms involved in the impact event and the subsequent evolution of the breaking event are the same as those presented in the existed literature.

7. The IPA solution has similar density to the freshwater (976kg/m^3 instead of 998kg/m^3) but smaller surface tension and kinematic viscosity, 0.0436N/m instead of 0.073N/m and 1.027*10^{-6}m^2/s instead of 1.005*10^{-6}m^2/s. Thus the model's We and Re increase significantly without distorting Fr; the difference

between seawater and IPA density remains equally small. This in combination with the observed differences on bubble sizes and numbers encourage the use of the fluid for other air-water related flow, even in larger scales. However, carefully controlled laboratory conditions are required in order to avoid the contamination of the fluid from the surrounding environment and the experimental cost is expected to increase. Characteristically, in the current project the cost for 165lt of IPA solution was £150.

Chapter 6

Micro-models as an investigation and development tool for engineering problems and novel concepts

6.1 Introduction

Results presented thus far show that micro-models are, under certain conditions, a valid tool for the modelling of near-shore processes such as wave shoaling, refraction, diffraction and wave breaking. Although fundamental, all these processes are seldom modelled alone and in most cases a physical model is employed in order to provide answers related to their effect on the coastal environment and / or on coastal structures. Such research is very often conducted in hired facilities (i.e. H.R. Wallingford), which are costly and have a limited availability. Accordingly any modelling study seeking to provide answers to engineering problems or develop new concepts needs to be very focused, well organised, and ideally to have a previous knowledge on the expected outcome and potential shortcomings.

Consequently the current chapter seeks to assess the possibilities of micro-models as an intermediate tool for the preliminary investigation of engineering problems and the development of new concepts and ideas. For this reason two individual case studies are presented here. The first refers to an engineering problem and deals with

the flushing of harbours and marinas and the second to the preliminary study of a novel idea for wave energy conversion based on overtopping. Experiments were conducted in a small and large scale and interesting findings regarding the effects of surface tension on overtopping and run-up are discussed.

6.2 Fundamental investigation of water flow in harbours through flushing culverts

Numerous harbours and marinas suffer from the deterioration of the water quality due to minimum water exchange. Natural flushing is mainly caused by wave action, tidal movement and wind, and is thus limited in well-protected and micro-tidal environments. As a result engineering solutions to stagnation problems have been utilized since ancient times. Franco (1996), reported harbours with two entrances and/or breakwater openings serving as flushing channels. Similarly contemporary approaches involve the use of flushing culverts and pumping systems for the enhancement of water exchange between the enclosed area and the open sea.

Bruun and Viggosson (1977), were the first to introduce a wave pump arrangement aimed to increase water discharge in a marina through the utilization of the incoming wave energy. The proposed structural layout amplified the wave height through two converging walls, causing the wave to break over the ramp section and to generate a significant volume flow into the marina. However Ozhan and Tore (1992) conducted physical model studies at a 1:80 scale of a marina incorporating such a system and reported that for deep water wave heights of 0.75m a very weak current was generated. They also observed that the flushing effects of two covered channels situated at mean water level and running through the breakwater were local and insignificant. On the contrary Stamou et al. (2004) used a Computational Fluid Dynamic surface flow model for a similar layout and reported flushing times reduced by 50%.

Furthermore, breakwaters with an embedded ability of seawater exchange driven by wave motion were developed and experimentally investigated. Ohmura (2006),

describes such a structure which utilises the piston-like mode wave resonance generated inside a wave chamber formed between a block- work mound and a vertical wall. Intake pipes were then used to channel the flow towards the protected area. Inflow rates ranging from 200 up to 2500 cm3/s were reported for increasing wave heights and wave periods, although the effect of the latter were less significant. Presented data also indicated the existence of an oscillatory motion within the intake pipes. Despite their effectivness such structures could significantly increase construction costs and cannot be retrofitted.

On the contrary the use of intake pipes or flushing culverts can be realized and/or be incorporated in existed defenses at a low cost. Although culverts are important and common hydraulic structures in irrigation systems their use in the coastal environment is mainly empirical and seldom have they been thoroughly investigated. Fountoulis and Memos (2005) highlighted the importance of the culvert dimension, location and shape with regards to flushing and excessive wave penetration. The transmission coefficient (K_t) or else the ratio of the transmitted to the incoming wave height is up to present utilised as a measure of the culverts effectiveness.

Tsoukala and Moutzouris (2009), derived an empirical equation for the calculation of Kt based on a three dimensional physical model. Rectangular shaped culverts were placed in mean water level resulting in transmission values smaller than 0.4; higher harmonics were generated inside them and were transmitted to the deep-water sheltered area. Needless to say, harbour tranquility is essential for berthing ships and for safe loading and unloading operations. Figure 6.1 suggests that during a storm a significant amount of energy may enter the sheltered area through the culvert. Even more, surface elevation measurements in a 3D environment can be 'contaminated' by diffracted and reflected waves while according to Ruol et al. (2004) the contribution of the water piling up (transmission through the porous material) behind the defensive structures cannot be easily quantified. Monioudi et al. (2006), studied the same rectangular culvert in a wave flume and reported increased K_t for larger culvert widths but similar values for various 'pipe' lengths.

Figure 6.1: Photograph of a wave passing through a culvert placed at MWL during a storm event, North Crete, Greece

It appears that despite the fact that flushing culverts are considered as potentially very interesting means to improve water quality, up to the present the importance of the culvert length, the submersion depth and the diameter, on water mass transmission have not been clearly clarified. It should be noted that the transmission of waves only indicates that energy, not necessarily volume, travels through the culvert. Therefore it stands to reason that the net transmission through a culvert under wave action, and without introduction of some sort of unidirectional flow condition, will be very limited. To the author's knowledge, no theory or study of the fundamental mechanics of flow through a culvert system has been published. The current work presents the preliminary results of an attempt to investigate the effects of culvert dimensions to K_t, and provide an insight to the water flow within the tube.

6.2.1 Experimental apparatus

6.2.1.1 Small scale model / micro-model

Two wave flumes with similar set up but different dimensions were used. The most extensive set of experiments was conducted in the small scale wave tank described in

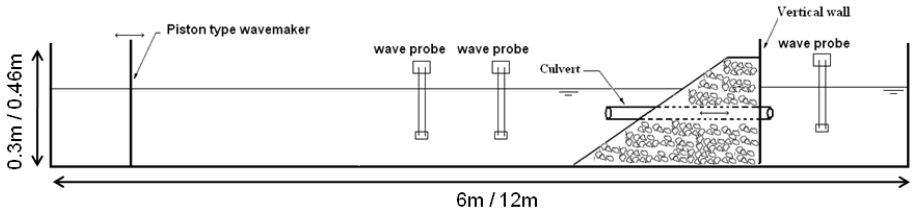

Figure 6.2: Experimental apparatus of the flushing culvert model; dimensions for both wave flumes used are given in the order of small / large.

chapter 5. The transparent walls of the tank offered an undisturbed overview of the phenomena taking place inside and the small size decreased significantly the model construction and set-up phase. An impermeable vertical wall was introduced near the far end of the tank and PVC pipes of various lengths (0.2, 0.3, 0.4m) and constant diameter (0.025m) were used as flushing culverts. Experiments were conducted for two absorbing slopes (1:1.5 and 1:2.5) installed on the front side of the breakwater, a constant depth of 0.1m, and for three different culvert submersion depths, 0.5, 0.7m and mean water level (MWL); the culvert submersion depth was estimated as the distance from the imaginary centre of the tube to the flume's bed (Fig. 6.2). Wave frequencies ranged between 0.5 and 2.5Hz and the surface elevation was measured offshore with two resistance type wave probes and inshore with one probe.

For the flow visualisation experiments, part of the slope was removed and the PVC tubes were replaced by transparent pipes with same length and diameter (Fig. 6.5). Blue ink diluted in water, was used to visualise the flow inside the culvert. The ink was introduced into the pipe prior to the start of each test, through a small opening drilled on the tube's top side. A medical siringe was used to control the inflow rate and a butterfly valve was employed to prevent water outflow. A light source was placed underneath the flume and a Casio Exilim F1 digital video camera was used to record the ink's motion. The video speed was set at 300fps which allowed for a 512x384p image resolution.

6.2.1.2 Large scale model

A second, larger model of a flushing culvert (0.9m and 1.12m long and 0.5m wide) was also built in a 12 m long, 0.46 m wide, and 0.46m deep wave flume. The model's

slope (1:2.5) was built from gravel (d_{50} = 0.04 m) and tests were conducted for a constant water depth of 0.3m and the wave frequency was ranged between 0.5 and 2 Hz. Resistance type wave probes were again used to measure surface elevation and two Nortek AS, Vectrino-ADV's (Acoustic Doppler Velocimeters) were deployed on the entrance and the exit of the culvert and measured simultaneously inflow and outflow velocities. The ADV emits an acoustic pulse and makes use of the Doppler phenomenon to return velocities of particles floating inside the water column. Both instruments were located in the middle of the wave flume and the maximum sampling depth was set at 0.07m from bed in order to avoid erroneous measurements due to side wall and / or bed reflections; to further improve measurements the flow was also seeded with tracer particles. Due to these restrictions and due to the very small flow velocities expected in the culvert's micro-model ADV's were not used in the small scale flume.

At this point it should mentioned that only one person (the author) worked on building and setting-up the micro-model of the breakwater, culvert and slope and all works were fully completed within three working days. On the contrary and despite the fact that in the large scale facility only two different culvert lengths were utilised, almost seven working days and two (ocasionally three) persons were required to fully build and set-up the model. Moreover the overall experimental time was signigficantly reduced in the micro-model since less than 30 minutes were needed in order to either replace the pipe or enven replace the whole model.

6.2.1.3 Incident and reflected wave separetion

The wave gauges placed off shore were also used to separate the incoming from the reflected wave. For this reason, a Matlab routine was written based on the method developed by Frigaard and Brorsen (1995). According to the authors the elevation signals from two wave probes can be phaseshifted in such ways that the incident parts of both wave signals will be in phase while the reflected parts will be in mutual and opposite phase. In this case the summary of the two manipulated signals will be proportional to and in phase with the incident wave signal. The amplification and phaseshift factors for each wave signal as given by Frigaard and Brorsen (1995) are:

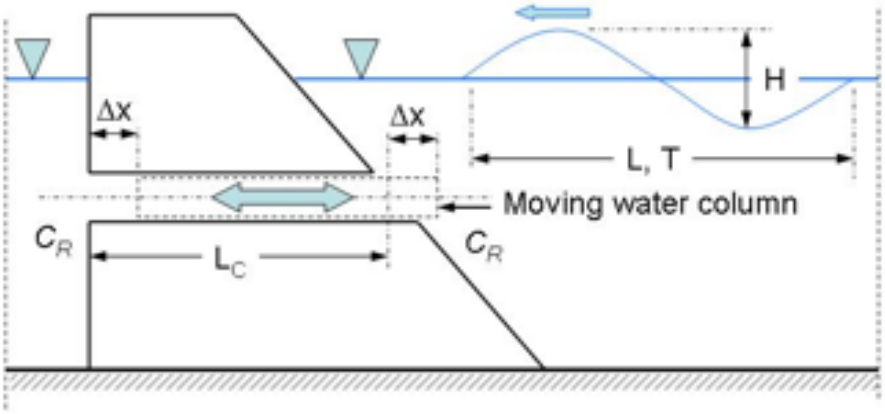

Figure 6.3: Schematic describing the principle of the theoretical model

$$\Phi_1^{theo} = k\Delta x + \frac{\pi}{2} + m\pi + n2\pi \tag{6.1}$$

$$\Phi_2^{theo} = -\frac{\pi}{2} - m\pi + n2\pi \tag{6.2}$$

$$C = \frac{1}{2cos(-k\Delta x - \frac{\pi}{2} - m\pi)} \tag{6.3}$$

where,

Φ_{1and2}^{theo} : is the phaseshift for wave probe 1 and 2 respectivelly,

C : is the amplification,

k : is the wave number,

Δx : is the distance between the two wave probes,

n and m : nϵ(0, $\pm$1, $\pm$2, ..) and mϵ(0, $\pm$1, $\pm$2, ..)

Although similar separation methods have been proposed by other authors like Goda and Suzuki (1976) and Mansard and Funke (1980), the one presented here was preferred because it could be applied using the two available wave probes and due to its clarity of approach.

6.2.2 Theoretical model

In order, to assess the properties of culvert flow under the effect of a wave with length L and height H, a simple theoretical model was developed. Figure 6.3 shows a cross section through a breakwater with a submerged culvert of length L_c . The volume inside the culvert moves a distance Δx for- and backward under wave action,

assuming the in- and outflow resistance factor C_r is the same in both directions. If the hypothetical wave exerts a hydrostatic pressure with maximum values of $\pm\rho g\frac{H}{2}$ on the culvert entrance, and if the culvert has a unit area, the movement of the water column in the culvert can be described as an enforced movement as follows:

$$\rho L_c \frac{d^2x}{dt^2} + \left(sgn\frac{dx}{dt}\right) C_R \frac{\rho}{2}\left(\frac{dx}{dt}\right)^2 = \rho g \frac{H}{2} sin(\frac{2\pi}{T}t) \tag{6.4}$$

where

ρ : is the water density

L_C : is the culvert's length

C_R : here is the loss factor of the water flowing in or out of the culvert

H : is the incoming wave height

T : is the wave period

g : is the accelaration due to gravity

A forward integration model was developed in Matlab to solve 6.4. The mass of the water has to be accelerated and decelerated in every cycle and the movement of the column was assumed to be symmetrical i.e. without mass flow. It will be shown that despite its simplicity the model agrees well with both physical models, and provides a satisfactory, preliminary insight to the overall problem. To the author's knowledge this is the first time that a theoretical analysis of a culvert system is conducted.

6.2.3 Results and discussion

6.2.3.1 Micro-model

Figure 6.4 presents the results on the wave transmission coefficient over the dimensionless kd (k is the wave number, $k = \frac{2\pi}{L}$ and d is the water depth, d = 0.1m) for several submersion depths (MWL, 0.07m and 0.05m), culvert lengths (20mm, 30mm and 40mm) and wave frequencies (0.5-2.5Hz). For all the graphs presented here, $K_t = \frac{H_t}{H_{inc}}$ and $H_{rms} = 2\sqrt{2}\sqrt{m_o}$, where H_t and H_{inc} are the transmitted and the incoming root mean square wave heights calculated based on the zero order moment (m_o) of the incoming and transmitted wave signal. Although the H_{rms} is commonly used for irregular wave analysis, several researchers amongst which Lozada et al. (1997) have used

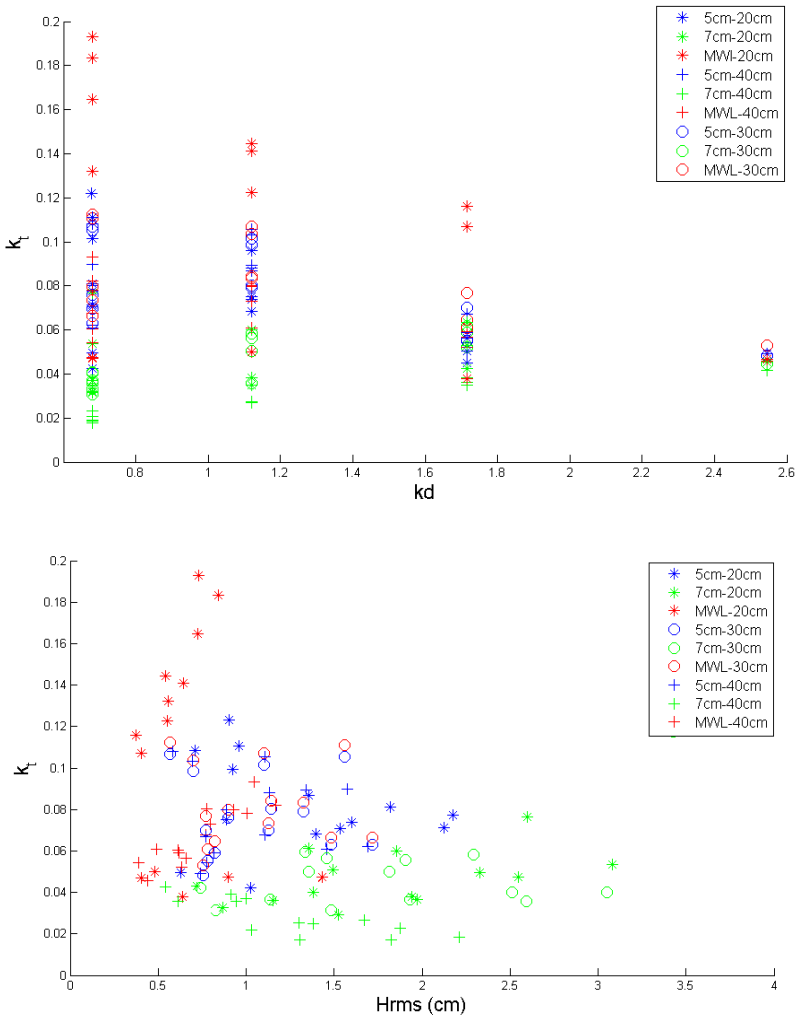

Figure 6.4: Plots of the transmission coefficient as a function of kh (above) and H_{rms} (below), for various culvert lengths and submersion depths

it to analyse regular waves as well.

It is seen that the largest transmission coefficient value is achieved when the culvert is placed at MWL but, when submerged, the culvert appears to be more efficient at 0.05m rather than when placed at 0.07m; however, the current experimental series could not provide convincing evidence that would explain this and further research is required. It is also pointed out that decreasing wavelengths cause a decrease on the transmission coefficient, which rapidly increases for very small kd. Nevertheless, when located at MWL smaller culvert lengths significantly influence K_t, which becomes maximum for larger wavelengths and shorter pipes. A similar trend is observed for submersion depths of 0.07m and 0.05m, where larger K_t are recorded for

smaller culverts and longer waves; the overall K_t values however, reduce significantly. When fully submerged the culvert appears to be less sensitive to the incoming wave length.

Moreover, it should be noted that although the wave transmission coefficient does not appear to be significantly affected by the incoming H_{rms} (Figure 6.4, right), a sharp increase was measured for the smallest wave heights and especially for the shorter culverts placed at MWL and at 0.05m. The latter observation is surprising since larger wave heights imply that a larger hydrostatic pressure will be exerted on the culverts entrance and thus higher waves should result on increased values of K_t. One possible explanation for this discrepancy could be that the culvert is exposed when a trough arrives and a strong backflow is caused but this could only apply for culverts placed at MWL. When fully submerged, an explanation could be provided by the fact that shorter waves are associated with smaller particle velocities, which in turn result in significantly smaller drag forces in the culvert. This is better expressed by:

$$F_d = C_D \frac{\rho v^2 A}{2} \tag{6.5}$$

where,

F_d : is the drag force

C_D : is the drag coefficient

ρ : is the density of fluid

v : is the flow velocity

A : is a characteristic frontal area

Experiments were also conducted for a steeper slope of 1:1.5 returned similar results. Again, shorter culverts placed in MWL or 0.05m returned larger values of K_t (slightly higher than before), which decreased for decreasing wavelength.

Thus far the micro-model's results do not fully agree with the published literature since they indicate a strong dependence of K_t on the ratio of culvert length and wavelength, while submerging the culvert appears slightly less effective then when

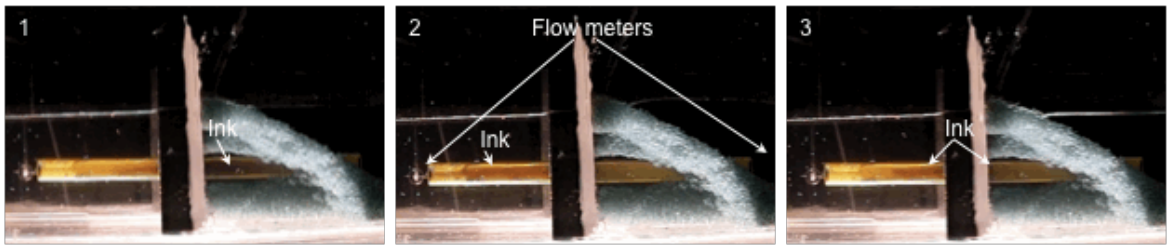

Figure 6.5: Water mass oscillation inside a 0.4m long, submerged culvert for T = 1sec and H=0.017cm. The position of electronic flow meters is also depicted.

placed at MWL. Needless to say that for the latter set up no significant disturbances of the protected water surface were observed. Nevertheless, the findings presented here do not indicate a clear trend between the transmission coefficient and the incoming wave height except in the case of very small waves. Consequently an attempt was made to visualize water flow through a submerged and transparent culvert and a similar set of experiments was repeated in the larger wave tank.

6.2.3.2 Flow visualisation inside the culvert

As previously mentioned, ink was utilized in order to visualize flow motion inside a culvert submerged at 0.05m. Videos were taken for two different tube lengths (20, 40cm), wave periods ranging from 0.5-2sec and various wave heights, and indicative results are now presented.

The first trough arriving on the structure has minor effects but as soon as the crest follows an inshore flow movement is observed. The flow continues as the water level retreats and the ink approaches the sheltered area. An oscillatory motion develops when the subsequent crest arrives and the water mass inside the culvert moves now offshore.

In general it was observed that waves with the same period (i.e. 0.66sec) but smaller heights produce a weaker burst when the first crest reaches the structure; for higher crest a significant inshore flow motion takes place. Soon after, that an oscillatory motion develops within the tube and depending on the experimental conditions (i.e culvert and wave length) water flows into the protected area, or not.

Specifically, for a short culvert (20cm), long and high waves caused the water to

fluctuate near the entrance of the pipe and an offshore motion was observed, whilst short and high waves generated the opposite effect. Experiments with longer culvert (40cm) yielded similar results, but the offshore motion was significantly reduced. This can probably be attributed to the fact that the oscillatory mass motion generated by the wave action was 'trapped' inside the pipe, as can be seen in Figure 6.5.

6.2.3.3 Large scale model

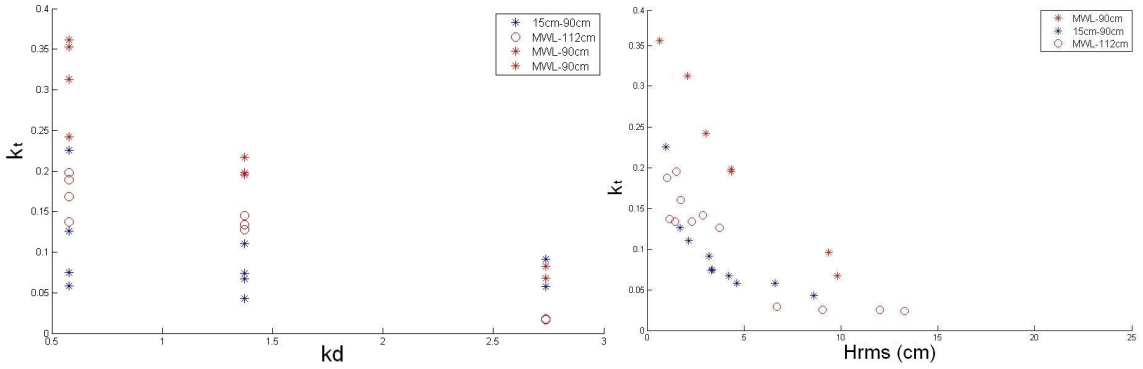

Figure 6.6: Large scale model results for K_t over kh (left) and H_{rms} (right). Experiments conducted for two, 0.9m and 1.12m long culverts, placed at MWL and at 0.15m.

Large-scale experiments were also conducted and their results are now presented. Figure 6.6 shows plots of K_t over kd and H_{rms}, for two, 0.9m and 1.12m long, culverts placed at MWL and 0.15m. It is seen that larger values of the transmission coefficient were again recorded for the former than the latter (Figure 6.6, left). A trend of increasing K_t for decreasing wavelengths is observed for the culvert placed at MWL but when submerged the transmission values appear to be less senssitive to the wavelength.

The shorter culvert (90cm) appears to be more efficient, but in general small wave heights result again in large transmission values which decrease for higher waves. The latter trend is more pronounced for the submerged culvert since when the culvert is placed at MWL, the K_t appears to be less dependent on H_{rms}; a similar behaviour can also be seen in the micro-model results (Figure 6.4). Nevertheless, during the course of the tests it was obvious that by placing the culvert at MWL, large surface disturbances were generated on the free surface of the sheltered area.

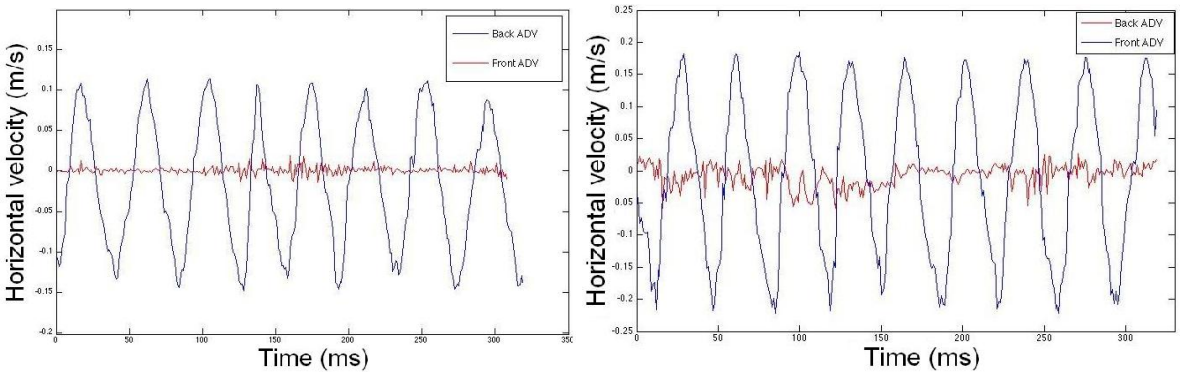

Figure 6.7: ADV flow measurements for a culvert (90cm) placed at 0.15m (left) and MWL (right), for T = 1sec

Figure 6.7 presents representative ADV results for the culvert placed at MWL (right) and at a depth of 0.15m (left). For both cases the ADV's were triggered prior to the wavemaker and were set to record a maximum number of 7500 samples with a sampling frequency of 50Hz. It is seen that an oscillatory motion develops on the exit of the submerged culvert but flow velocities are extremely small.

Although the ADV's were located deeper than the culvert for the MWL tests, an oscillatory motion was observed as well (Figure 6.7, right). Inflow and outflow velocities were larger than before but they oscillated around zero and only a small net flow was recorded. On the contrary an offshore flow was observed during the measuring period which was the result of the culvert's exposure by the wave trough. Overall net positive flow was mainly observed for the fully submerged culvert, a fact that partly contradicts data presented here (Figure 6.6) and published previously; based on surface elevation measurements. The latter suggests that although energy may enter the protected area through the culvert, actual water flow might be limited.

6.2.3.4 Theoretical model

Figure 6.8 shows the maximum horizontal movement normalized with the wave height as a function of the ratio of culvert length to incident wavelength L_C / L. It is seen that a significant horizontal motion is possible, with the maximum amplitude decreasing rapidly for increasing ratios of L_C / L.

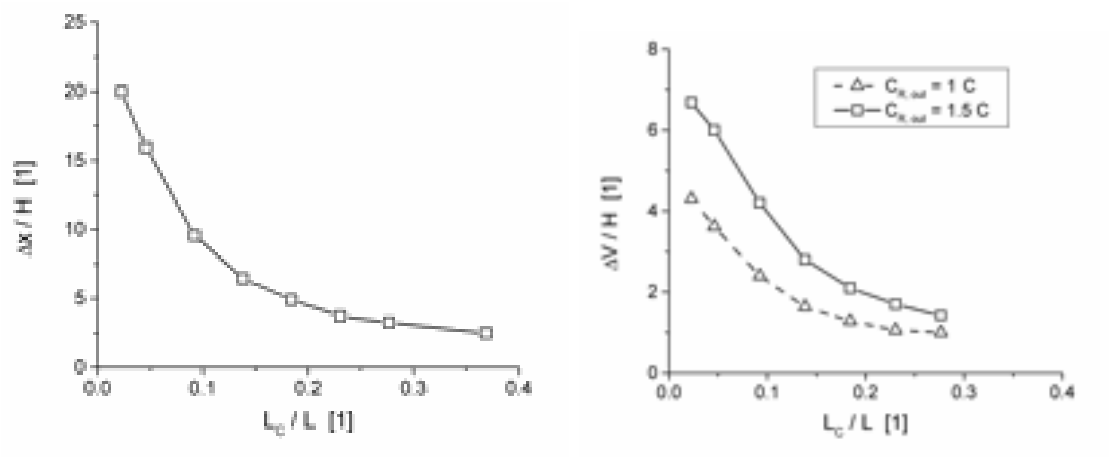

Figure 6.8: Plots of the maximum horizontal oscillatory movement (left) and volume transport (right) over L_C / L

Figure 6.8 shows the effect of uneven loss factors (this could be achieved by e.g. having a funnel type inflow on one side) in the entrance and the exit of the culvert. The ratio of flow volume is depicted normalised by the incoming wave height (assuming again unit area of the culvert) and over L_C / L. It can be seen that even for $C_{R,in}$ = 1.5 $C_{R,out}$, significant volume flow in one direction is possible; $C_{R,in}$ and $C_{R,out}$ are the loss factor on the culvert's entrance and exit respectively.

However, it should be noted that in reality for a culvert with an opening below MWL the acting pressures caused by the wave will be smaller than the here assumed hydrostatic pressures, caused by the water surface displacement.

6.2.4 Conclusions

Decreased water quality is one of the major problems of most existed harbours and marinas. As a solution flushing culverts have been used in many cases but their design was mainly based on engineering experience as they were considered as a black box. Previous studies reported significant K_t values and based on that suggested the use of culverts placed at MWL as an effective flushing mechanism. However field and laboratory observations show that the protected area can be significantly disturbed by the wave energy passing through the culvert. Even more, data presented here show that submerged culverts can be almost as efficient as those placed at MWL; in terms of K_t.

A very good qualitative agreement was also observed between the two physical models. The micro-model was found to be able to reproduce the same trends in the dimensionless transmission coeffiecient results, while a good qualitative agreement was also observed. For both cases smaller waves heights resulted on increased transmission values, especially when the culvert was fully submerged. This can probably be attributed to the reduced drag force caused by the decrease in particle velocities for shorter waves. When placed at MWL a strong backflow motion was observed during the presence of the wave's trough. Even more, the micro-model agrees with the theoretical model and shows that for shorter culverts K_t increases for longer waves.

In conclusion a combination of experimental and theoretical work showed that:

- Wave transmission does not necessarily mean a net volume flow.
- The efficiency of the culvert depends on the ratio of culvert to wave length and should be as small as possible.
- There is no reason for a culvert to be placed at MWL, were it's entrance will be exposed to breaking waves.
- When placed a MWL, the wave's energy passing through the culvert during a storm can result to significant and unwanted disturbances on the water surface of the protected area.
- A useful net flow might only be possible in assymetric culverts
- Previous ideas about culverts as flushing elements need to be revised in view of the new insights.

6.3 Composite seawalls for wave energy conversion

Wave energy generation at the shoreline is attractive from the point of view of access and ease of construction; it is however limited by the fact that the available wave energy reduces with decreasing water depth and by the exposure to the extreme

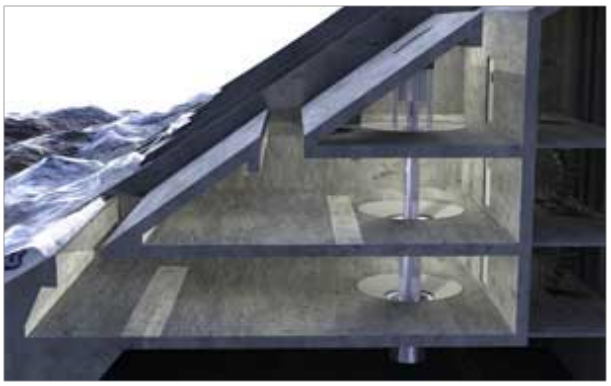

Figure 6.9: Lateral section of a three-levels SSG device with Multi-stage Turbine (MST), after Margheritini et al. (2009).

conditions created by breaking waves. Many different wave energy converters have been developed; from the point of view of construction and operation however overtopping devices are attractive because of their simplicity, their independence of wave period and – although to a lesser extent - their independence of wave direction.

The Wave Dragon, described by kofoed et al. (2004), is an offshore floating wave energy converter. It consists of a basin and a sloped front which both extend above MWL and a turbine. The wave run-up on the sloped front spills into the basin and generates a head difference, which then drives the turbine. More recently, a shoreline overtopping device, which consists of three stacked concrete containers with a slotted inclined front wall, has been proposed by Margheritini et al. (2009). In this concept, run-up from the waves is collected at three different height levels and then fed into turbines, so that maximum use is made of the potential energy generated (Fig. 6.9). Both devices, the Wave Dragon and the SSG wave energy converter, are however rather complex structures. In addition, both employ a specially developed Kaplan turbine but Senior et al. (2008) suggested that such turbines are usually considered not economical and environmentally questionable for situations with very low head differences.

Composite sea walls, i.e. sea walls on a high rubble mound which have an energy absorbing screen or a slit wall in front of the impermeable wall, have been recently constructed as described in Mori et al. (2008). Field measurements showed that such structures reduce wave loading on the seawall and overtopping, since the energy of

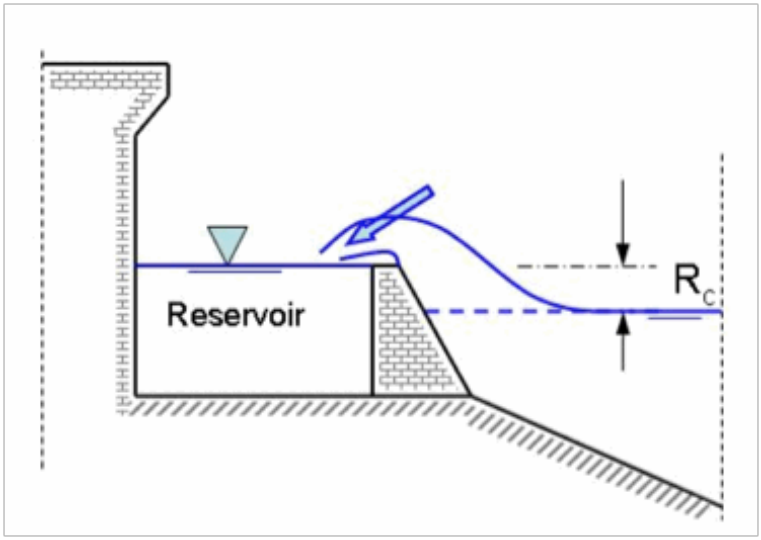

Figure 6.10: Schema of an energy capturing sea wall

breaking waves is dissipated by the screen, and by the turbulence created by the impact of the breaker's jet onto the water between screen and wall. A similar concept has also been proposed by Geeraerts et al. (2006) for the reduction of wave ovetopping on sea dikes. A basin is placed in between two walls and the incoming wave impacts on the seaward wall, directs upwards and drops in the basin were most of its energy is dissipated. The current research involves the slight modification of the silt wall which may allow for the generation of energy as well as the protection of a shoreline. The same principle of energy conversion employed by the Wave Dragon is used and as a concept it was originally published in Muller et al. (2009). Moreover, the overtopping data used and presented here have been produced along the lines of the work reported in Maravelakis (2009), who conducted an extensive set of small (micro-model) and larger scale experimental measurements.

6.3.1 Theoretical description

The concept of a water retaining composite seawall is depicted in 6.10. It is believed that in combination with the availability of novel energy converters it may allow to capture the low head potential energy from wave action. If the lower part of the seaward screen is impermeable, with an upper crest at a distance Rc above MWL, wave run-up will transport water into the basin between screen and sea wall. The head difference generated however will probably be small (in the range of the wave

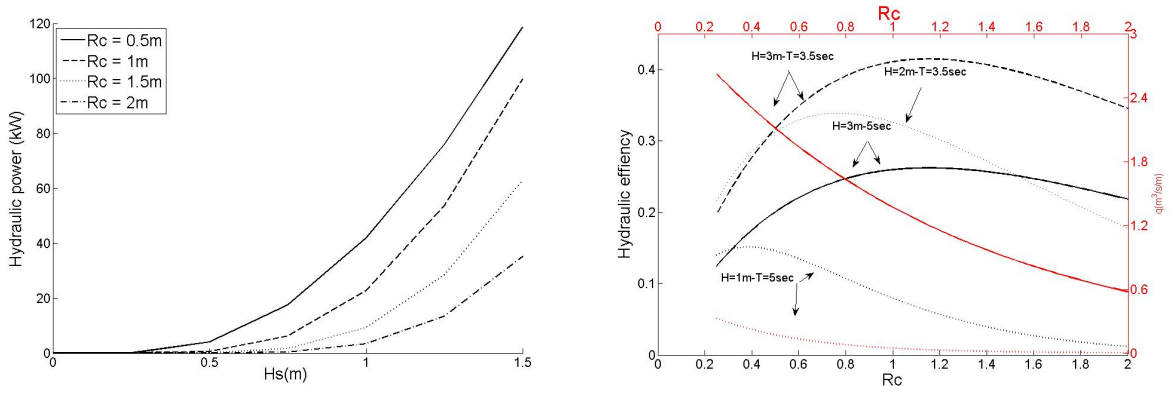

Figure 6.11: Theoretical power as a function of the significant wave height (H_s) for various freeboards (R_C) (left) and theoretical hydraulic efficiency as a function of R_C and overtopping volume (q), for various H_s and a constant depth of 6.5m.

height). Nevertheless, such a sea wall would have two main advantages:

- the linear nature of the structure allows for a long capture length without a supporting floating structure as is required for the Wave Dragon. Its fundamental dimension is matched to the linear character of the wave crest,
- the structure is a double purpose structure, providing protection and energy generation, thereby increasing its cost-effectiveness

Figure 6.11(left) shows the theoretical power production (hydraulic power) for a 50 m strip of seawall, for different freeboard ratios of 0.5, 1.0, 1.5 and 2.0 m and significant wave heights of up to 1.5 m. The hydraulic power is a function of the freeboard and the overtopping rate which was determined using the formula proposed by van der Meer and Janssen (1994). The latter formula was preferred since it had the best fit on the data presented in the following section; all the equations used for the current project can be found in Table 6.2. It is seen that even for 2m freeboard, power production is still possible. Assuming for example H_s = 1.0m, Rc = 0.5 m, the maximum power level of 38 kW appears acceptable.

The sea wall is envisaged to capture energy for average wave heights, and to dissipate energy for large breaking wave events. A combination of roles however may mean

that no one role can be fulfilled completely. Figure 6.11(right) shows that there is an optimum crest length (R_c), which can be determined for individual locations, as a function of the local wave climate. In opposition to most existed wave energy converters (period dependent) the performance of the wall appears to depend mainly on the incoming wave height, rather than the wave period. It is seen that although the maximum efficiency is larger for waves with larger T, the overtopping rate remains the same.

On the contrary q increases for smaller freeboards and higher waves. Accordingly the optimum design of the wall involves the selection of the freeboard's height based primarily on the significant wave height (H_s) rather than the wave period, since an optimum combination of large overtopping rates and large efficiencies is desired. If for example H_s = 3m, maximum performance can be achieved for a freeboard ranging between 0.8m and 1m, where the ovetopping rate will be approximately 1.5m^3/s/m and the efficiency will range from 24% to 39%, for wave periods between 3.5sec and 5sec. Nevertheless, the performance of such a wall will be insignificant for H_s = 1m since the water collected in the reservoir will be minimum and despite the fact that the efficiency will remain more than 10%. As a result data collected in the current work are analysed with respect to the wave height and not the wave period. Such an approach is also supported by van der Meer and Janssen (1994) and Goda (2009) who do not consider the wave period in their overtopping equations.

Overall, possible disadvantages of the composite seawall for energy conversion can be listed as:

- The structure's performance will be strongly influenced by water levels / tides.
- Energy dissipation for larger waves may be lower compared with the composite wall proposed by Mori et al. (2008).
- The outflow detail needs to be designed so as to be unaffected by wave action. This is dictated by the hydropower converter which requires a smooth inflow.

The exploitation of wave energy with such a seawall however critically depends on whether a cost-effective hydropower converter for very low head differences exists.

Senior et al. (2008) suggested that standard Kaplan turbines are restrictivly expensive for power ratings below 500 kW. Hence a potentially very effective converter for very low head differences – the Hydrostatic Pressure Wheel (HPW) – was developed in parallel with the current project by Muller and Senior (2007).

6.3.2 Experimental apparatus

Over the past years wave run-up and overtopping were the focus of several research studies. De Rouck et al. (2005) and Kortenhaus et al. (2005) amongst others compared field measurements with extensive physical model results and concluded that run-up and overtopping are underestimated in laboratory conditions. These discrepancies were mainly attributed to the absence of wind and the increased importance of surface tension and viscosity 1effects in scaled models. Accordingly a micro-model of a composite wall was originally used and later on experiments were also conducted in a large scale model as well. The latter was considered necessary in order to evaluate the results obtained by the micro-model, where the influence of scale effects is increased.

6.3.2.1 Small scale model / micro-model

The micro-model experiments were conducted in the 7m long, 0.2m wide and 0.3m deep wave tank described in the previous chapter. For the current tests a constant water depth of 0.13m was adopted (coresponding to a prototype water depth of 6.5m) and a 1:10 slope was installed at the end of the tank. The water depth was chosen as such in order to allow simulations with a variety of unbroken waves.

Assuming a Froude scale of 1 : 50, a small scale model of the composite sea wall was built out of 5mm thick, transparent, Perspex sheets, in the laboratory workshop. Costs associated with the model construction referred only to the building materials which cost approximately £30. The structure consists of two sloping parts and three vertical walls which form the water collection chamber (Figure 6.12, left). The lower sloping part was specifically designed in order for the structure to fit on the 1:10

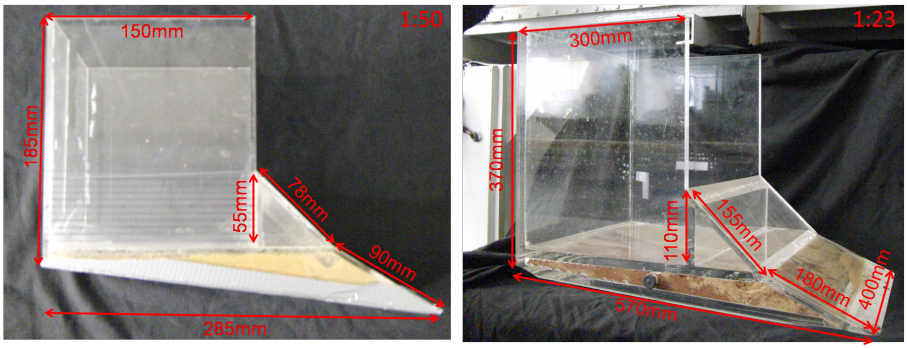

Figure 6.12: Photographs of the modified composite sea wall for the micro-model (left) and the large scale model (right).

Prototype	1 : 50 model	1 : 23 model
10	1.4	2.1
7.1	1	1.5
6.3	0.9	1.3
5	0.7	1.1
4.2	0.6	0.9
3.5	0.5	0.7

Table 6.1: Prototype and model scale periods in seconds.

slope and for the chamber's level to be parallel to the still water level. The upper sloping part, which from now on will be referred to as the ramp, replaced the slit wall proposed by Mori et al. (2008) and had an angle of 45^o to the vertical; more details on the wall's design can be found in Maravelakis (2009).

Since the beginning of the project it was decided that the wave periods used should be representative of an actual case study. Accordingly, the Aegean Sea was chosen due to its very low tidal regime (< 0.03m) and information on the predominant wave periods was aquired from Soukassian et al. (2009). Table 6.1 presents the prototype wave periods selected along with their corresponding values for each model scale.

Regular waves were considered appropriate for the current experimental series since no resonance effects were employed, and since it is the average wave height during operational conditions which is of main interest and not any extreme event. For each micro-model experiment, a wave train of six waves was generated and wave heights ranged between 0.02m and 0.05m. Since an active wave absorption system was not available, using a small number of waves was necessary in order to avoid unwanted

effects (i.e standing waves) generated due to the reflected and re-reflected waves. Surface elevation was recorded by three resistance type wave gauges plugged into a DataTaker DT800, with a sampling frequency of 20Hz. The output signal was calibrated with the same method described in Chapter 5.

A Casio Exelim F1 camera was placed parallel to the structure and videos for each test case were created. The videos were later used to calculate the number of waves that overtopped the ramp and spilled inside the chamber. Accordingly the average wave height (H_{av}) was calculated based on these observations and the wave probe measurements. Although two wave gauges were placed at the toe of the structure and on top of the slope, only the signal of the third probe, placed at a distance of 2m from the structure, was used in the current study. The latter probe was selected since in most field studies wave measurements are seldom available at the structure's toe i.e Franco et al. (2009). Even more, Goda (2009) reanalysed selective CLASH datasets and suggested that in overtopping model studies the nearshore wave height is to be used as the wave height at the toe of the structure.

Experiments were conducted for two different freeboard heights, $R_{cmodel} = 0.02$m and $R_{cmodel} = 0.03$m, corresponding to prototype values of $R_c = 1$m and $R_c = 1.5$m. The freeboard is the vertical distance between the still water level and the top end of the ramp and is also equal to the available hydraulic head. The performance of the composite sea wall with each freeboard was tested for 20 different wave conditions. After the end of the current experimental series the water depth was raised up to the ramp's limit as a qualitative test of the wall's performance in extreme situations.

For each experiment, a manual pump and a medical siringe were used to transfer the water collected in the reservoir into calibrated beakers and measure its volume; the chamber was then left empty for the next test. Overtopping volumes (q) and the average wave height (H_{av}) were used for the calculation of the wall's hydraulic efficiency and power. The results were also compared with the thoretical values given by predictive equations proposed by previous reserachers. Table includes all the formulas used in the current study.

Parameter	Formula	Author(s)
Overtopping rate (non-breaking waves $\xi_{m-1,0} > 2$)	$\frac{q}{\sqrt{gH_{m0}^3}} = 0.2exp(-2.6\frac{R_c}{H_{m0}\gamma_f\gamma_\beta})$	van der Meer and Janssen (1994)
Overtopping rate	$\frac{q}{\sqrt{gH_{m0}^3}} = exp[-(a + b\frac{R_C}{H_{s,toe}})]$	Goda (2009)
Dimensionless overtopping rate	$Q^* = \frac{q}{(gH^3)^{\frac{1}{2}}}$	van der Meer and Janssen (1994); Goda (2009)
Dimensionless freeboard	$R^* = \frac{R_c}{H}$	van der Meer and Janssen (1994); Goda (2009)
Wave power	$P_{wave} = EC_g$	
Hydraulic power of water in the crest	$P_{crest} = qR_C\rho g$	
Hydraulic efficiency	$H_{ef} = \frac{P_{crest}}{P_{wave}}$	
Experimental mean overtopping rate	$\frac{V}{tw}(\frac{m^3}{sm})$	
q : is the overtopping rate, H_{m0} : is the zero moment spectral wave height, T_{m0} : is the zero moment spectral wave period, γ_f, γ_β: are correction factors set to here 1, $\xi_{m-1,0}$: is the breaker parameter		
a and b : correction factors depending on the seabed slope (here $0.1_{micromodel}$ and $0.05_{large\ scale\ model}$), the water depth at the toe (here 1.25m and 1.75m for each freeboard) and the structure's slope (here 1)		
E : is the wave energy, C_g : is the wave group velocity		
V : is the total water volume measured, t : is the period summary of the waves that overtopped the structure, w : is the slope's width		

Table 6.2: Formulas used in the current study.

Freshwater was used for the majority of the micro-model experiments. However tests for the larger freeboard (0.03m) were also repeated with the same IPA solution used in Chapter 5. Kortenhaus et al. (2005) produced extensive datasets of wave run-up and overtopping in laboratory conditions and suggested that similarity of Fr, We, and Re is required. Of course the importance of the latter and the former number increases as the scale decreases. Accordingly the use of a fluid with similar viscosity to freshwater but significantly reduced surface tension might mitigate the scale effects expected in micro-models; De Rouck et al. (2007) compared prototype and scaled measurements and found that run-up and overtopping are underestimated in the model.

6.3.2.2 Large scale model

A geometrically similar experiment procedure was conducted in the 12m long, 0.5m deep and 0.45m wide wave tank. Assuming a model to prototype scale of 1:23 a larger scale model of the composite sea wall was constructed by an external contractor with an overall cost of £250; the 15mm thick Perspex sheets used were provided by the laboratory to the contractor. Figure 6.12 (right), depicts all the structure's dimensions in more detail.

The main difference of the larger scale model was that the structure was placed on top of the pre-existed 1:20 slope which was followed by a plateau. Accordingly experiments for both freeboard heights (here 0.044m and 0.065m respectively) were only possible with a water depth of 0.255m. Wave heights ranged between 0.03m and 0.09m and three resistance type wave gauges again measured the surface elevation. Once more the signal returned from the probe located at a distance of 4.4m from the structure, was used for all the subsequent calculations.

6.3.3 Results and discussion

6.3.3.1 Hydraulic power and efficiency

The hydraulic power expresses the amount of kW that can be available in the structure and is a function of the freeboard and the overtopping rate (Table 6.2). Figure 6.13

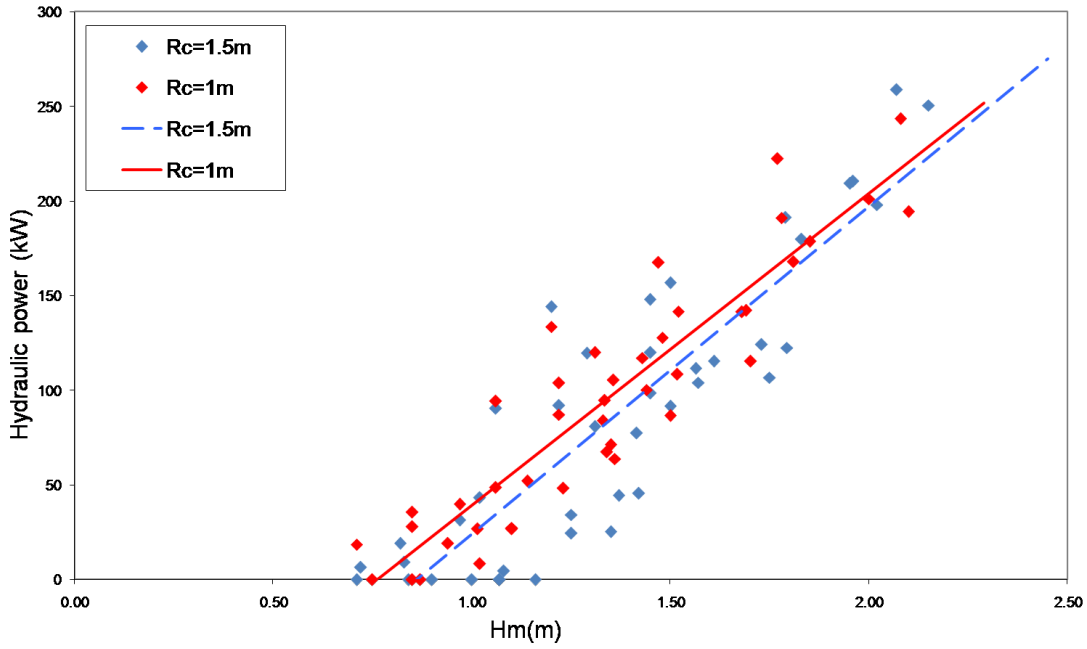

Figure 6.13: Hydraulic power over the wave height.

presents the hydraulic power for the two different freeboard heights of 1m and 1.5m plotted over the wave height for a 50m strip of sea wall; power calculations (Table 6.2) are based on overtopping rates measured in both physical models.

It is seen that the hydraulic power of the structure increases for larger wave height and smaller freeboard. This comes as no surprise as the combination of low freeboard and high waves allows for more overtopping to occur on the structure and thus for more water to be collected in the reservoir. Nevertheless the difference between the two freeboards appears to decrease for higher waves but a solid conclusion can not be drawn for heights larger than 2m since more measurements are required. In any case a power output of 1.5kW / m for waves of only 1m looks very interesting. According to the power measurements provided by Margheritini et al. (2009), a three deck Sea wave Slote cone Generator (SSG with $R_c = 5$m) will have exactly the same power output for 1m high waves.

Although important, the hydraulic power can be misleading without reference to the hydraulic efficiency of the structure and the efficiency of the potential to electrical energy convertor. The hydraulic efficiency of the composite sea wall is plotted in Figure 6.14 over the dimensionless ratio of the wave height to freeboard ratio. It is

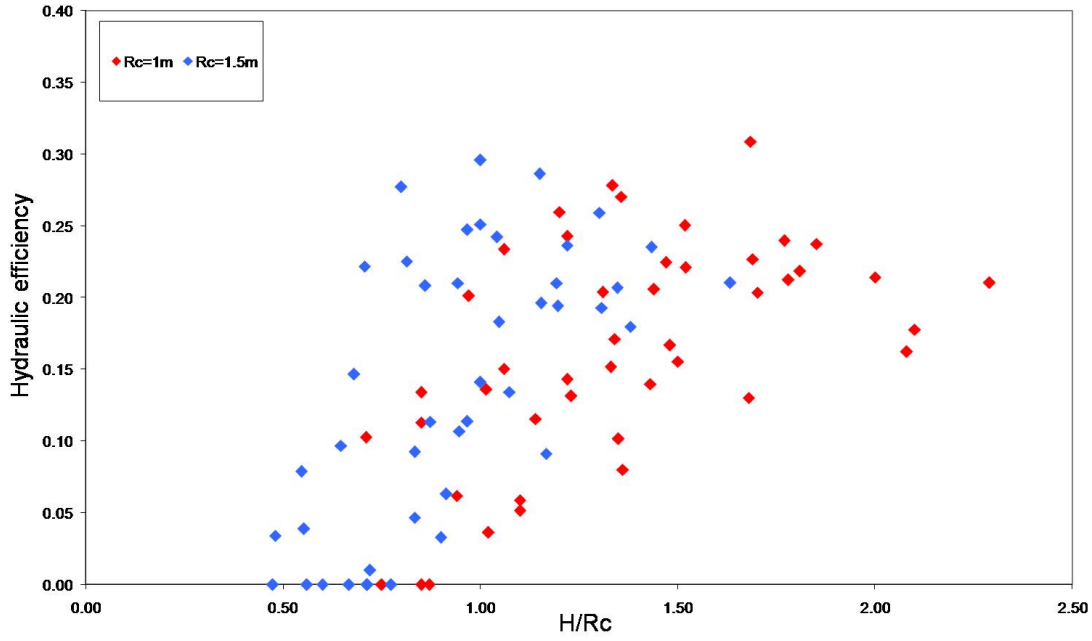

Figure 6.14: Hydraulic efficiency plotted over the dimensionless ration of the wave to freeboard height.

seen that for both freeboard heights the efficiency increases with the relative wave height and reaches its maximum of approximately 30% for relative heights ranging between 1m and 1.5m. A very good agreement is found when the measurements are compared with the theoretical predictions (Figure 6.11). Indeed for wave and freeboard heights between 1m and 2m and 1m and 1.5m respectively, theoretical efficiencies range between approximately 6% and 32% while measured efficiencies are in the order of 4% to 30%. The corresponding hydraulic efficiencies reported in Margheritini et al. (2009) ranged from 30% to 40% but for larger wave heights than those used in the current study (i.e 0.6m $<$ H $<$ 8.9m).

In any case, the energy converter is outside the scope of the current project and for more details the keen reader is referred to Maravelakis (2009).

6.3.3.2 Theoretical case study

As previously mentioned wave periods were chosen as such in order to resemble the wave climate of the Greek seas. This section presents a theoretical application of the

Figure 6.15: Satelite photo of Greece.

Significant wave height (m)	Occurance probability (%)
0.5 - 0.99	42
1 - 1.49	22
1.5 - 1.99	11
2 - 2.5	8

Table 6.3: Occurence probabilities of significant wave heights in northern Crete.

composite sea wall on the northern part of the Hellenic island of Crete. The specific location was originally proposed by Maravelakis (2009), who worked alongside the present author on the composite sea wall project for a period of 4 months, and was finally chosen due to the absence of tides and the beneficial wave climate. Soukassian et al. (2009) used a numerical model and wave buoy data, and provided estimations for the annual mean significant wave height and the mean spectral period that ranged between 0.9m and 1.2m and 5.97sec respectively. The authors also calculated the probabilities of occurrence for significant waves heights and those related to the current study are presented in Table 6.3.

Based on these probabilities the hypothetical power production per meter of a composite sea wall can be calculated by multiplying the hydraulic power of the structure to the probability of occurrence transformed into number of hours. SinceSoukassian et al. (2009) reported probabilities for a single wave period of 5.97sec thus Table 6.4 gives the structure's power potential in kWh / y for the two different freeboards and all the different wave heights measured for a wave period of

R_C = 1.5m				R_C = 1m			
T(sec)	H_s(m)	Probability(%)	kWh / y	T(sec)	H_s(m)	Probability(%)	kWh / y
6	0.97	42	2291	6	0.97	42	2962
6	1.29	22	4596	6	1.31	22	4683
6	1.5	11	3502	6	1.5	11	3266

Table 6.4: Table of theoretical annual power production per m of composite sea wall in Crete island, Greece.

6sec; measurements from the large scale physical model were preferred for this theoretical analysis since the larger size of the model implies less scale effects. It is seen that although the highest probabilities of occurrence correspond to the smaller wave heights, the summary of all the possible power outputs results approximately to 10.5MWh / y per meter wall for a 1.5m high freeboard and 11MWh / y. Even more the annual power production of 2962kWy / h for R_C = 1m, T=6sec, and H_s = 0.97m is directly comparable to the 3153kWh / y which is the annual production of the SSG for T=6.1sec, and H_s = 1m in a theoretical case study on the island of Kvitsøy, Norway, Margheritini et al. (2009).

According to the Greek national company of electricity, kWh prices for domestic use may vary between 0.07449€ / kWh and 0.16426€ / kWh depending on demand (source: www.dei.gr). Hence if we assume a 50m long composite seawall, a freeboard of 1m and a wave period of 6sec, and a 65% efficiency for the energy converter, then the annual return of such structure in € will range between approximately 37,000€ and 60,000€; of course these numbers are only indicative. The structure's overall performace is expected to increases if more wave periods are considered but if oblique wave aproach is also considered than an average decrease of 5% on the hydraulic efficiency is also expected, Margheritini et al. (2008).

6.3.3.3 Extreme conditions

Qualitative tests were conducted with a high water level (HWL) at the crest of the primary wall (ramp) and wave heights which created plunging breakers in order to assess the wall's performance under extreme conditions. The results were encouraging. Breaking waves were tripped by the wall, resulting in a jet plunging

into the basin. It appeared that a significant amount of the energy of the breaking wave was dissipated in turbulence in the basin, and that loadings and overtopping were reduced. Figure 6.16 shows the impact and uprush. The direct collision of the wave with the vertical wall does not take place any more, only the jet of the wall hits the bottom slab. The observations appeared to indicate that overtopping and wave loadings were significantly reduced. Preliminary impact experiments on the sea wall of the structure and a vertical sea wall placed at the ramp's location, resulted in 5 times smaller pressure measurements for the former than the latter; details on the measurements are reported in Soler (2009) but further investigation is required.

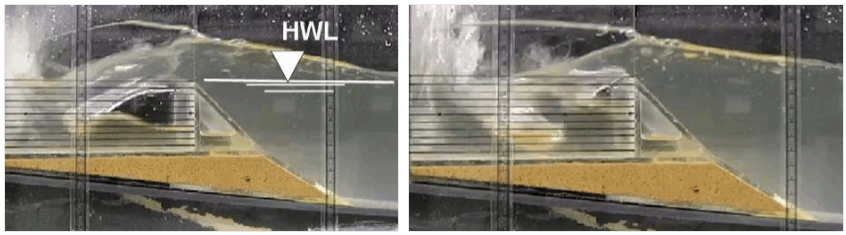

Figure 6.16: The composite sea wall under extreme conditions; the initial jet impact is shown (left) and the subsequent impact, uprush and turbulence generation (right).

6.3.4 Conclusions

An exploratory research project was conducted in order to assess the potential of a modified composite seawall to generate low head hydropower with head differences in the range from 0.5m to 1.5m. The regular waves are hereby assumed to simulate an average wave height occurring over a prolonged period of time. Nevertheless:

- With a hydraulic power of 1.5kW per m length of seawall available for a wave height of 1m, the initial results of the power generation with a composite seawall look promising.
- The overall power potential of the composite sea wall is directly comparable to the previously developed SSG.
- The structure needs to be specifically optimised for each location, since an optimum freeboard exists as a function of the wave height and the probability of occurrence. In general though, smaller freeboards appear to be more effective.

- The theoretical application of the composite sea wall on an actual case study shows favourable economic considerations.
- Observations from the model tests indicated that the modified composite seawall leads to reduced wave loading and overtopping.

A number of questions have however not yet been addressed by the work presented here:

- The effect of tidal variations on power generation.
- Observations on reduced loading and overtopping need to be verified for extreme conditions.
- Experiments are required for an intrergrated model of the composite sea wall and the hydrostatic pressure wheel. Questions like the exit of the water from the wheel at mean water level need to be answered.

6.4 Comparison of wave overtopping in the micro-model and the large scale physical model

Figure 6.17 presents the scaled overtopping rates measured in the micro-model and the large scale model over the wave height. It is seen that for both freeboards the micro-model predicts smaller overtopping rates than the large scale model. Even more as the wave height decreases the number of waves that do not overtop the structure in the micro-model increases. These results agree with previous authors like Kajima and Sakakiyama (1994) and Schulz (1992), who also recorded smaller overtopping volumes for smaller physical models. De Rouck et al. (2005), also observed similar differences and suggested that they occur mainly for small overtopping rates but are very important since the model predicts zero overtopping for a prototype condition with overtopping. Indeed Figure 6.17 implies that for larger wave heights and overtopping rates the micro-model's predictions are closer to the large scale model.

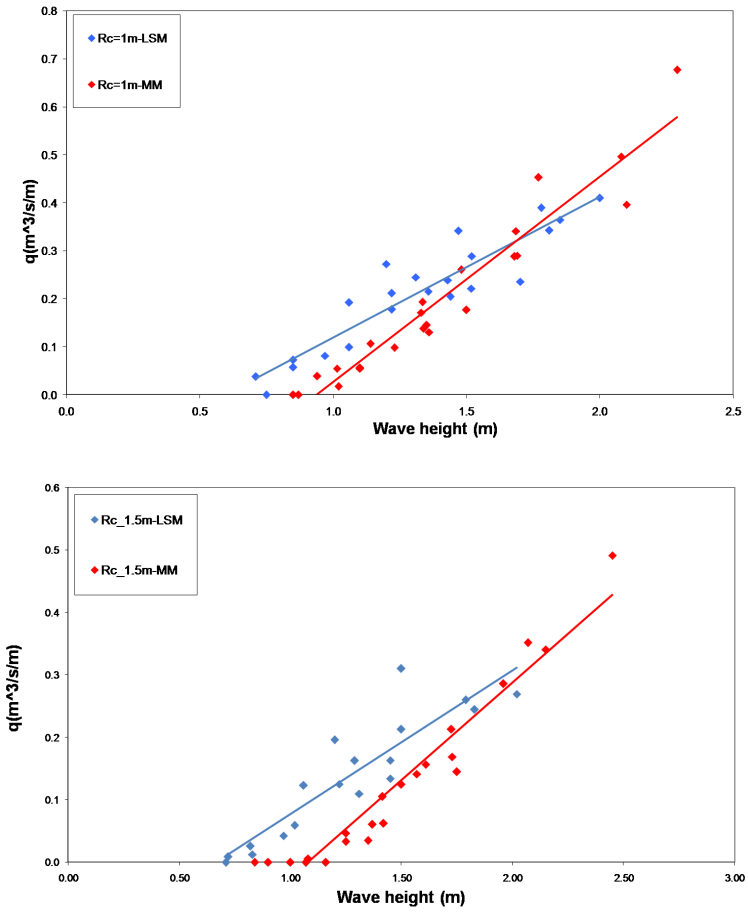

Figure 6.17: Overtopping rate as a function of the incoming wave hight in the micro-model and the large scale model for R_C = 1m (left) and R_C =1.5m (right); MM is the micro-model and LSM is the large scale model.

Furthermore the discrepancies on overtopping rates (e.g. $0.12m^3/s/m$) between the micro-model and the large scale model increase for the higher freeboard (R_c= 1.5m). This is in accordance with Schuttrumpf (2001) who suggested that viscosity effects are more pronounced for high freeboards since critical values of the overtopping Reynolds number ($< 10^3$) are achieved for freeboard heights near the wave rup-up height; surface tension and viscosity effects on wave run-up and overtopping in micro-models are better discussed in the following section. Nevertheless the results from both models are also compared to the predictions given by the overtopping rate formulas proposed by van der Meer and Janssen (1994) and Goda (2009).

The dimensionless relative overtopping rate (see 6.2) is plotted over the freeboard to wave height ratio in Figure 6.18. The curves fitted on the theoretical overtopping predictions are presented with blue for van der Meer and Janssen (1994) and red

(dashed for R_C = 1m) for Goda (2009). In general overtopping rates seem to be underpredicted by both formulas but a better fit is observed between the micro-model's results (above) and van der Meer and Janssen (1994), while Goda (2009) is closer to the experimental data only for the higher freeboard. Surprisingly enough a significant difference is recorded for the large scale model (below), were the theoretical values are much smaller than the test results.

Given the fact that both equations are empirical and have been developed on the basis of large scale experiments, one would expect them to fit better with the overtopping rates measured in the larger model. Since the method used here for the measurement of the water volume collected in the reservoir is accurate beyond any dispute, one possible explanation for this discrepancy would be the presence of a smoother slope and a plateau which may imply more intense wave reflection. On the contrary both previous authors used data for steeper (i.e 1 : 2 to 1 : 4) and rougher slopes which according to Battjes (1974) should result in smaller wave reflections and larger energy dissipation during the run-up, Bruce et al. (2006). Further support to this is provided by Maravelakis (2009) who reported observations of larger overtopping volumes occurring by the first incoming -and unaffected by reflections- wave.

In any case though both models appear to follow the same trends as those indicated by the theory. The relative overtopping rates are larger for the smaller freeboard and decrease as the freeboard to wave height ratio increases. Even more the selection of van der Meer and Janssen (1994) for the theoretical analysis of the structure is justified by its better fit on the data presented here.

On the contrary a good agreement is observed between the theoretical predictions and the micro-model's results, especially for the formula proposed by van der Meer and Janssen (1994). Goda's (2009) equation slightly overpredicts overtopping for the 1.5m freeboard and underpredicts them for the 1m crest freeboard. In general though it could be said that the micro-model agrees well with theory except when the overtopping volume is small.

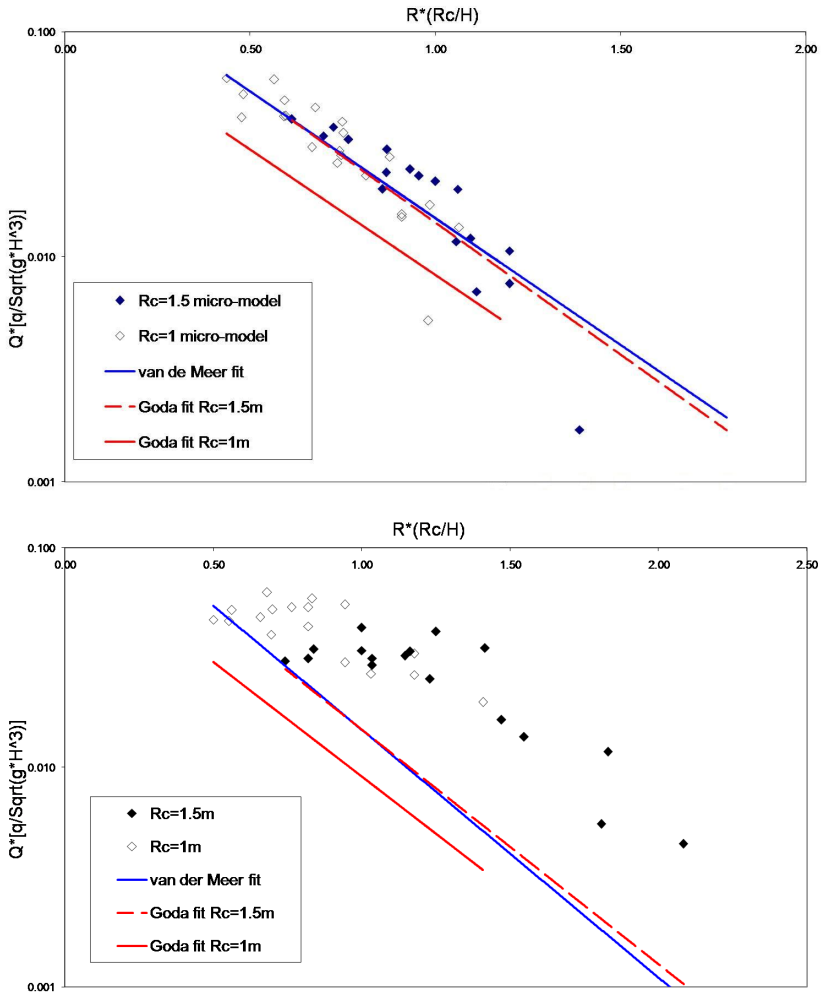

Figure 6.18: Plots of the relative overtopping rate against the relative crest freeboard for the micro-model (above) and the large scale model (below). Blue lines represent overtopping predictions according to van der Meer and Janssen (1994) and red lines predictions according to Goda (2009).

6.4.0.1 Scale effects influencing overtopping and run-up in micro-models

Surface tension and viscosity are the main fluid properties affecting overtopping and run-up and their influence increases for low overtopping rates, LeMehaute (1976), Wiegel (1976).

To present surface tension is considered to influence violent overtopping events and specifically the break-up of green water to spray and the air content in the run-up water. Kortenhaus et al. (2004a) argues that less air entrainment in model scale results in a small increase in the density of the water mass involved in the run-up, which in turn leads to smaller run-up heights and overtopping. Accordingly surface

tension effects are considered of minor importance compared to viscosity effects and especially for We_R larger than 10, Schuttrumpf (2001); were We_R is the run-up Weber's number.

Viscosity is a measure of the internal resistance of the fluid and influences its interaction with the slope during run-up, the flow state at model scale and the transport of spray by wind, Pullen et al. (2009). Schuttrumpf (2001), argues that for small overtopping rates the turbulent sublayer seize to exist and a transmission from hydraulic rough flow to smooth or transitional flow occurs. This is related to higher energy losses since the drag coeffient increases for smaller Reynolds number; the author placed the limit below which viscosity effects on wave run-up and overtopping are important to a critical overtopping Reynolds number of about 10^3.

To investigate the surface tension and viscosity effects on wave run-up and overtopping in micro-models, experiments in small scale were repeated using the same IPA solution used in Chapter 5. Unfortunately during the current project the measurement of the fluid's properties were not posssible and thus surface tension is again assumed to be 0.0436N / m, as reported in McDonald (2005), and viscosity $1.027*10^{-6}N^2$ / s, as calculated previously.

Nevertheless wave run-up could not be measured in the current set-up due to the small length of the ramp. Accordingly the composite sea wall was removed and the experiments were repeated for both fluids. Run-up heights were manually measured for waves plunging over the 1:10 slope. As the run-up height was considered the distance of the maximum point on the slope reached by the run-up water, from the still water level (SWL). To minimise the experimental error measurements were repeated 4 times for each wave set and the average run-up value was considered as the final run-up height; maximum differences of 15% were recorded.

Experiments were conducted with wave heights ranging between 0.015m and 0.05m, run-up Reynolds number between approximately 100 and 10^4 and Weber's number smaller than 10. Accordingly it is expected that run-up and overtopping in the micro-model will be influenced by both surface tension and viscosity.

6.4.0.2 Surface tension effects

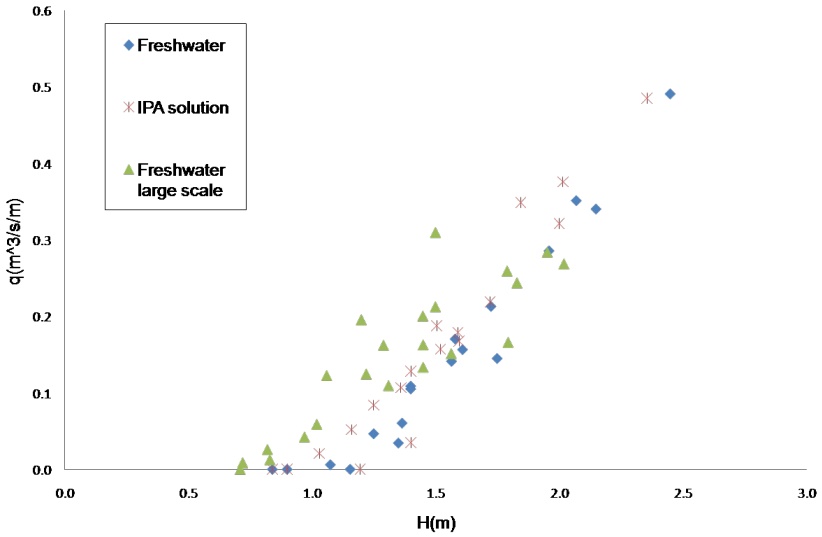

Figure 6.19: Overtopping rates over wave height for the micro-model with freshwater, the IPA solution and the large scale physical model.

The overtopping rates measured for the IPA solution are plotted over the wave height in Figure 6.19 along with the overtopping rates for freshwater in small and large scale. It is seen that when the surface tension was reduced in the micro-model, overtopping was increased and moved closer to the large scale model results but a significant difference is still observed.

In order to theoretically investigate the effects of surface tension on run-up the wave run-up velocity equation proposed by Schuttrumpf (2001) was used:

$$v_R = k^* \sqrt{2gR} \tag{6.6}$$

were,

v_R : is the run-up velocity at SWL,

k^* : is a factor counting for the influence of friction and thus it depends on Re,

R : is the wave run-up height.

If the influence of surface tension is to be considered and assuming an inviscous fluid ($k^* = 1$) then 6.6 is transformed to:

$$v_A = \sqrt{2g(R + sigma)} \tag{6.7}$$

where,

sigma : is the increase in run-up height due to surface tension and is expressed by:

$$sigma = \frac{\sigma}{\rho g h_R} \tag{6.8}$$

where,

σ : is the surface tension value,

ρ : is the density of the fluid,

h_R : is the run-up layer water thickness at SWL, which is equal to:

$$h_R = c_2 n R \tag{6.9}$$

where,

c_2: is an empirical coeficient and is a function of the slope. Schuttrumpf and Oumeraci (2005) calculated to be equal to 0.028 for a 1:6 dike slope; despite the steeper slope (1:10) used in the present study c_2 is assumed to be the same,

n : is the slope steepness.

Figure 6.20 presents the non-dimensional ratio of the run-up heights over the run-up Weber's number; $We_R = \frac{v_R^2 h_R \rho}{\sigma}$. It is seen that when freshwater is used, surface tension significantly influences run-up as the experimental values differ from the theoretical predictions. Although the run-up magnitude is similar for both cases the theory predicts larger We_R. Since σ, ϱ, and h_R are the same this might implies that

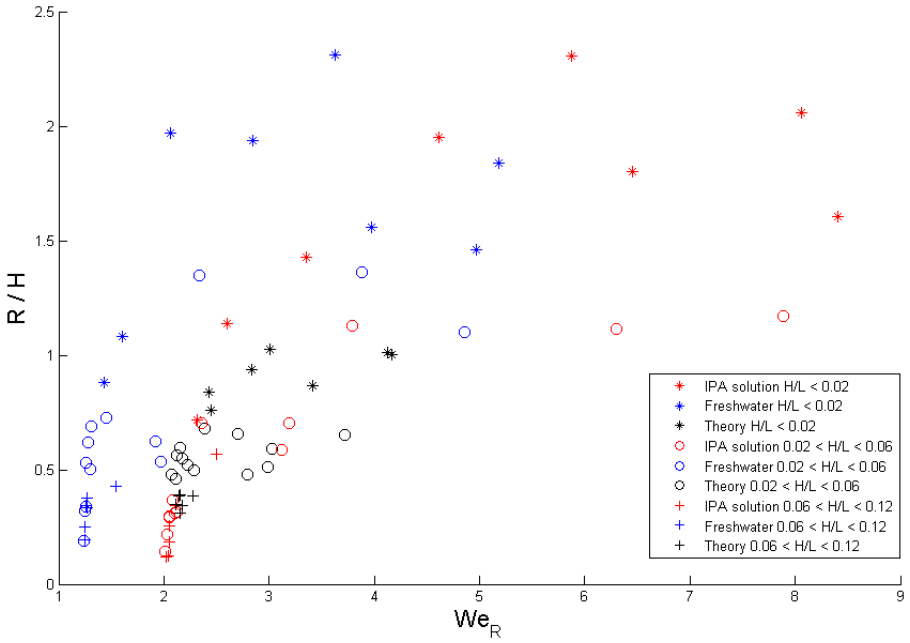

Figure 6.20: Plot of the run-up height normalised with the wave height over the Weber number. Theoretical values consider only surface tension effects.

run-up velocities are smaller in the micro-model than it should. This could be the result of smaller air content in the flow as suggested by Kortenhaus et al. (2004a).

On the contrary a good agreement is observed between the theoretical results and the experimental measurements for the IPA solution. In a similar way like above, this implies that when the surface tension is reduced the run-up velocity increases.

Although both experimental values appear to follow the same trend, smaller run-up values are recorded for the IPA solution. This is in accordance with the findings presented in Chapter 5, where it was shown that when the surface tension is reduced, more air is indeed entrained but in the same time more energy is consumed during breaking. As a result less energy is introduced to the run-up. Diffences between Figure 6.19 (larger overtopping volumes) and 6.20 (smaller run-up) are explained by the fact that breaking waves are considered here.

6.4.0.3 Viscosity effects

To investigate the theoretical influence of viscosity on wave run-up equation 6.6 was again used. If surface tension effects are neglected then the run-up velocity can be re-written as:

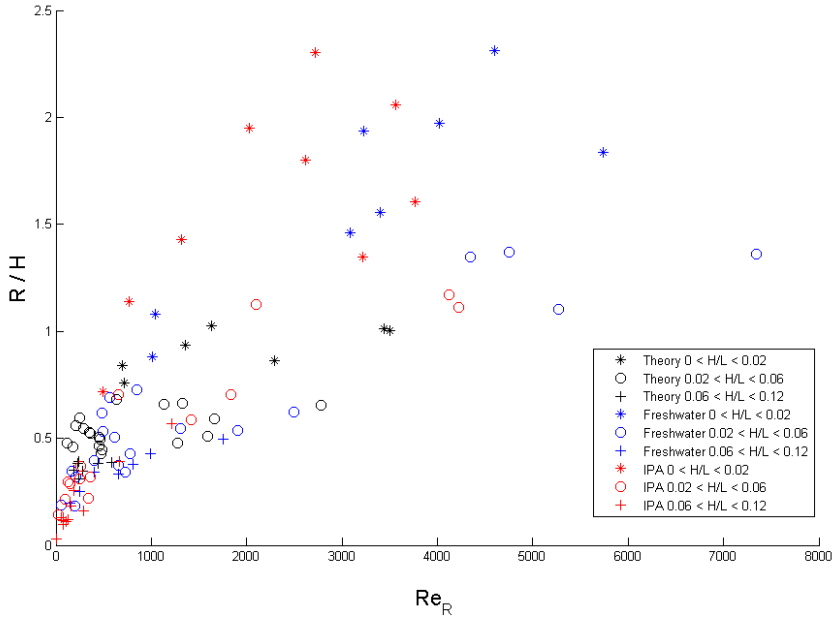

Figure 6.21: Plot of the run-up height normalised with the wave height over the Reynolds number. Theoretical values consider only viscosity effects.

$$v_R = \sqrt{\frac{1}{1-\alpha}}\sqrt{2gR} \tag{6.10}$$

where,

α: expresses the contribution of viscosity on run-up and $\alpha = \frac{fRn}{h_R}$.

The experimental ratio of the run-up height is plotted over the Reynolds number in Figure 6.21 and theoretical values are presented as well. It is observed that the influence of viscosity for smaller $\frac{H}{L}$ values results in reduced run-up heights than those predicted by theory for both fluids; as Re_R increases viscosity effects reduce. Once more the same trend appears for both cases but as expected the viscosity effect is slightly increased for the more viscous IPA solution but becomes negligible for $\mathrm{Re}_R > 10^3$.

Overall results presented here show that scale effects on run-up and overtopping due to viscosity are important but the influence surface tension is not as negligible as

previously suggested. Figure 6.19 clearly shows that larger overtopping rates are achieved for a fluid which is slightly more viscous than freshwater but has almost half its surface tension value. This is despite the fact that the comparison between experimental and theoretical measurements indicates a stronger effect of viscosity on the run-up height (Figures 6.20 and 6.21).

6.5 Summary and conclusions

A great deal of work is presented in the current chapter. micro-models have been used for the study of an engineering problem and the development of a novel idea.

The artificial flushing of a marina and / or a harbour through the use of flushing culverts has been investigated in a micro-model and results were verified by a large scale physical model as well. It was shown that simple culverts transmit energy instead of volume and as such they are not expected to be efficient flushing elements. In view of the new insights, previous studies need to be revised. The use of asymmetric culverts was also proposed for further study.

The micro-model of a composite seawall was used in order to assess the potential of the proposed structure to generate low head hydropower. Thus far composite seawalls have been proposed for the reduction of wave impact loads and to the author's knowledge this is the first time that the power generation scenario is investigated. With a hydraulic power of 1.5kW per m length of seawall available for a wave height of 1m the structure is directly comparable with other, more complicated, inshore wave energy devices like the SSG and thus its further development is encouraged.

For both studies two physical models having half the scale of the micro-models were used and the flow through flushing culverts was also analysed with a simple theoretical model. Subsequent conclusions are:

- Engineering structures can be modelled in micro-models.

- Micro-models can be used for the preliminary development and investigation of wave energy converters.

- Overtopping and run-up measurements in micro-models are subjected to scale effects, but the good agreement observed between experimental data and theoretical predictions implies that useful qualitative results can be acquired. Nevertheless, the influence of surface tension on run-up can be mitigated using a 10% isopropyl alcohol and distilled water solution.

- The trends on wave transmission through a flushing culvert appear to be similar for the micro-model and the large scale model. This entails that the same physical processes take part in both physical models.

- Micro-models are a very good complementary tool for the preliminary theoretical analysis of wave related engineering problems. The effectiveness of culverts as flushing elements has been assessed with the use of a simple theoretical model, a micro-model and a large scale physical model, and useful conclusion have been extracted.

- Micro-models provide a complementary option to large scale physical models. They are associated with low development costs, and reduced experimental time required, whilst the experimental arrangement can be easily altered and / or replaced.

- Micro-models should not be used as a standalone tool without further consideration, as the influence of scale effects could result in faulty conclusions. Overtopping rates for example are underestimated and larger values should be expected at full scale.

- Micro-models are an excellent screening tool as the same physical processes occurring in large and full scale can be easily recorded and displayed for demonstration and analysis. Results produced during the current studies have been successfully presented in major conferences, Stagonas et al. (2009) and Muller et al. (2009).

Chapter 7

Micro-modelling of wave fields: the Ostia-Rome yacht harbour case

7.1 Introduction

The findings reported thus far show that the micro-modelling of wave fields is possible for water depths larger than 0.025m and wave periods larger than 0.3sec. Under these conditions the effects of surface tension and viscosity are negligible and no wave damping occurs. Furthermore, wave breaking and run-up can also be modelled but a liquid with reduced surface tension should be used. Micro-models can also be used for 2D complementary studies of engineering problems but 3D micro-model studies of complex layouts (i.e. harbour layout) should be conducted in a wave basin longer and wider than 1.6m and 0.8m respectively.

When it comes to the design of a new harbour maybe the most important question faced by the designer refers to the efficiency of the proposed layout on reducing the incoming wave height. Although the first step of the design process involves the use of theoretical knowledge and engineering intuition the second involves the use of a numerical or a physical model, or in some cases both.

Despite the impressive advances of the past years, i.e Johnson et al. (2005), numerical models either can not accurately describe and predict the highly non linear processes

occurring between waves and complicated harbour layouts or require a large and often expensive computational effort, Kofoed et al. (2005). On the contrary, physical models include by definition all the non-linear wave-structure interactions involved in such schemes but they are associated with high construction and experimental costs. Hence their use is either prohibited or restricted to very specific investigations and thus the testing of more than one design scenarios is commonly not an option.

However the combination of wave micro-models with the full field mapping method proposed here could provide the scientists and engineers with a useful tool, which may allow for the inexpensive, quick and reliable testing of different design solutions. For this reason the micro-model of a yacht harbour is presented in the current chapter. Obviously the principal goal is not to extensively investigate the effectiveness of the harbour but rather to answer the question, if two different design options can be compared with a wave micro-model. Depending on the final result. such a tool could save precious computational and experimental time and even provide valuable data for the further development (e.g. calibration, validation) of numerical models.

Accordingly the Ostia-Rome yacht harbour was selected due to its impressive, innovative and complex shape and because useful and required information (i.e. breakwater dimensions etc) was available in the literature, i.e. Franco et al. (2009), Bellotti (2007) and Briganti et al. (2005).

7.2 The study area

The Ostia yacht harbour is located about 25km from Rome, on the south-west of the river Tiber, facing the Tyrrhenian Sea in central Italy (Figure, 7.1a.). The harbour has a unique design consisting of two rubble mound breakwaters, which converge to a central straight entrance to form an elliptic-shaped outer harbour, whilst the gravel beach (1:3) located opposite to the entrance is used to absorb the part of wave energy that penetrates the harbour. The outer harbour can be viewed as a filter that reduces transmission of wave energy except for certain incoming waves pertaining to

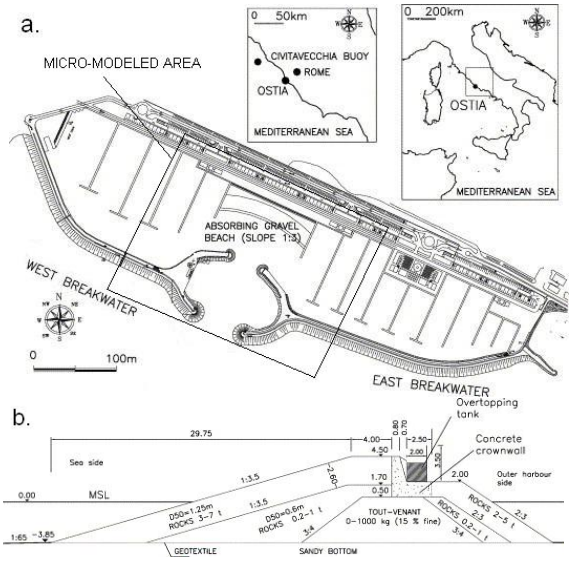

Figure 7.1: a. Layout and location map of Ostia-Rome yacht harbour and b. Design cross-section of the breakwater, after Briganti et al. (2005).

the frequency band of its resonating modes (i.e. $\omega = 0.13 rad/sec$), Bellotti (2007). According to Nakamura et al. (1996), when specific wave frequencies approach the harbour, the outer basin resonates and reduces the amount of energy transmitted towards the inner harbour.

Figure 7.1b summarises the structure's dimensions. The water depth at the breakwater's toe is 4m and its seaward slope is equal to 1:4.

7.3 Experimental apparatus

7.3.1 The wave basin and measuring equipment

The Ostia yacht harbour micro-model was facilitated in a 3x1.5x0.3m wave basin, as shown in Figure 7.2. The basin was equipped with a computer controlled, piston type wavemaker capable to generate regular waves but no active wave absorption was available. Optical observations were possible from every angle view thanks to the transparent side walls.

The PIV method, described in chapter 3, was used to map the wave field evolution within the basin. For this reason a F1-Exilim Casio camera was mounted over the

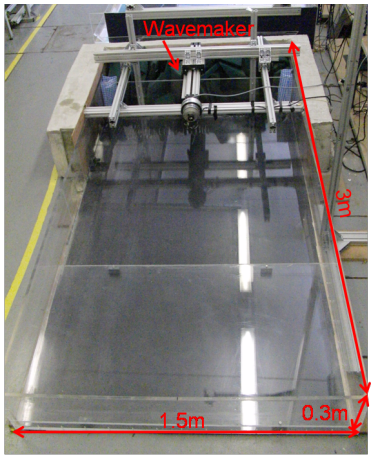

Figure 7.2: Picture of the large wave basin.

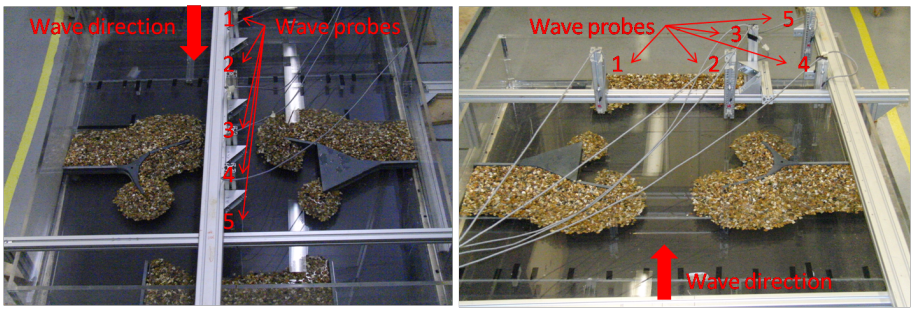

Figure 7.3: Ostia-Rome yacht harbour wave probe locations.

basin at a distance of 2.5m. High definition images were captured with this newly released camera at a recording speed of 60fps. The increased resolution of each frame, 1920x1080p instead of 640x480p, allowed the mapping of a larger area with a denser interrogation grid; in other words the PIV images could now be analysed at a much higher resolution.

Surface elevation measurements were also conducted with 5 resistance type wave probes at 10 different locations along the outer and inner area of the harbour (Fig. 7.3). The main purpose of these measurements was to provide a base of comparison for the aforementioned mapping technique. Accordingly wave height data were collected from several locations since, although accurate, wave gauges can only provide single point measurements.

7.3.2 The physical model

Figure 7.4 shows the construction process of the Ostia yacht harbour physical model. Model development, from design (day 1) to building (day 2), was done exclusively by the author and lasted for 3 days, while all the technical work required was conducted in the workshop of the hydraulics laboratory. The overall expenditure including the costs for the wavemaker and the wave basin was smaller than £4000.

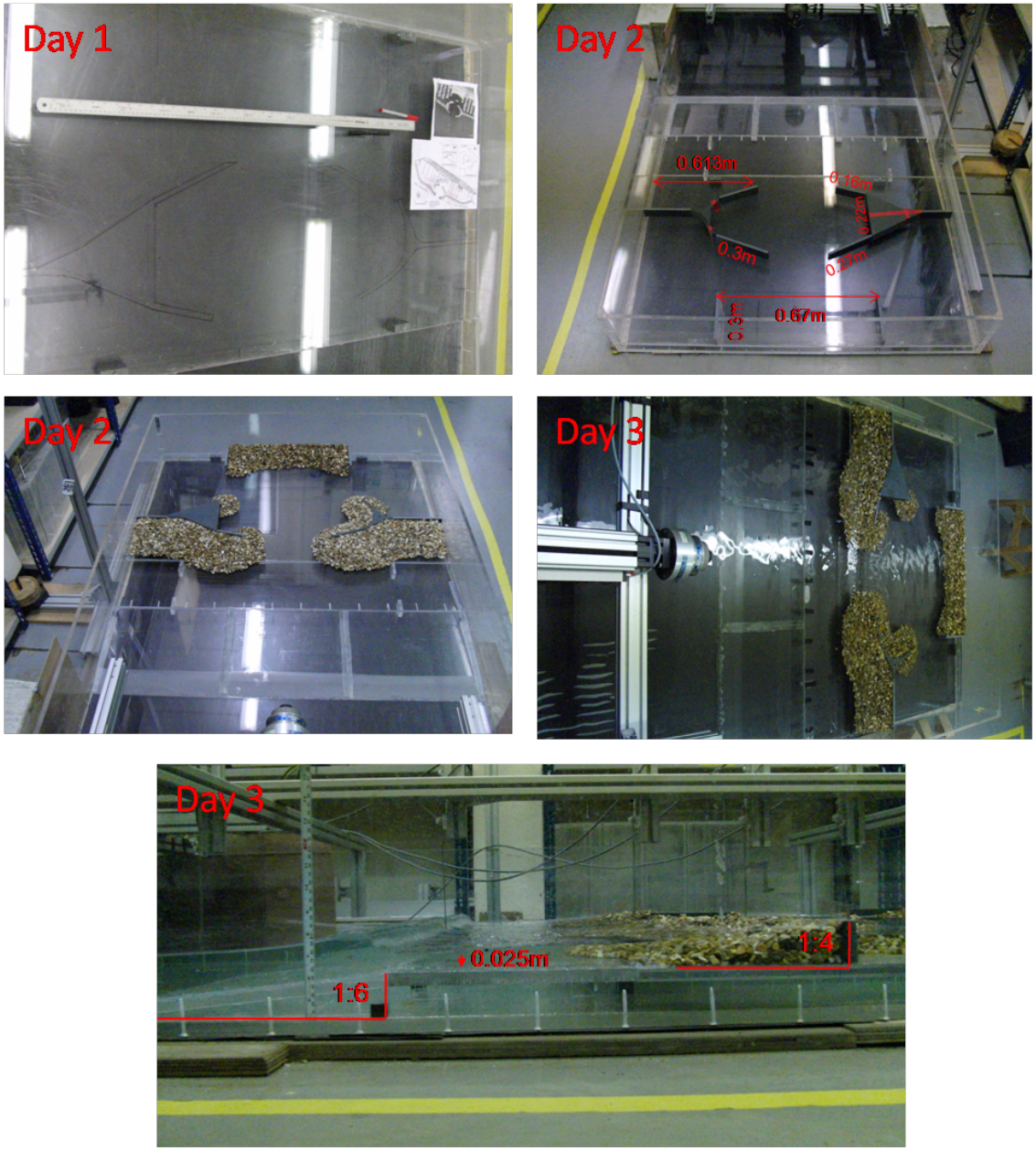

Figure 7.4: Construction process, from day 1 to day 3, of the Ostia yacht harbour micro-model.

Prototype harbour dimensions and wave climate information were extracted from Briganti et al. (2005) and scaled down. Primarily the length scale was decided based

	Prototype				Micro-model			
Wave period (sec)	8.39	7.37	9.56	10.90	0.66	0.58	0.75	0.85
Wave height (m)	2.22	2.15	2.26	2.40	0.014	0.013	0.014	0.015

Table 7.1: Prototype and laboratory wave conditions for the Ostia yacht harbour micro-model.

on the water depth limit for accurate micro-modelling of wave fields (see chapter 4). Hence a prototype water depth of 4m at the toe of the breakwater should correspond to 0.025m in the model, which results in a scale of 1:163. Accordingly Froude's law was used for the calculation of all other model dimensions required.

However with a 1:163 scale the model's length exceeded the width of the basin and as a result only part of the original harbour was built; the part had a real life length of 250m and is depicted in Figure 7.1a. The sea bottom of the modelled area consisted of a 1:6 slope and a level plateau, both made out of transparent, 15mm thick, Perspex plastic. The same but thinner material was used for all the breakwater components and the armour rocks were modelled by gravel with $d_{50} =$ 7.7mm. Obviously the purpose of such a physical micro-model is to simulate only the fundamental wave-structure interaction features, like wave diffraction. The very small scale used here and thus the large distortion between model and prototype Re prohibits the modelling of phenomena such as water flow through the breakwater and wave overtopping. Support for the latter is provided by Burcharth et al. (1999), as well as by the findings presented in the previous chapter.

Finally, Table 7.1 summarizes the prototype and model wave characteristics.

7.4 Results

As mentioned previously the aim of the experimental effort carried out in the current chapter was to investigate the potentials of wave micro-models as a tool for testing different design scenarios and preparing large scale experiments and / or numerical simulations. Such a tool could be used in cases where the wave-structure interactions

are complex enough so not to be dealt with theoretically and even more, where the veracity of numerical solutions can be disputed.

For this reason a micro-model of the newly built Ostia-Rome yacht harbour was constructed. The shape of its entrance makes this harbour unique in design, as it employs curved elements to form a secondary harbour in order to reduce the transmitted wave energy (Fig. 7.1). Accordingly the main question posed refers to the effectiveness of such an entrance and thus two different design scenarios were tested in the micro-model. For the first scenario, the rear breakwaters (enclosing the secondary harbour) have been removed (Fig. 7.8a.) and then put back in place for the second scenario (Fig. 7.8b.).

The wave field evolution and surface elevation were mapped and measured, with the PIV method described in Chapter 3, for regular waves with the characteristic periods referred to in Table7.1. Figure 7.5 presents the velocity vector fields for both scenarios and waves with T = 0.55sec. It is directly evident that the energy transmitted inside the harbour is significantly reduced when the secondary protective elements (breakwaters) are put in place. Surface flow velocities are reduced and the disturbance of the water surface is only limited within a narrow area located at the exit of the secondary harbour.

This is better illustrated in Figure 7.6 were the incoming wave height is equal to approximately 2cm and is reduced to 1.4cm for the first design scenario (a.) and 1cm for the second (b.). Since the wave energy is a function of the wave height squared the energy transmitted into the primary harbour is decreased by 51% and 75% respectively.

Moreover, in the absence of the rear breakwaters the stimulation of the water surface expands over a larger area within the primary harbour and extends over the limits of the absorbing beach (Fig. 7.5a.). The increased surface velocities observed adjacent to the beach can have a direct effect on the functionality of the harbour as they entail the reflection of the propagated wave by the sea wall; water oscillations like those can limit berth operativity and even induce high mouring forces Miles (1974).

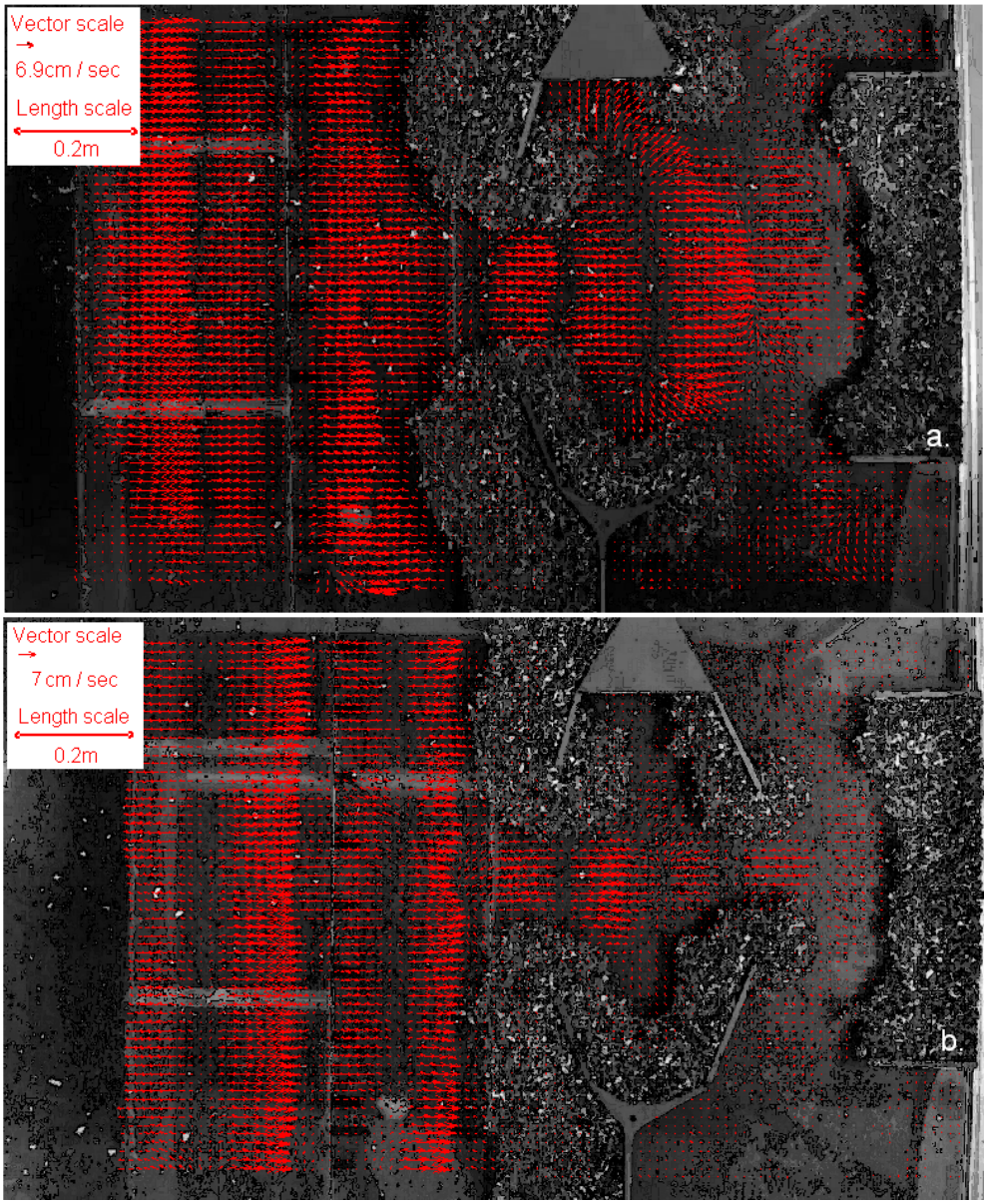

Figure 7.5: Surface velocities vector map for the Ostia yacht harbour micro-model, a. design scenario 1 without the outer harbour, and b. design scenario 2 with the outer harbour.

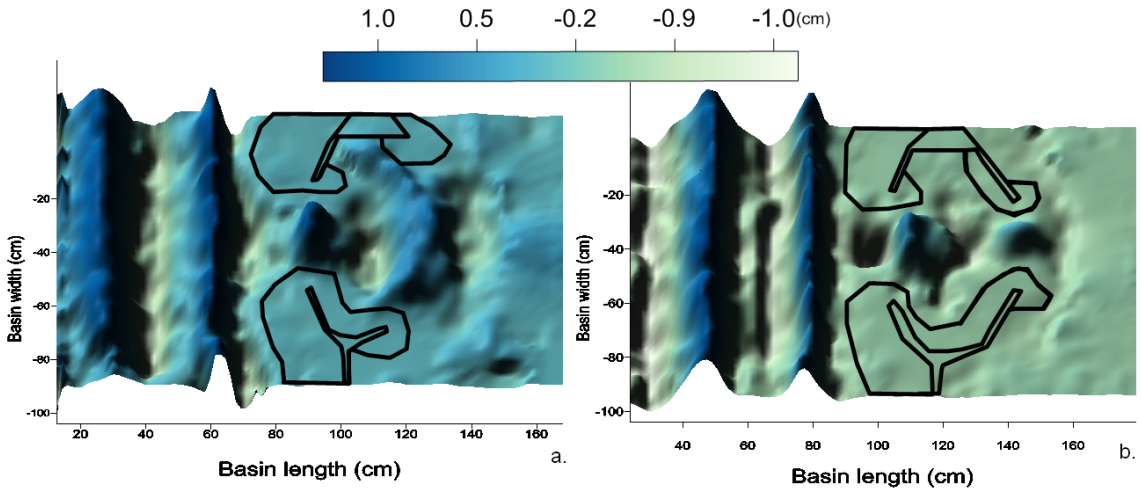

Figure 7.6: 3D represantation of the wave field in Ostia yacht harbour micro-model for a. design scenario 1 without the outer harbour, and b. design scenario 2 with the outer harbour. T = 0.55sec.

The presence and absence (for the second scenario) of such unwanted waves is better depicted in Figure 7.6 a. and b., where it seen that the maximum wave height near the sea wall has been reduced from approx. 0.35cm (no rear breakwaters) to almost 0cm (0.05cm). On the contrary the wave height at the inner toe of the breakwater is similar for both cases, at approximately 0.15cm. Figure 7.7 also illustrates that wave transmission is further enhanced for longer waves (T = 0.7sec) but only for the first case scenario. Unfortunately the width of the interrogation was restricted by almost 0.5m due to limits on the camera's focal plane. As result the evolution of the wave field further inside the harbour could not be mapped.

To verify all the above observations, wave probes were also used to measure the surface elevation inside the investigation area. Figure 7.8 a. and b. depict each probe's location and the recorded outcome. It is seen that for both cases the incoming wave height is 1.7cm or 18% smaller than the one calculated with the PIV method. In accordance the reduction in energy transmission is 22% (instead of 51%) when the rear breakwaters were not included but otherwise it remains at a high 70% which is along the limits of the previous estimation for 75%. However, wave probe measurements near the sea wall and the inner part of the breakwater agree very well with the surface elevation values attributed in the mapped wave field.

Nonetheless, the qualitative agreement between the two methods is very good. It is highly possible that the use of linear theory for the conversion of flow velocities to

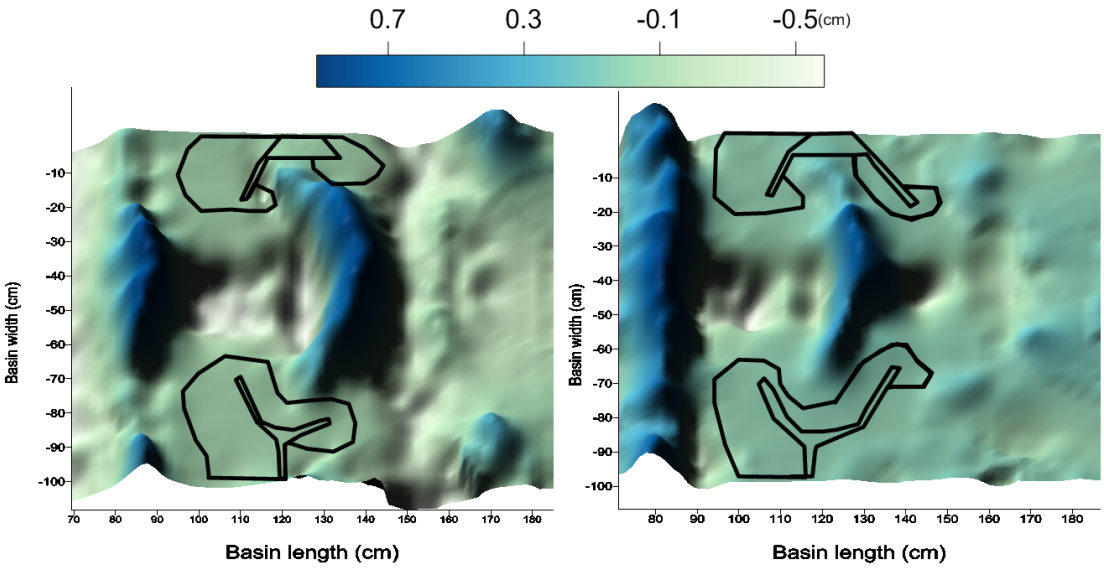

Figure 7.7: 3D represantation of the wave field in Ostia yacht harbour micro-model for a. design scenario 1 and b. design scenario 2. T = 0.7sec. The image has been intentionally truncated in order to emphasise on waves inside the sheltered area.

surface elevation is responsible for the observed quantitative differences. Some support to that is provided by Svendsen (2006) who argues that linear solutions can at least give the order of magnitude of all relevant quantities except for strongly non-linear cases. In any case, since a non-linear solution for the mapping method is not available here this arguement can not be further developed.

Despite their decreased accuracy Figures 7.5 and 7.6 provide information regarding the surface flow and wave direction, which can not be noticed with the wave gauge measurements. Figure 7.5a. for example illustrates that part of the incoming flow is strongly directed towards the unprotected, vertical part of the right-hand breakwater. Since such a flow-structure interaction could result into unwanted events as increased reflection, overtopping etc, it cannot be neglected. More importantly Figure 7.5b. clearly shows a flow movement from the sides towards the middle of the outer harbour but definitely further research is required in order to verify the existence / absence of resonating conditions.

In summary the combined use of micro-models with the PIV mapping method and wave probe measurements, indicates that the final design of the Ostia yacht harbour is the most effective in terms of reducing the transmitted wave energy. Figures 7.6

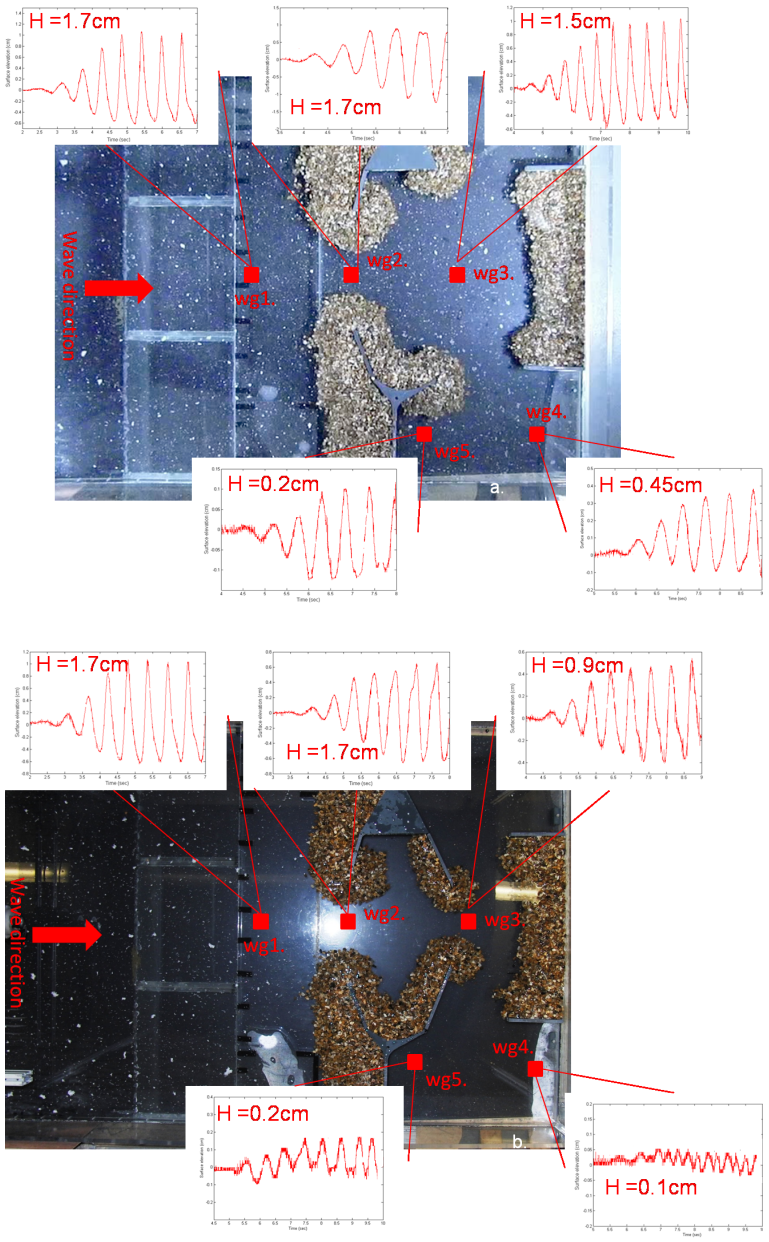

Figure 7.8: Wave probe locations and recorded surface elevation for, a. design scenario 1, and b. design scenario 2.

and 7.7 indicate that the principle energy dissipation comes from the diffraction of the wave and the absorption on the arms of the outer harbour. This is in initial agreement with the beneficial effects of the outer harbour as referred to in Bellotti (2007) who also reported reduced wave transmission in the inner basin due to the outer harbour. However if more wave frequencies are to be considered then further research is required although due to their small length micro-models will not be able to facilitate very long wave components.

Accordingly it is seen that within 6 days (overall experimental time) two different design options were built and tested, a task which is hardly possible in any large physical model. Hence, although the micro-model cannot provide final answers it can set the base for a more comprehensive large scale experiment. Finally the mapping of the flow / wave field presented in this chapter provides for the first time the opprtunity of a full field comparison with the corresponding numerical results.

7.5 Conclusions

The micro-model of an existed yacht harbour was presented in the current chapter in an attempt to investigate the use of micro-models as a robust tool for testing alternative design options and preparing large scale experiments and / or numerical simulations. For this reason the efectiveness of the unique shape of the Ostia-Rome yacht harbour was compared against a simpler alternative at a scale of 1 / 163. The model's length scale was selected based on the minimum water depth limits set in chapter 4 (d = 2.5cm) and the time scale was calculated according to Froude's law. The effects of both design options on the wave field and the transmitted wave energy were investigated for regular waves with an incident direction of 90^o. Wave probes were used to measure surface elevation and the wave field evolution was mapped for different wave periods. The main conclusions are:

- The findings presented here encourage the use of wave micro-models for the initial investigation of various design options for coastal structures. Once the alternative scenarios are eliminated the investigation can move further to a better targeted large scale experiment and / or to a numerical simulation.

- Although not 100% accurate, the combined use of wave micro-models with the PIV gives a good estimation upon the magnitude of the surface flow and wave phenomena taking place inside the wave basin. In contrast with traditional measuring equipment, this new tool provides full field surface flow and elevation data.

- The use of micro-models minimises the experimental time, effort and staff requirements along with the overall experimental expenditure.

- Compared with the alternative option examined here the present shape of the Ostia-Rome yacht harbour was found to be more efficient on reducing the energy transmitted inside the inner basin.

Chapter 8

Conclusions and future work

The present thesis is the first investigation of the validity and potentials of very small scale (i.e. $<$ 1:50) physical models of waves, termed wave micro-models. The critical review of the existed literature suggests that waves can be modelled at very small scales (e.g. d = 0.02m and T = 0.35sec) but the micro-modelling of wave fields for coastal engineering purposes, has never been considered before.

A novel wave field mapping method was developed first, which allows, for the first time, the full three-dimensional mapping of a wave field inside a small scale wave basin. Theoretical work and a large experimental effort established the validity limits for wave propagation and diffraction in micro-models, whilst the micro-modelling of breaking waves was investigated using a fluid with reduced surface tension. Finally, micro-models were successfully used to investigate a coastal engineering problem (harbour flushing through culverts), develop a novel breakwater type for wave energy conversion and compare two alternative design options for a yacht harbour. The results presented within every chapter were discussed in conjunction with theoretical considerations based on the existed literature and the main conclusions drawn from this effort are summarised here.

- Theoretical and experimental work established that for water depths larger than 0.03m and wave periods longer than 0.35sec scale effects are negligible and thus the micro-modelling of wave propagation and wave diffraction is valid.

- Wave breaking at micro-scales was demonstrated to be dominated by surface tension effects. Replacing freshwater with a fluid with reduced surface tension it was shown that wave breaking and subsequently energy dissipation can be modelled at very small scales. Such a fluid can be of use to future researchers studying air-water interactions.

- The micro-modelling of wave run-up and overtopping is improved when a fluid with reduced surface tension is used. The qualitative similarity between the micro-models and the large scale models is encouraging but the results should always be interpreted with care and for sure further research is required.

- The wave flow and surface elevation field were visualised over the full dimensions of a physical model for the first time, using a novel, PIV based, method. Although linear theory is used, the mapping method gives a satisfactory estimate at the magnitude of non-linear wave-structure interactions like, for example, wave diffraction. In any case and for non-breaking waves, the technique provides a very good overview of the temporal and spatial wave field evolution.

- The combination of micro-models with the mapping method can reveal the presence of unwanted surface flows, which are otherwise ignored by traditional measuring techniques (e.g. wave gauges).

- Expenses and time requirements associated with micro-models are very small, especially if compared with large scale physical models. Support to that is provided by the low model building cost and the low requirements for space and technical and experimental staff.

All the above yield that:

- Wave micro-models constitute a robust tool that can be used for the preliminary investigation of wave related coastal engineering problems and applications.

- Wave micro-models can be used for the initial development and testing of novel ideas, for testing geometry variations of a proposed design and preparing large scale experiments.

- Wave micro-models are of particular interest in combination with theoretical / numerical models.

8.1 Future work

The findings of the large experimental effort presented here showed that micro-models allow for the utilization of area rather than point measurement techniques, and can be employed for the simulation of wave fields and the cost-effective testing of novel ideas and geometry variations of a proposed design. This section presents three recommendations for future work.

1. Although robust the Particle Image Velocimetry (PIV) mapping method, described in Chapter 3, utilises linear theory which reduces its capacity to capture non-linear phenomena like for example reflected waves (superimposed wave field). Accordingly it is suggested that a numerical model should be developed that will allow for the accurate application of the method to non-linear processes. The model could be based on the work Madsen et al. (2002) who expressed the kinematic and dynamic surface conditions in terms of velocity variables defined on the free surface (eqs. 8.1, 8.2 and 8.3). Ignoring originally the non-linear terms, which include the unknown vertical velocity, the model will be inputted with the surface velocities extracted from the PIV method and calculate the surface elevation at each point of the interrogation grid for a single time step. The vertical velocity component can then be calculated from equation 8.1 and subsequently the surface elevation estimation can be iteratively improved (eq. 8.2). Defining the initial and boundary conditions -especially when complex geometries are involved- as well as methods for verifying the convergence of the iteration system are significant challenges for the development of such numerical model.

$$\eta_t - \tilde{w} + \nabla\eta \cdot \tilde{\mathbf{u}} = 0 \tag{8.1}$$

$$\tilde{V} + g\nabla\eta + \nabla(\frac{\tilde{V}\cdot\tilde{V}}{2} - \frac{\tilde{w}}{2}(1 + \nabla\eta\cdot\nabla\eta)) = 0 \tag{8.2}$$

$$\tilde{V} \equiv \tilde{\mathbf{u}} + \tilde{w}\nabla\eta \tag{8.3}$$

where,

η : is the surface elevation,

$\tilde{\mathbf{u}}$: is the horizontal velocity vector,

$\tilde{w}$: is the vertical velocity vector,

∇ : is the horizontal gradient operator defined by $\nabla \equiv \begin{pmatrix} \partial & \partial \\ \partial x & \partial y \end{pmatrix}$

2. The results presented in chapter 5 encourage further research on the use of the Isopropyl-alcohol (IPA) and distilled water solution in small scale physical models. The larger air entrainment and subsequent bubble formation observed imply that this fluid could potentially allow for a more accurate modelling of any air-water turbulent flow, like i.e. wave impact on vertical walls, hydraulic jumps etc. Accordingly it is suggested that for validation purposes, detailed void fraction measurements as those of Blenkinsopp (2007) and turbulent flow velocity measurements should be conducted. Nonetheless, the large energy dissipation values reported here for breaking waves entail that the complicated processes involved in these intense phenomena have not yet been fully understood.

3. Finally, the small scale wave basin could be modified to include wave generated longshore currents. Initially, the shallow water zone will be represented by an inclined and a horizontal platform which reduces the water depth, induces breaking, and thus generates mass transport onto the shallow zone. The side walls in the shallow zone will be permeable at bed level (out- and inlet) and will be connected through a channel running along the back side of the basin (Fig. 8.1 left). Inlet sizes will may vary near the bottom; the current working hypothesis being that the current concentrates just above the bed. Water levels will be measured at both in- and outlet, and it is expected that due to the flow resistance of the openings a head difference between them (in- and outlet) will develop (Fig. 8.1 left). LDA and PTV measurements could be conducted in the shallow zone (Fig. 8.1 right) in order to establish flow paths and actual flow velocities as a function of wave height, wave

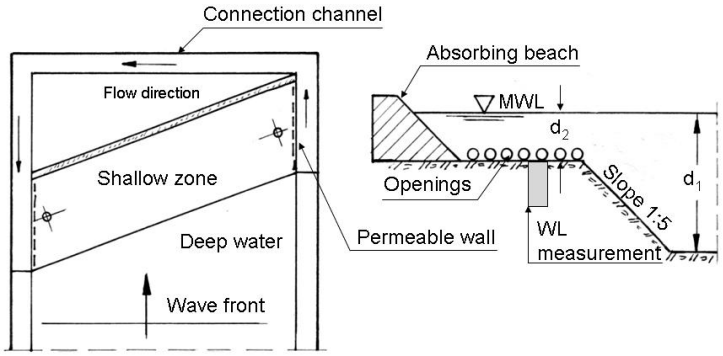

Figure 8.1: Proposed experimental apparatus for a wave micro-model including longshore currents.

period and distance from the seabed. At a first stage these tests are definitely not meant to model reality but they are merely intended to assess whether or not wave induced longshore currents can be generated in a physical model.

References

Adamsom, A. (1990). *Physical Chemistry of Surfaces*, John Whiley & Sons, Inc.

Alam, S. (2009). Let us try to save the vanishing mississippi river delta, *Louisiana Civil Engineer* **2**: 6–13.

ASCE (2000). *Hydraulic modelling*, U.S Association of Civil Eng.

Banner, M. and Peregrine, D. (1993). Wave breaking in deep water, *Annu. Rev. Fluid Mech.* **25**: 373–397.

Battjes, J. (1974). Surf similarity, Vol. Proceedings 14TH International Conference on Coastal Engineering.

Bauer, B. and Greenwood, B. (1988). Surf-zone similarity, *Geographical Review* **78**: 138–147.

Beckett, A. and Marshall, S. (1983). Design and construction of muara deep water port, brunei., *Proc. of the Inst. of Civil Eng. London.*

Beckett, T. (1992). Hydraulic mini-models studies, *Proc. of the 2nd Intern. Conf. in Marina Technology*, pp. 283–.

Bellotti, G. (2007). Transient response of harbours to long waves under resonance conditions, *Coastal Engineering* **54**: 680–693.

Benjamin, T. (1967). Instability of periodic wave trains in non-linear dispersive systems, *Proc. of the Roy. Soc. A299*, pp. 59–75.

Benjamin, T. and Feir, J. (1967). The disintegration of wave trains on deep water, part 1, *Journal of Fluid Mech.* **27(3)**: 417–430.

Blenkinsopp, C. (2007). *Air entrainment, splash and energy dissipation in breaking waves*, Master's thesis, School of Civil Engineering and the Environment.

Blenkinsopp, C. and Chaplin, J. (2007). Validity of small-scale physical models involving breaking waves, *22nd International workshop on water waves and floating bodies, Plitvice*.

Blue, F. and Johnson, J. (1949). Diffraction of water waves passing through a breakwater gap, *Trans. Amer. Geophys. Union* **30**: 705–718.

Bonmarin, P. (1989). Geometric properties of deep water breaking waves, *Journal of Fluid Mech.* **209**: 405–433.

Briganti, R., Belloti, G., Frano, L., De Rouck, J. and Geeraerts, J. (2005). Field measurements of wave overtopping at the rubble mound breakwater of rome-ostia yacht harbour, *Coastal Engineering* **52**: 1155–1174.

Brown, J. (2004). Hydraulic micro model sedimentation study of the middle mississippi river at buffaloisland, *24th USSD Annual Meeting and Conference Proceedings*.

Bruce, T., van der Meer, J., Franco, L. and Pearson, J. (2006). A comparison of overtopping performance of different rubble mound breakwater armour., *30th International Conference on Coastal Engineering, ICCE*, number 1705, San Diego, USA.

Bruun, P. and Viggosson, G. (1977). The wave pump: conversion of wave energy to current energy, *Journal of the Wat. Port, Coastal and Ocean Division, Proc. of the ASCE* **103(4)**: 449–469.

Bullock, G., Crawford, A.R. andHewson, P., Walkden, M. and Bird, P. (2001). The influence of air and scale on wave impact pressures, *Coastal Engineering* **42**: 291–311.

Burcharth, H., Liu, Z. and Troch, P. (1999). Scaling of core material in rubble mound breakwater model tests., *Proceedings of the 5th International Conference on Coastal and Port Engineering in Developing Countries (COPEDEC V), Cape Town, South Africa*.

Carosi, G. and Chanson, H. (2006). Air-water time and length scales in skimming flows on a stepped spillway. application of the spray characterisation, *Technical report*, Report No. CH59/06. Division of Civil Eng., The University of Queensland, Brisbane, Australia.

Carr, J. and Stelzriede, M. (1952). Diffraction of water waves by breakwaters, *Technical report*, U.S. National Bureau of Standards, Circular No. 521,109-125.

Ceniceros, H. (2003). Dynamic generation of capillary waves, *Phys. Fluids* **11**: 1032–1050.

Ceniceros, H. and Hou, T. (1999). Dynamic generation of capillary waves, *Phys. Fluids* **11**: 1032–1050.

Chanson, H. (1997). *Air bubble Entrainment in Free-Surface Turbulent Shear Flows*, London:Academic Press.

Chanson, H. (2009). Turbulent air-water flows in hydarulic structures: dynamic similarity and scale effects, *Environ. Fluid Mech* **9**: 125–142.

Chanson, H., Aoki, S. and Hoque, A. (2002). Scaling bubble entrainment and dispersion in vertical circular plunging jet flows: Freshwater versus seawater, *Proceedings of 5th International Conference on Hydrodynamics ICHD2002, Taiwan,*, pp. 431–436.

Chanson, H., Aoki, S. and Hoque, A. (2006). Bubble entrainment and dispersion in plunging jet flows: freshwater versus seawater., *J. Coastal Research* **22(3)**: 664–677.

Chanson, H., Aoki, S. and Maruyama, M. (2002). Unsteady air bubble entrainment and detrainment at a plunging breaker: dominant times scales and similarity of water level variations, *Coastal Engineering* **46**: 139–157.

Chanson, H. and Lee, J. (1995). Characteristics of plunging breaking waves, *Research Report CE150*, Department of Civil Engineering.

Chanson, H. and Toombes, L. (2002). Experimental study of gas liquid interfacial properties in a stepped cascade flow, *Environ. Fluid Mech* **2(3)**: 241–263.

Couriel, E., Horton, P. and Cox, D. (1998). Supplementary 2-d physical modelling of breaking wave characteristics., *Technical report*, WRL Technical Report 98/14, Water Research Laboratory, University of New South Wales, Sydney.

Craeye, C., Sobieski, P., Bliven, L. and Guissard, A. (1999). Ring-waves generated by water drops impacting on water surfaces at rest, *IEEE Journal of Oceanic Engineering* **24 (3)**: 323–332.

Curtis, R., Hathaway, K., T., H. and Seabergh, W. (2002). Video-based wave direction measurements in a scale physical model, *Coastal and Hydraulics Engineering Technical Note ERDC/CHL CHETN IV-49, U.S. Army Engineer Research and Development Center, Vicksburg, MS.*

Dalrymple, R. (1985). *Physical modeling in Coastal Engineering.*

Dalrymple, R. (1989). *Physical modelling of Littoral Processes*, Kluwer Academic Publishers, Dordrecht, The Netherlands, chapter Recent Advnaces in Hydraulic Modelling, pp. 567–588.

Dalrymple, R., Eubanks, R. and Birkemeier, W. (1977). Wave-induced circulation in shallow basins, *Journal of the waterway, port, coastal and ocean division* **49**: 117–135.

Davinroy, R. (1994). *Physical sediment modeling of the mississippi river on a micro scale.*, Master's thesis, University of Missouri-Rolla, Rolla, Mo.

Davinroy, R. (2004). Micro modeling success stories, *24th USSD Annual Meeting and Conference Proceedings.*

De Rouck, J., Geeraerts, J., Troch, P., Kortenhaus, A., Pullen, T. and Franco, L. (2005). New results on scale effects for wave overtopping at coastal structures, *Proc. ICE Coastlines, Structures and Breakwaters*, pp. 29–43.

De Rouck, J., Van de Walle, B., Troch, P., van der Meer, J., van Damme, L., Medina, J., M., W. and Frigaard, P. (2007). Wave run-up on the zeebrugge rubble mound breakwater: Full scale measurements results versus laboratory results, *Journal of Coastal Research* **23**(3): 584–591.

Dean, G. and Stokes, M. (2002). Scale dependence of bubble creation mechanisms in breaking waves, *Nature* **418**: 839–844.

Dean, R. and Dalrymple, R. (1984). *Water wave mechanics for engineers and scientists*, World Scientific.

Dimas, A. (2007). Large-wave simulation of microscale breaking waves induced by a free-surface drift layer, *Wave Motion* **44**: 355–370.

Dold, J. and Peregrine, H. (1986). Water-wave modulation, *Proc. of the 20th Conf. Coastal Engineering, ASCE*, Vol. 1, pp. 163–175.

Dommermuth, D., Lin, D., Rap, R., Chan, E. and Melville, W. (1988). Deep water plunging breaker: a comparison between potential theory and experiments, *Journal of Fluid Mech.* **189**: 423–442.

Duncan, H. (2001). Spilling breakers, *Annu. Rev. Fluid Mech.* **35**: 519–547.

Duncan, J., Haibing, Q., V., P. and Wenz, A. (1999). Gentle spilling breakers: crest profile evolution, *Journal of Fluid Mech.* **379**: 191–222.

Duncan, J., Philomin, V., H., Q. and Davis, L. (1994b). The fomration of spilling breaker, *Phys. Fluids* **6**.

Duncan, J., Philomin, V., Qiao, H. and Davis, L. (1994a). The fomration of spilling breaker, *Phys. Fluids* **6**: 2558–2560.

Ebuchi, N., Wawamura, H. and Toba, A. (1987). Fine structure of laboratory wind wave surfaces studies using an optical method, *Boundary Layer Met.* **39**: 133–151.

Elshof, I., Janssen, T. and van Dongeren, A. (2001). Video observation of laboratory waves, *The Fourth International Symposium on Ocean Wave Measurement and Analysis (Waves2001), San Fransisco, ASCE.*

Ettema, R. (2001). A framework for evaluating micro-models, *Technical report*, LimitedDistribution Report No. 295, Iowa Institute of Hydraulic Research,The Univ. of Iowa, Iowa City, Iowa.

Ettema, R., Fujita, I., Muste, M. and Kruger, A. (1997). Particle image velocimetry for whole field measurement of ice velocities, *Cold Regions Science and Technology* **26**: 97–112.

Ettema, R. and Maynord, R. (2002). Framework for evaluating very small hydraulic models of channel - control works, *Technical report*, Hydraulic Measurements and Experimental Methods, ASCE, Reston, U.S.

Ettema, R. and Muste, M. (2004). Scale effects in flume experiments on flow around a spur dike in flatbed channel, *Journal of Hydraulic Engineering* **130(7)**: 635–646.

Fairley, I. and Davindson, M. (2008). A two dimensional wave flume investigation into the effect of multiple vertical steps on the form of breakin waves, *Journal of Coastal Research* **24**: 51–58.

Falvey, H. (1999). Letter to Editor, Misuse of term model, *Civil Engineering Magazine, ASCE, Reston* **69**.

Fan, L. and Tsuchiya, K. (1990). *Bubble wake dynamics in Liquids and Liquid-Solid Suspensions*, Butterworth-Heinemann, Boston.

Fountoulis, G. and Memos, C. (2005). Optimization of openings for water renewal in a harbour basin, *Journal of Marine Env. Eng.* **7**(4): 297–306.

Franco, L. (1996). Ancient mediterranean harbours: a heritage to preserve, *Ocean and Coastal Management* **30(2-3)**: 115–151.

Franco, L., Geeraerts, J., Briganti, R., Willems, M., G., B. and De Rouck, J. (2009). Prototype measurements and small-scale model tests of wave overtopping at shallow rubble-mound breakwaters: the ostia-rome yacht harbour case, *Coastal Engineering* **56**: 154–165.

Freeman, J. (1929). *Hydraulic laboratory practice*, American Society of Mechanical Engineers, New York.

Frigaard, P. and Brorsen, M. (1995). A time domain method for separating incident and reflected irregular waves., *Coastal Engineering* **24**: 205–215.

Fuhrboter, A. (1986). Model and prototype tests for wave impact and run-up on a uniform 1 : 4 slope, *Coastal Engineering* **10**.

Fujita, I., Muste, M. and Kruger, A. (1998). Large scale particle image velocimetry for flow analysis in hydraulic engineering applications, *Journal of Hydraulic Research* **36**: 397–414.

Funke, E. and Mansard, E. (1987). A rationale for the use of the deterministic approach to laboratory wave generation, *Proc. of Wave Analysis and Generation in Laboratory Basins, 22nd Congress IAHR.*

Gaines, R. and Maynord, S. (2001). Microscale loos-bed hydraulic models, *Journal of Hydraulic Engineering* pp. 335–338.

Galvin, C. (1968). Breaker type classification on three laboratory beaches, *Journal of Geoph. Research* **73**: 3651–3659.

Garrett, G., Li, M. and Farmer, D. (2000). The connection between bubble size spectra and energy dissipation rates in the upper ocean, *Journal of Physical Oceanography* **30**: 2163–2171.

Geeraerts, J., De Rouck, J., Beels, C. and Gysens, S. (2006). Reduction of wave overtopping at seadikes: Stilling wave basin (swb), *30th International Conference on Coastal Engineering*, Vol. 5, pp. 4680–4691.

Goda, Y. (2000). *Random seas and design of maritime structures*, 2nd edn, World Scientific, Singapore.

Goda, Y. (2009). Derivation of unified wave overtopping formulas for seawalls with smooth impermeable surfaces based on selected clash datasets, *Coastal Engineering* **56**: 385–399.

Goda, Y. and Suzuki, Y. (1976). Estimation of incident and reflected waves in random wave experiments, *Proc. 15th Int. Conf. Coastal Eng., ASCE, New York*, pp. 828–865.

Gonzalez, C. and Chanson, H. (2004). Interactions between cavity flow and main stream skimming flows: an experimental study, *Can. Journal of Civil Eng.* **31**: 33–44.

Gorman, R. (1999). Crvfit software, *Technical report*, National Institute of Water and Atmospheric Research, Hamilton, New Zealand.

Govender, K., Mocke, G. and Alport, M. (2002). Video-imaged surf zone wave and roller structures and flow fields., *Journal of Geophysical Research* **107**: 1–21.

Graf, W. (1971). *Hydraulics of sediment transport*, McGraw-Hill, New York.

Grant, I., Stewart, J. and Padilla-Perez, I. (1990). Topographical measurments of water waves using the projection moire method, *Applied Optics* **29(28)**: 3981–3983.

Gray, C. and Bruce, T. (1995). The application of particle image velocimetry (piv) to offshore engineering, *Proceedings of the 5th Int. Offshore and Polar Eng. Conf., ISOPE'95*, Vol. 3, pp. 701–708.

Grune, J. and Breteler, M. (2010). Introduction, *Proc. of the Hydralab III Joint User Meeting, Hannover, February*.

Haas, K. and Svendsen, I. (2002). Laboratory measurements of the vertical structure of rip currents, *Journal of Geophysical Research* **107(C5)**: 3047.

Haines, M. and Johnson, B. (1995). Injected bubble populations in seawater and freshwater measured by a photographic method, *Journal of Geophysical Research* **100**: 7057–7068.

Haque, M., Klaassen, G. and Enggrob, H. (2006). Scale effects in movable bed models of rivers with dominant suspended load, *Examining the Confluence of Environmental and Water Concerns. Proceedings of the World Environmental and Water Resources Congress*.

Hirschfelder, J. (1954). *Molecular theory of gases and liquids*, Wiley, New York.

Horikawa, K. (1988). *Nearshore Dynamics and Coastal Processes*, University of Tokyo Press.

Huang, Z. (2007). An experimental study of the surface drift current in a wave flume, *Ocean Engineering* **34**: 343–352.

Hughes, S. (1993). *Physical models and laboratory techniques in coastal engineering*, World Scientific.

Hull, P. and Muller, G. (2002). An investigation of breaker heights, shapes and pressures, *Ocean Engineering* **29**: 59–79.

Hunt, J. (1952). Viscous damping of waves over an inclined bed in a channel of finite width., *La Houille Blanche* **7**: 836.

Hwung, H., Chyan, J. and Chung, Y. (1992). Energy dissipation and air bubbles mixing inside the surf zone, *Proc. 23rd Int. Conf. on Coastal Eng., ASCE, Venice, Italy*, Vol. 1, pp. 308–321.

Irribarren, C. and Nogales, C. (1949). Protection des ports 2, *17th Int. Navig. Congress, Lisbon*, pp. 31–80.

Iversen, H. (1952). *Laboratory study of breakers*, National Bureau of Standards, Circular.

Jansen, P. (1986). Laboratory observations of the kinetics in the aerated region of breaking waves, *Coastal Engineering* **9**: 453–477.

Jensen, O. and Klinting, P. (1983). Evaluation of scale effects in hydarulic models by analysis of laminar and turbulen flows, *Coastal Engineering* **7**: 319–329.

Johnson, H., Karambas, T., Avgeris, I., Zanuttigh, B., Gonzalez-Marco, D. and Caceres, I. (2005). Modelling of waves and currents around submerged breakwaters, *Coastal Engineering* **52**: 949–969.

Johnson, J. (1952). Generalized wave diffraction diagrams, *Proc. Second Conf. Coastal Eng. Berkeley, Calif.: The Eng. Foundation Council on Wave Research*, pp. 6–23.

Kajima, R. and Sakakiyama, T. (1994). Review of works using criepi flume and present work., *Coastal Dynamics.*, Barcelona, Spain.

Kamphuis, J. (1973). Short-wave models with fixed bed boundary layer, *Journal of the waterways harbors and coastal engineering division* **4**: 471–482.

Kamphuis, J. (1974). Practical scaling of coastal models, *Proc. of the Conf. on Coastal Eng.*, pp. 2086–2101.

Kapdasli, M. and Turker, U. (2002). The wave breaking phenomena as a tool for environmentally friendly shore protection., *Water Science and Technology* **46**: 153–160.

Karambas, T. (2004). *Computational wave mechanics and coastal engineering: a theoretical approach with educational and operational software. (in Greek)*, Mitilini.

Keulegan, G. (1950a). The gradual damping of a progressive oscillatory wave with distance in a prismatic rectangular channel, *Technical report*, (unpublished-in Hughes 1993) National Bureau of Standards, Washington D.C.

Keulegan, G. (1950b). *Wave motion*, J. Wiley & Sons, pp. 711–768.

Kittle, P. (2002). Removing foam particles with foam medium, *A2C2 Magazine: Contamination control of life sciences and microelectronics* .

Kofoed, H., Kerper, D., Sørensen, O. and Kirkegaard, J. (2005). Simulation of long wave agitation in ports and harbours using a time-domain boussinesq model, *Proceeding of the Fifth COPRI International Conference on Ocean Wave Measurement and Analysis, WAVES, 2005, Madrid, Spain, paper n. 077.*

kofoed, J., Frigaard, P., E., F.-M. and Sorensen, H. (2004). Prototype testing of the wave energy converter wave dragon, *World Renewable Energy Conference VIII (WREC 2004).*

Kortenhaus, A., Oumeraci, H., Geeraerts, J., De Rouck, J., Medina, J. and J.A., G.-E. (2004a). Laboratory effects and other uncertainities in the wave overtopping measurments., *29th International Conference on Coastal Engineering*, Lisbon, Portugal.

Kortenhaus, A., van der Meer, J., Burcharth, H., Geeraerts, J., Pullen, T., D., I. and Troch, P. (2005). Clash workpackage 7-quantification of measurement errors, model

and scale effects related to wave overtopping, *Technical report*, Leichtweib Institute for Hydraulics, Germany.

Koterayama, W. and Hu, C. (1996). Wave forces on horizontal cylinders at low keulegan-carpenter and reynolds numbers, *International Journal of Offshore and Polar Engineering* **6(2)**.

Lamarre, E. (1993). An experimental study of air entrainment by breaking waves.

LeMehaute, B. (1965). Wave absorbers in harbours, *Technical report*, Report No. 2-122, US Army Waterways Exp. Station, Vicksburg.

LeMehaute, B. (1970). A comparison of fluvial and coastal similitude, *Proc. of the Conf. on Coastal Eng., Washington, D.C.,*.

LeMehaute, B. (1976). Similitude in coastal engineering, *Journal of waterways, harbors and coastal engineering division* **102**.

LeMehaute, B., Divoke, D. and Lin, A. (1968). Shallow water waves: A comparison of theories and experiments, *Proc. 11th Int. Conf. on Coastal Engineering.*

Lighthill, J. (1975). *Waves in Fluids*, Cambridge, Cambridge University Press.

Liu, X. and Duncan, J. (2003). The effects if surfactants on spilling breaking waves, *letters to nature* **421**: 520–523.

Liu, X. and Duncan, J. (2006). An experimental study of surfactant effects on spilling breakers, *J. Fluid Mech.* **567**: 433–455.

Longuet-Higgins, M. (1982). Parametric solutions for breaking waves, *Journal of Fluid Mech.* **121**: 403–424.

Longuet-Higgins, M. (1994). Shear instability in spilling breakers, *Proc. R. Soc. Lon. A 446*, pp. 399–409.

Longuet-Higgins, M. (1996). Capillary jumps on deep water, *Journal of Phys. Ocean.* **96**: 1957–1965.

Longuet-Higgins, M. (1997). Progress towards understanding how waves break, *Symp. Nav. Hydrodyn. 21st, Trondheim, Nor. June 1996, pp. 7-28.*

Longuet-Higgins, M. and Cleaver, R. (1994). Crest instabilities of gravity waves: The almost highest wave, *Journal of Fluid Mech.* **258**: 115–129.

Longuet-Higgins, M. and Cokelet, E. (1978). The deformation of steep surface waves on water, *Proc. Royal Soc. London* **A**: 364.

Longuet-Higgins, M. and Dommermuth, D. (1997). Crest instabilities of gravity waves. part . non-linear development and breaking, *Journal of Fluid Mech.* **336**: 33–50.

Lozada, I., Patterson, M. and Lozada, M. (1997). Harmonic generation past a submerged porous step, *Coastal Engineering* **31**: 281–304.

Ltd, C. C. (2001). *Wave Monitor Manual*, Unit 2, Ind. Estate, Berkshire, England.

Madsen, P., Bingham, H. and Liu, H. (2002). A new boussinesq method for fully non-linear waves from shallow to deep water, *Journal of Fluid Mech.* **462**: 1–30.

Mansard, E. and Funke, E. (1980). The measurement of incident and reflected spectra using a least squares method, *Proc. 17th Int. Conf. Coastal Eng., ASCE, New York*, pp. 154–172.

Maravelakis, N. (2009). *Experimental investigation of a novel composite seawall for wave energy conversion*, Master's thesis, Civil Eng. and the Env., University of Southampton.

Margheritini, B., Vicinanza, D. and Frigaard, P. (2009). Ssg wave energy converter: Design realiability and hydraulic performance of an innovative overtopping device, *Renewable Energy* **34**: 1371–1380.

Margheritini, L., Vicinanza, D. and Frigaard, P. (2008). Sea slote cone generator overtopping performace in 3d conditions, *International Offshore and Polar Engineering Conference, ISOPE*, number 18, ISSN 1098-6189, Vancouver, Canada.

Masterton, S. R. and Swan, C. (2008). On the accurate and efficient calibration of a 3d wave basin, *Ocean Engineering* **35(8-9)**: 763–773.

Maynord, S. (2002). Comparison of surface velocities in micro-model and prototype, *Technical report*, US Army Engineer Research and Development Center, Coastal and Hydraulics Laboratory, Navigation Branch.

Maynord, S. (2006). Evaluation of the micromodel: an extremely small-scale moveable bed model, *Journal of Hydr. Eng.* **132**: 343–353.

McCleave, B., Greer, H. and Briggs, M. (1999). Wave generation instrumentation in hydraulic models, *OCEANS apos;99 MTS/IEEE. Riding the Crest into the 21st Century*, Vol. 1, pp. 119–125.

McDonald, K. (2005). *Experimental investigation of small-scale breaking waves : flow visualization across the air-water interface*, Master's thesis, Massachusetts Institute of Technology. Dept. of Ocean Engineering.

Mead, S. and Black, K. (2001). Predicting the breaking intensity of surfing waves, *Journal of Coastal Research* **SI29**: 103–130.

Melville, W. (1982). The instability and breaking of deep-water waves, *Journal of Fluid Mech.* **115**: 163–185.

Miche, M. (1944). Mouvements ondulatoires de la mer en rpofondeur constant ou decroissante, *Annales de Ponts et Chassees* .

Miles, W. (1974). Harbor seiching, *Annu. Rev. Fluid Mech.* **6**: 17–35.

Müller, G., Kauppert, K. and Bruce, T. (2002). Particle image velocimetry: a simple technique for complex surface flows, *Proc. Riverflow 2002 Conference, Louvain-la-Neuve, Belgium.*

Monioudi, I., Akylas, A., Tsoukala, V., Stamou, A. and Moutzouris, K. (2006). Investigation of wave transmission through a renewal pipe at breakwaters, *4rth Panellenic Conf. of Harbor works* pp. 219–228.

Mori, M., Yamamoto, Y. and Kimura, K. (2008). Wave force and stability of upright section of high mound composite seawall, *in* J. Simth (ed.), *Proc. of the 31st International Conference*, Vol. 4, pp. 3164–3172.

Morse, P. and Rubinstein, R. (1938). The diffraction of waves by ribbons and slits, *Physical Review* pp. 895–898.

Muller, G. (2003). Characteristics of pressure pulses propagating through water-filled cracks., *Coastal Engineering* **49**: 83–98.

Muller, G., Canning, A., Magagna, D., Stagonas, D. and Warbrick, D. (2009). Composite seawalls for wave energy conversion, *Coasts, Marine Structures and Breakwaters, EICC, Scotland, UK.*

Muller, G. and Senior, J. (2007). Die wasserdruckmaschine mit freier oberfläche – ein neuer energiewandler für sehr niedrige fallhöhen (the hydrostatic pressure converter with a free surface – a novel energy converter for very low head differences, in german), *in* R. V. (ed.), *Zehntes Internationales Anwenderforum Kleinwasserkraftwerke, Ostbayerisches technologie-Transfer Institut (OTTI)*, pp. 26–31.

Nairn, R. (1988). Statistical vs variance definitions of wave parameters in the surf zone, *postscropt to Prediction of wave height and mean return flow in cross-shore sediment transport modelling, IAHR symposium on math, modelling of sed. transp. in the coastal zone, Copenhagen, Denmark.*

Nakamura, T., Mochizuki, H. and Morita, S. (1996). Performance of a resonator designed by the wave filter theory -applicability to a harbor, *Proceedings of the 25th International Conference on Coastal Engineering held in Orlando, Florida*, pp. 1280–1292.

Nece, R. (1985). *Physical Modelling of Tidal Exchange in Small-Boat Harbors*, Numerical and Physical Modelling of Ports and Harbors, Birmingham, England, Dept. of Civil Engineering of Brimingham University and International Association for Hydraulic Researsh.

Oguz, H. and Prosperetti, A. (1989). Surface tension effects in the contact of liquid surfaces, *Journal of Fluid Mechanics* **203**: 149–171.

Ohmura, Y. (2006). Wave set-up induced flow in seawater exchange structures with blockwork mounds, *Proc. Coastal Engineering, ICCE* **4**: 4374–4385.

Oumeraci, H. (1984). Scale effects in coastal hydraulic models, *Proc. Symposium on Scale Effects in Modelling Hydraulic Structures, IAHR.*

Ozhan, E. and Tore, E. (1992). Studies for improving flushing ability of marmaris marina, *Marina Technology, Computational Mechanics and Thomas Telford, London* pp. 267–281.

Penny, W. and Price, A. (1944). Diffraction of sea waves by breakwaters, *Technical report*, Directorate of miscellaneous weapons development, Technical History No. 26, Artificial Harbors, Sec. 3D.

Penny, W. and Price, A. (1952). The diffraction theory of sea waves by breakwaters, and the shelter afforded by breakwaters, *Phi. Trans. Royal Soc. (London)* **244**: 236–253.

Peregrine, D. (1983). Breaking waves on beaches, *Annu. Rev. Fluid Mech.* **15**: 149–178.

Perlin, M. and He, J. (1996). An experimental study of deep water plunging breakers, *Phys. Fluids* **8**: 2365–2374.

Perlin, M. and Schultz, W. (2000). Capillary effects on surface waves, *Annu. Rev. Fluid Mech.* **32**: 241–274.

Prosperretti, A. and Oguz, H. (1997). Air entrainment upon liquid impact., *Philosophical Transactions of the Royal Society London* **A355**: 491–506.

Pullen, T., Allsop, W., Bruce, T. and Pearson, J. (2009). Field and laboratory measurements of mean overtopping discharges and spatial distributions at vertical seawalls, *Coastal Engineering* **56**: 121–140.

Putnam, J. and Arthur, R. (1948). Diffraction of water waves by breakwaters, *Trans. Amer. Geophys. Union* pp. 481–490.

Qiao, H. and Duncan, J. (2001). Gentle spilling breakers: crest flow-field evolution, *J. Fluid Mech.* **439**: 57–85.

Rankine, G. (1991). Mini models for the hydarulic design of ports, *The Dock and harbor authority.*

Rapp, R. and Melville, W. (1990). Laboratory measurements of deep water breaking waves, *Philosophical Transactions of the Royal Society London* **A331**: 735.

Ruol, P., Faedo, A. and Paris, A. (2004). Physical model study of water piling-up behind low crested structures, *Proc. 29th Int. Conf. on Coastal Eng.* pp. 4165–4177.

Sayce, A., K., B. and Gorman, R. (1999). Breaking wave shape on surfing reefs, *Proceedings of Coasts and Ports '99, Perth, Australia*, pp. 596–603.

Schäffer, H. (1996). Second order wavemaker theory for irregular waves, *Ocean Engineering* **23(1)**: 47–88.

Schäffer, H. and Jakobsen, K. (2003). Non-linear wave generation and active absorption in wave flumes, *Proc. Long. Waves Symposium,Thessaloniki, Greece.*

Schulz, K. (1992). *Maßstabseffekte beim Wellenauflauf auf glatten und rauhen Böschungen.*, PhD thesis, Mitteilungen des Leichtweiß-Instituts für Wasserbau der Technischen Universität Braunschweig., Germany.

Schuttrumpf, H. (2001). *Wellenüberlaufströmung bei Seedeichen – Experimentelle und Theoretische Untersuchungen.*, PhD thesis, Technishe Universitat Braunschweig, Germany.

Schuttrumpf, H. and Oumeraci, H. (2005). Layer thicknesses and velocities of wave overtopping flow at seadikes, *Coastal Engineering* **52**: 473–495.

Senior, J., Wiemann, P. and Muller, G. (2008). The rotary hydraulic pressure machine for very low head hydropower sites, *Hidroenergia*, p. Session 5B.

Slauenwhite, D. and Johnson, D. (1999). Bubble shattering: Differences in bubble formation in fresh water and sea water, *Journal of Geophysical Research-Oceans* **104(C2)**: 3265–3275.

Soler, A.-C. (2009). *Pressure measurements on the composite sea wall*, Master's thesis, School of Civil Engineering and the Environment.

Soukassian, T., Tzortzi, E. and Kokkali, A. (2009). Spatiotemporal behaviour of wind sea states in the hellenic seas, *Proc. 19th. Offshore and Polar Engineering Conference*, pp. 792–799.

Spinnekena, J. and Swan, C. (2009). Second-order wave maker theory using force-feedback control. part i: A new theory for regular wave generation, *Ocean Engineering* **36(8)**: 539–548.

Stagonas, D. (2005). *Micro-modelling of wave fields*, Master's thesis, School of Civil Eng. and the Env.

Stagonas, D., Müller, G., Magagna, D. and Warbrick, D. (2009). Fundamental investigation of water flow in harbors through a flushing culvert, *Proceedings of the 33rd IAHR congress, Water Engineering for a Sustainble Environment*, Vancouver, Canada.

Stamou, A., Katsiris, I. and Moutzouris, C.and Tsoukala, C. (2004). Improvement of marina design technology using hydrodynamic models, *Global nest* **6**: 63–72.

Stokes, G. (1880). Considerations relative to the greatest height of oscillatory irrotational waves which can be propagated without change of form, *Math. Phys. Papers* **1**: 225–228.

Svendsen, I. (1985). *Physical modelling of water waves. In Physical modelling in coastal engineering*, Rotterdam: A.A Balkema, Inc., chapter 2, pp. 13–45.

Svendsen, I. (2006). *Introduction to nearshore hydrodynamics*, World Scientific.

Svendsen, I. and Haas, K. (1999). Interaction of undertow and rip currents, *In Proc. Vth COPEDEC, Cape Town*, Vol. 1, pp. 218–229.

Svendsen, I. and Jonsson, I. (1994). *Hydrodynamics of coastal regions*, Den private ingeniorfont- Technical university of Denmark.

Svendsen, I., Madsen, P. and Buhr Hansen, J. (1978). Wave characteristics in the surf zone, *Proceegings of the 16th Coastal Engineering Conf.*, Hamburg, pp. 520–539.

Swan, C. (1990). Convection within an experimental wave flume, *Journal of Hydraulic Research* **vol. 28 (3)**: 273–282.

Ting, F. and Kirby, J. (1995). Dynamics of surf zone turbulence in a strong plungin breaker, *Coastal Engineering* **24**: 177–204.

Ting, F. and Kirby, J. (1996). Dynamics of surf zone turbulence in a spilling breaker, *Coastal Engineering* **27**: 131–160.

Tirindelli, M., Lamberti, A., Paphitis, D., Vidal, C., Hawkins, S., Morchella, P. and Sanchez-Arcilla, A. (2000). Wave action on rubble mound breakwaters: the problem of scale effect, *Technical report*, DELOS EVK3-CT-2000-00041.

Tsoukala, V. and Moutzouris, C. (2009). Wave transmission in harbours through a flushing culvert, *Ocean Engineering* **(available online)**.

Tulin, M. (1996). *Breaking of ocean waves and downshifting*, In Wave and Nonlinear Processes in Hydrodynamics, pp. 177–190.

Tzivanaki, A. (2007). *Simultaneous measurements of surface water waves in space and time*, PhD thesis, School of Civil Eng., Imperial College London.

USACE (2004a). Rep. on the 68th meeting, micromodeling, *Technical report*, Committee on Channel Stabilization, Mississippi Valley Division, Vicksburg, Miss.

USACE, U. A. C. o. E. (2004b). Rep. on the 68th meeting, micromodeling,, *Technical report*, Committee on Channel Stabilization, Mississippi Valley Division, Vicksburg, Miss.

Valembois, J. (1951). Methods used at the national hydraulic laboratory of chatou (france) for measuring and recording gravity waves in models, *Proceedings of the NBS Semicentennial Symposium on Gravity Waves, NBS*, pp. 18–20.

van der Meer, J. and Janssen, J. (1994). Wave run-up and wave overtopping of dikes. wave forces on inclined and vertical wall structures, *Technical Report 485*, Delft Hydraulics.

Wang, Y. and Tulin, M. (1996). Surface tension effects on breaking waves-longtank simulation, *Tech. Rep. 95-132. University of California, Santa Barbara* .

Watson, D. (2002). *Practical ship design*, Vol. 1, Elsevier Ocean Engineering Book Series, Elsevier Science Ltd.

Watson, O. (2007). *Micro-modelling of wave fields*, Master's thesis, School of Civil Eng. and the Env., University of Soutahmpton.

Whalin, R. and Chatham, C. (1974). Design of distorted harbor wave models, *Proc. of the 14th Coastal Engineeering Conference, ASCE*, Vol. 3, pp. 2102–2121.

Wiegel, R. (1962). Diffraction of waves by semi-infinite breakwater, *J. Hyd. Div., Proc. ASCE* **88**: 27–44.

Wiegel, R. (1976). *Oceanographical engineering.*

Williams, J. (1981). Limiting gravity waves in water of finite depth, *Phi. Trans. Royal Soc. (London)* **302**.

Willson, C. (2009). Small-scale physical model, *Louisiana Civil Engineer* **2**: 14.

Wood, I. (1991). *Air entrainment in free-surface flows. IAHR hydraulic structures design manual no.4, Hydraulic design considerations*, Balkema Publ. Rotterdam, The Netherlands.

Yalin, M. (1965). Similarity in sediment transport by currents, *Technical report*, Hydraulics Research Paper No. 6, Hydraulics Research Station, Wallingford, U.K.

Yalin, M. (1971). *Theory of hydraulic models*, McMillan, London.

Yasuda, T., Mutsuda, H., Mizutani, N. and Matsuda, H. (1999). Relationships of plunging jet size to kinematics of breaking waves with spray and entrained air bubbles., *Coastal Engineering Journal* pp. 269–280.

Yeh, H. (1995). *Free-Surface Dynamics*, World Scientific Co., pp. 1–74.

Yeung, R. and Ananthakrishnan, P. (1997). Viscosity and surface tension effects on wave generation by a translating body, *Journal of engineering mathematics* **32**: 257–280.

Yoo, D. (1986). *Mathematical modelling of wave-current interacted flow in shallow waters*, PhD thesis, Univ. of Manchester.

Yuksel, M. and Kapdasli, M. (1994). *Two-Phase Flow Structure in Breaking Waves.*, World Scientific., chapter Sediment Transport Mechanisms in Coastal Environments and Rivers., pp. 299–307.

Zhanq, H. and Schäffer, H. (2008). Approximate stream function wavemaker theory for highly non-linear waves in wave flumes, *Ocean Engineering* **34**: 1290–1302.

Appendix A

Observations on air entrainement

In Chapter 5, section 5.3.4 it was shown that in micro-models, waves with the same initial conditions brake in a more intense manner for larger We and a larger amount of air is trapped under the plunging jet. Moreover, the formation of clean plunging breakers was also made possible for the smallest wave parameters employed in the current project.

However in order for similarity to be achieved between a micro-model and the prototype several aspects of the breaking event need to be in similitude. These aspects contribute to the dissipation of energy and include the mechanisms evolved during breaking, the amount of entrained air, the formation and distribution of bubbles etc. Although research focused on scale effects in turbulent air water flows (i.e hydraulic jumps) and especially in air entrainment by breaking waves has been contacted in the past, the information available is contradictory. Key findings related to the current observations are referred to here:

- Dean and Stokes (2002), suggested that for plunging breakers the air entrainment and bubble creation is driven by the jet-water impact and the cavity collapse. The latter flow feature is responsible for the generation of bubbles larger in radius than 1mm, while smaller bubbles are produced by the former and the subsequent splashing. The limit between these two processes is set by the Hinze scale which is the scale where turbulent fragmentation ceases. The authors found that the location of change in the Hinze scale is the same for laboratory and oceanic breaking waves and put this forward as evidence that the bubble formation mechanisms are the same in model and prototype and that the distribution of bubble sizes should also be the same at all scales.

- Based on Garrett et al. (2000), air is originally entrained into larger bubbles which break up into smaller ones by the turbulent motion produced as the cavity collapses. The central idea behind this turbulent fragmentation is that bubbles break up when the differential pressure forces exceed the restoring force of surface tension, or else when a critical value of We_b (commonly between 3 and 4.7) is exceeded:

$$We_b = \frac{\rho u^2 d}{\sigma} \tag{A.1}$$

were We_b is the bubble Weber number, ρ is the fluid density, σ is the surface tension, u is the turbulent velocity field on the scale of the bubble, and d is the bubble diameter.

- Fan and Tsuchiya (1990), argued that air bubbles also oscillate inside the fluid and thus the bubble Reynolds number,

$$Re = \frac{ud}{\nu} \tag{A.2}$$

were, ν is the fluid kinematic viscosity should be considered as well.

- Chanson, Aoki and Hoque (2002) and Lamarre (1993) observed significantly smaller air entrainment by plunging jets in saline water than in freshwater. Further, less air was entrained in natural than artificial sea water and Chanson et al. (2006) proposed that the presence of surfactants and the physical, biological and chemical properties should be taken into account in any physical model study.

- Chanson (2009), conducted experiments of highly aerated flows like hydraulic jumps and flows over stepped spillways, in different scales. He observed that in small scales turbulence levels are lower and larger in length, less air is entrained and larger bubbles are formed; lesser turbulence levels impliesalso lesser rate of energy dissipation. Accordingly the author concluded that even large size scale models based on Froude similitude, with Re $< 5*10^5$ drastically underestimate turbulence levels, mass transfer rates and air-water interactions.

- Blenkinsopp and Chaplin (2007), presented measurements of void fractions for waves breaking in freshwater and saline water that disagree with all previous researchers. They observed no significant difference in air entrainment and bubble sizes between the different fluids, except on the formation of very fine bubbles ($d_b < 0.3$mm, $d_b$is the bubble radius) during the final stages of the plume evolution for the seawater case. The number of these bubbles increased over repeated breaking events. Blenkinsopp (2007) also reported observations that for the seawater case foam was formed on the water surface. The author also noted that the generation of foam and the bursting of bubbles caused a continuous fizzing noise.

- Blenkinsopp (2007), presented results showing that the time scale of bubble plume evolution follows the length scale instead of the square root of the length scale suggested by Froude scaling. He also conducted numerical calculations and concluded that in model scale the bubble plume disperses more rapidly while at field scale it accumulates over repeated breaking events.

- Blenkinsopp (2007), observed no difference in energy dissipation between saline and freshwater.

- Chanson, Aoki and Maruyama (2002) related larger bubble penetration depths with larger energy dissipation. This is possibly explained because part of gravity wave's energy needs to be spend against the buoyancy force acting on each bubble.

In summary the existed literature suggests that the veracity of a physical model strongly depends upon its size/scale, the effects of which are more important than the influence of the water type. Even when the same mechanisms are evolved (i.e. plunging breakers of Blenkinsopp (2007)) important flow features like the plume evolution, can not be accurately reproduced if the scale selected is not sufficiently large. Consequently it is seen that all previously published studies prohibit the modelling of breaking wave in micro-models due to their very small size and mainly due to the increasing importance of surface tension. However, observations are now presented which show that if the surface tension effects are mitigated then the micro-modelling of breaking wave might be possible.

A.1 Observations on air entrainement: Jet impact and splash-up

All the qualitative characteristics of breaking waves, presented in Chapter, compare very good with those attributed to laboratory and prototype plunging breakers by authors like those Blenkinsopp (2007), Chanson and Lee (1995), and Dean and Stokes (2002) (see 2.3.4). Although this comparison extends all the way down to the

smaller scales employed here, further quantitative research is required in order to assess the validity of waves with L $>$ 0.3m and $H_i <$ 0.03m. Ovservations show that when the length scale increases that much, air entraiment could become unrealisticly small but such waves could be usefull in studies related to wind generated waves and bow ship waves, Yeung and Ananthakrishnan (1997).

Furthermore, the enhanced splash-up could further explain the larger energy dissipation by breaking waves in the IPA solution. The increase in the maximum height of the first reactionary splash-up might imply a stronger impact on the free water surface which in turn will result in a larger second reactionary slash-up and stronger vortex-like structures (red arrows in Figure 5.5 and Figure Figure 5.9 on page 96). Further support to that is provided by Peregrine (1983), who noted that the splash-up motions result in high turbulent intensity and high levels of energy dissipation.Moreover, Jansen (1986) estimated that the wave height reduces by 20-25% during the first jet and splash impact and by 10-15% during every subsequent splash. Accordingly it can be assumed that since the formation of a clean plunging jet is obscured in the freshwater case a reduction in energy dissipation should be expected.